Aalto University
School of Chemical
Technology

**School of Chemical Technology**
**Degree Programme of Chemical Technology**

Mohammed Refaat

# Investigation and ranking antiscalants and biocides in a new monitoring system for reverse osmosis desalination and benchmarking results to the conventional system

**Master's thesis for the degree of Master of Science in Technology submitted for inspection, Espoo, 7 April, 2017.**

Supervisor: Professor Ville Alopaeus

Instructors: Dr. Eng. Mehrdad Hesampour
M.Sc. Tech. Elsa Olmos

Aalto University
School of Chemical
Engineering

Aalto University, P.O. BOX 11000, 00076 AALTO
www.aalto.fi

**Abstract of master's thesis**

**Author** Mohammed Refaat

**Title of thesis** Investigation and ranking antiscalants and biocides in a new monitoring system for reverse osmosis desalination and benchmarking results to the conventional system

**Department** Department of Biotechnology and Chemical Technology

**Major** Chemical Engineering

**Thesis supervisor** Professor Ville Alopaeus

**Thesis advisor(s) / Thesis examiner(s)** Dr. Eng. Mehrdad Hesampour, M.Sc. Tech. Elsa Olmos

**Date** 07.04.2017 **Number of pages** 79+8 **Language** English

**Abstract**

Reverse osmosis (RO) membranes are growing to be the dominant technology for water purification applications. However, fouling is the primary obstacle affecting the RO technologies, and it forces the operator to apply higher operating pressure and use more cleaning chemicals. Therefore, the membrane research major objective is to develop complementary approaches to control fouling based on the development of effective antiscalants and biocides to control fouling and biofouling. Moreover, useful tools for quantitative online monitoring of fouling at early stages and evaluation of cleaning steps. The three experimental research chapters in this thesis are covering the two approaches.

Three antiscalants were assessed in Chapter 7 to investigate the promotion of the RO recovery percentage despite the high saturation indices of feed water. The study was carried out on a model reject brine solution. Two cross-flow RO membrane units were utilised in the test. The scaling experiments were carried by circulating the feed solution through membrane modules for 90 hours in a total recycle mode at a flow rate of 48 L/h, the temperature was kept between 20 to 25 $^{o}$C, and the operating pressure was controlled at 10 bars. The assessment was based on the normalised permeate flux decline and the normalised pressure drop in the absence of antiscalant dose and (2, 10 and 20 mg/L antiscalant doses). Additionally, at the end of each scaling run, membrane autopsies were carried out on a fouled membrane to provide a quantitative and quantified analysis.

Two biocides were evaluated in chapter 8. The study was focusing on simulating biofouling accumulation in the cross-flow RO filtration units by utilising fresh bacterial inoculum and nutrients and exposing the system to biocide dose for cleaning. The feed water was recirculated through the system at flow rate 18 L/h in a total recycle mode for two weeks. The tank temperature was kept at 40 $^{o}$C to keep the bacteria growing. The operating pressure was controlled at 10 bars. The biocide was added stepwise when the permeate flux dropped by 10-15 % of initial values. The permeate flux and normalised pressure drop were continuously monitored to verify the ability of biocide to control biofouling on RO membrane. At the end of the test, the membrane coupons were examined to determine the effect of biocide on the biofilm accumulation.

The research objective of chapter 9 was to develop a prototype for real-time monitoring membrane fouling. The primary aims were to verify the device accuracy for detecting fouling of the spacer grids and membrane surface in the early phase, the device response to chemical addition (Biocide and Antiscalants), and its capability to classify and distinguish between biofouling and fouling.

**Keywords** Reverse osmosis; Desalination; (Bio)fouling; Antiscalants; Biocides; Real-time monitoring; membrane fouling simulator

# Foreword

The master's thesis has been conducted from June 2016 to February 2017 at Kemira Espoo Research Center for membrane desalination program.

There are so many people have made my thesis journey a lot easier than I thought it was going to be. I wish to thank Pentti Pekonen for giving me the opportunity to write my master's thesis at Kemira. I would like to thank especially Mehrdad Hesampour who has selflessly given me great guiding and help in every aspect of my research. I would also like to thank Elsa Olmos for her guidance and encouragement. I also extend my deepest of gratitude towards Vesa Vuori, Satu Ikävalko, Jaakko Ekman and Anne Mäki for providing indispensable advice and information. I am also very grateful for all the input and comments from professor Ville Alopaeus.

Much of my experimental work would not have been completed without the assistance of Tytti Larinoja, Merja Huotarinen, Pirkko Valkeinen, Joonas Toukkari, Jouni Koski, and Tiina Pajunen. Also, I wish to thank Markus Honkanen from Pixact Oy for his help during operating the monitoring device.

And last but not least, I would like to thank my friends and family, for supporting and encouraging me during this project.

Espoo, March 21, 2017

Mohammed Refaat

# Table of Contents

# List of Figures

# List of Tables

# List of Abbreviations and Nomenclature

## Abbreviation

| | |
|---|---|
| AA-AMPS: | 2-acrylanmido-2-methylpropanesulfonic acid |
| aNDP: | Average net driving force |
| AS1: | Antiscalant product one |
| AS2: | Antiscalant product two |
| AS3: | Antiscalant product three |
| ATMP: | Amino trimethylene phosphonic acid |
| ATP: | Adenosine tri-phosphate |
| BWRO: | Brackish water reverse osmosis |
| CA: | Cellulose acetate |
| CCPP: | Calcium carbonate precipitation potential |
| DI: | Deionized water |
| DMO: | Direct microscopic observation |
| DOTM: | Direct observation through the membrane |
| ED: | Electrodialysis |
| EDAM: | Electronic Diode Array Microscope |
| EDS: | X-ray spectrometry analysis |
| EIS: | Electrical Impedance Spectroscopy |
| EPS: | Extracellular polymeric substance |
| EXSOD: | EX-situ Scale Observation Detector |
| FCP: | Feed spacer channel pressure drop |
| LMH: | Litres of water per membrane area $m^2$ per hour |
| MED: | Multi-effect distillation |
| MFS: | Membrane fouling simulator |
| MSF: | Multi-stage flash distillation |
| NF: | Nanofiltration |
| NMR: | Nuclear Magnetic Resonance |
| NOM: | Natural Organic Matter |
| NP: | Normalised pressure |
| NPF: | Normalised permeate flow |
| PA: | Polyamide |

| | |
|---|---|
| PASP: | Poly aspartic acid |
| PESA: | Polyepoxysuccinic acid |
| PIV: | Particle Image Velocimetry |
| PPCA: | Poly-Phosphino Carboxylic Acid |
| RO: | Reverse osmosis |
| SANS: | Small-angle neutron scattering |
| SEM: | Optical imaging scanning electron microscopy |
| SI: | Supersaturation index |
| SWRO: | Sea water reverse osmosis |
| tATP: | Total ATP |
| TCF: | Temperature correction factor |
| TDS: | Total dissolved solids |
| TMP: | Transmembrane pressure |
| UTDR: | Ultrasonic time-domain refractometry |
| VCD: | Vapour compression distillation |
| XRD: | Powder X-ray diffraction |
| XRF: | X-ray fluorescence spectrometry |

## Nomenclature

| | |
|---|---|
| $IAP$ | Ion activity product |
| $K_{sp}$ | Solubility product |
| $\Delta P$ | Pressure drop across the membrane cell, mbar |
| $f$ | Friction coefficient |
| $v$ | Cross-flow velocity, m/s |
| $\rho$ | Fluid density, kg/m$^3$ |
| $L_m$ | Membrane cell length, m |
| $d_h$ | Hydraulic diameter, m |
| $\varepsilon$ | Spacer porosity |
| $S$ | Specific surface of membrane, m$^2$/m$^3$ |
| $w$ | Spacer width, m |
| $h$ | Height of spacer, m |
| $Re$ | Reynolds number |
| $\eta$ | Dynamic viscosity, Pa.s |

# 1. Introduction

Water is the primary source of living and the base of life on earth. 70% of our planet earth is covered with water which is about $1.4x10^9$ $km^3$ (El-Dessouky and Ettouney, 2002a). The fresh water present only 2.5% of the total amount of water and most of it is frozen in the icecaps (Voutchkov and Semiat, 2008). The rest is salted water located in the oceans; Table 1 illustrates the allocation of water sources. In additional to the small amounts of fresh water, it is not readily available, not accessible and not evenly distributed and the consumption of water doubles every 20 years. The majority of salted water is located in the oceans, and the main natural source of energy to form fresh water out of the oceans is the solar energy. The solar power creates a temperature difference forcing water to evaporate forming clouds. Due to the wind speed and direction, other geographical conditions, and different elevations, the precipitation of rain is not evenly distributed. Most of the lakes, rivers, and underground fresh water are formed due to rains (Miller, 2003).

One of the common classification methods for water category is based on salinity which refers to the quantity of total dissolved solids (TDS) in the water. A TDS concentration of 1,000 mg/L is the upper limit of freshwater. Water containing more than 1,000 mg/L up to 3,000 mg/L is used for daily purposes and domestic supply in areas where fresh water is not available. The above category is the brackish water which lies between 3,000-5,000 mg/L TDS, and water is considered saline if it exceeds 10,000 mg/l. The highest category is referred to as Brine with salinity greater than seawater (which is typically range from 18,000 to 35,000 mg/L) (El-Dessouky and Ettouney, 2002a;Strathmann, 2010).

In addition to the limited natural resources of fresh water, the level of development of the economy in the countries is one of the factors of increasing the water consumptions. Moreover, the increase in the population and the high living standards in the majority of the industrial countries leading to one of the biggest problems in this century which is the water scarcity. Basically, water shortages are the gap between water supply and demand. Top engineers have reported its impact to human development since half of the world population; mainly in the developed countries, are suffering from disease and death resulting from low-quality water, and water scarcity is expected to affect four times the number of population in the next twenty-five years. (Miller, 2003).

*Table 1. Water Resources guide across the world (El-Dessouky and Ettouney, 2002a).*

| Resource | Volume $Km^3$ | Percent of total water | Percent of fresh water |
|---|---|---|---|
| Atmospheric water | 12900 | 0.001 | 0.01 |
| Glaciers | 24064000 | 1.72 | 68.7 |
| Ground Ice | 300000 | 0.021 | 0.86 |
| Rivers | 2120 | 0.0002 | 0.006 |
| Lakes | 176400 | 0.013 | 0.36 |
| Marshes | 11470 | 0.0008 | 0.03 |
| Soil Moisture | 16500 | 0.0012 | 0.05 |
| Aquifers | 10530000 | 0.75 | 30.1 |
| Lithosphere | 23400000 | 1.68 | |
| Oceans | 1338000000 | 95.81 | |
| Total | 1396513390 | | |

Various research plans have been advanced to handle the water shortage and how to develop the water conservation and quality. Sequentially, the approach is to limit the effect of water scarcity by increasing the water reuse efficiency and finding non-traditional sources of fresh water like the sea water (Fritzmann et al., 2007). The sea water can be refined for industrial application and water reuse, one of the first and current technologies is the desalination of water.

# LITERATURE REVIEW

## 2. Desalination

Desalination is the process of separation the salts from salty water. It is broadly applied for water purification and industrial applications, and currently, it is growing rapidly worldwide to overcome the water scarcity. Particularly in the Middle East and North Africa are facing water shortages, and are the largest users of desalination technology. In Europe, Spain has the most desalination plants. More than 120 countries start to use desalination as a solution and source of fresh water. Desalination process has been developing towards decreasing the capital cost and energy consumption. The process demands energy mainly in the removal of the salts. Multiple technologies have been utilised, and they form primarily two categories; Thermal and membrane methods (Tsiourtis, 2001). Figure 1 represents a simple process diagram of desalination, showing the inputs and outputs of the process.

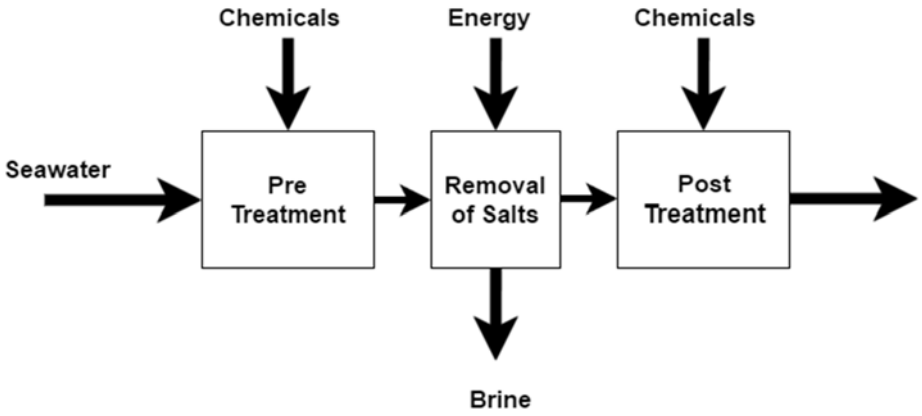


*Figure 1. Simple process diagram of desalination process (Tsiourtis, 2001).*

The thermal method is simply separating the salts from water based on evaporation and the subsequent condensation of the treated stream. On the other hand, the membrane method where water diffuses through the membrane and the salts are effectively retained. The most utilised desalination technologies are given in Table 2.

*Table 2. Various desalination technologies (Fritzmann et al., 2007).*

| Thermal desalination technologies | Membrane-based desalination technologies |
|---|---|
| Multi-stage flash distillation (MSF) | Reverse osmosis (RO) |
| Multi-effect distillation (MED) | Nanofiltration (NF) |
| Vapour compression distillation (VCD) | Electrodialysis (ED) |

The desalination technology is chosen based on the availability of the energy (The energy study) and the location of the plant. The energy cost represents about 25-40% of the total cost of a desalination plant (Tsiourtis, 2001). Therefore, in the Middle East, where the largest capacity of the desalination plant is located, the dominating technology is the thermal processes because of the low cost of fossil fuel. On the other hand, the reverse osmosis is dominant in Europe since it is less on the energy consumption (Tsiourtis, 2001). Table 3 shows the comparison between the two desalination alternatives based on the operation principles. The electrical energy in MSF is significantly higher than RO since it requires energy for operating various pumps in recycling, cooling water moves in heat exchangers and distillate product. Besides the advantage of RO over MSF on the operation principles, the production capacity can be scaled up and down since the process is based on modules and the process can be shifted from batch to continuous process. Besides, space requirement of the process is smaller than thermal technologies.

*Table 3. Comparison between thermal and membrane desalination based on the operation principles (Al-Karaghouli and Kazmerski, 2013).*

| | MSF | RO |
|---|---|---|
| Thermal Energy Consumption [MJ/$m^3$] | 190-282 | None |
| Electrical energy [kWh/$m^3$] | 19.58-27.25 | 4-6 |
| Typical salt content of raw water (mg/L TDS) | 30,000-100,000 | 1,000-45,000 |
| Product water quality (mg/L TDS) | <10 | <500 |

## 3. Membrane Separation

The membrane can be simply defined as a boundary to separate two states and limit the transport of particular component. The pressure difference is critical in choosing the separation techniques since the pressure difference needs to be constantly higher than the osmotic pressure. In other words, for efficient membrane separation process, the hydrostatic force must overcome osmotic pressure to remove unwanted molecules and ions from the water. The particle size range is the primary factor for choosing the separation technique. NF works on a particle size range of 5 nm to 50 nm and RO on a particle size between 0.1 nm to 5 nm (El-Dessouky and Ettouney, 2002b). Additionally, Figure 2 illustrates separation abilities of RO, NF, and other pressure driven separation process related to water desalination and treatment. The main advantage of NF over RO is that it has a different transport mechanism of the solution, NF allows monovalent salts like sodium and calcium chloride and not pass the multivalent salts or the small organic compounds (Fane et al., 2011).

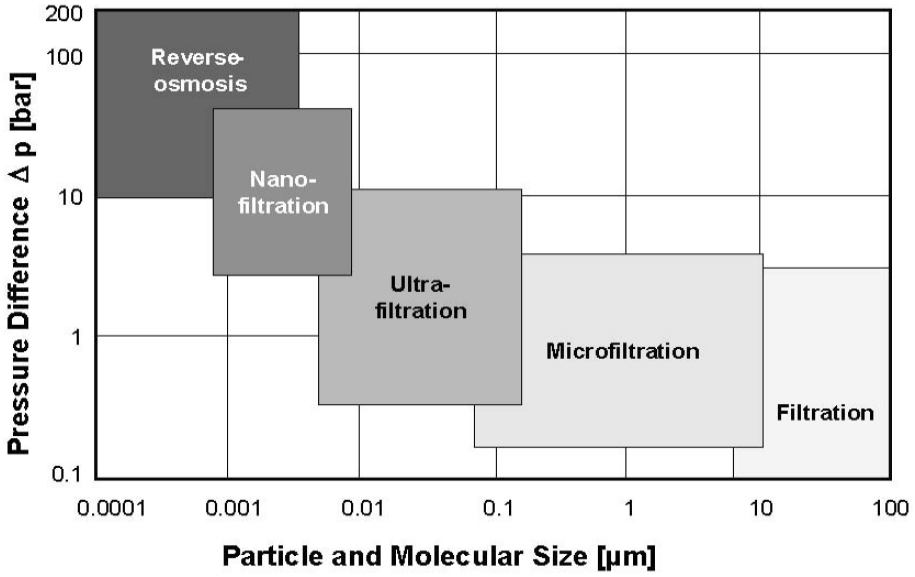


*Figure 2. The separation abilities of RO and Nanofiltration (Melin and Rautenbach, 2007).*

### 3.1 High-pressure membrane configuration

The high pressure driven membranes are principally applied in the water desalination for the removal of salts, particularly, the mono and divalent ions. The water sources are the seawater and the brackish water, and typically the transmembrane pressure (TMP) is between 5 to 55 bars (Crittenden et al., 2012). In the membrane applications and

particularly in water treatment application, the membranes are patterned into modules. The most common modules are plate and frame, spiral wound and hollow fibre modules (Fane et al., 2011). Besides, the difference in the geometric shapes of the modules, the membrane surface to volume ratio is the critical diversity between the modules. The plate and frame module surface to volume ratio is about 328–492 $m^2/m^3$, 656–820 $m^2/m^3$ for spiral wound modules and 6,562–13,123 $m^2/m^3$ for hollow fibre modules (Fane et al., 2011). It is common to locate a feed channel spacer in every membrane module, as it creates turbulence and minimises the concentration polarisation by 10-20 % in each module (El-Dessouky and Ettouney, 2002b).

The first module used for the desalination process was the hollow fibre module due to its excellent area to volume ratio. However, currently, the spiral wound is more implemented in the desalination process since it offers a right balance in term of permeability although it has a small membrane surface to volume ratio (Fritzmann et al., 2007). Figure 3 represents the spiral wound module where the membrane leafs adhere together creating a membrane element.

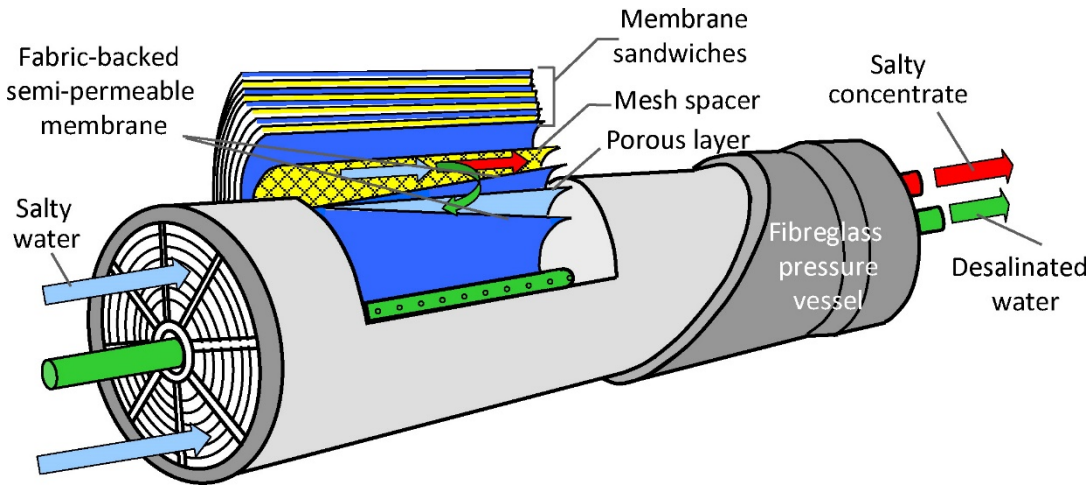


*Figure 3. The flow through a spiral wound module (Fane et al., 2011).*

In addition to the various modules which affects the membrane separation, the flow inside the membrane has a significant influence on the flux. The flow is classified into two separate flow directions; the cross-flow and the dead-end flow. In the cross-flow, the direction of the water is parallel to the membrane surface, and the permeate flow is nearly small. On the other side, in the dead-end, the flow of water is perpendicular to

the membrane surface, and there is one path for the water to exit the membrane, resulting in higher permeate flow than in the cross-flow (Crittenden et al., 2012).

## 3.2 Membrane materials

The membrane performance is mainly based on the physical and chemical properties of the membrane material. Various materials are involved in the manufacturing from ceramics, glasses to different polymers. The chemical stability in a wide pH range and mechanical strength are the main criteria for choosing the construction material of membrane module (Ren and Wang, 2011). The hydrophobicity is a critical feature, and it mainly affects the permeate flux and fouling rate. The hydrophobicity of a membrane is measured as the angle of contact between the liquid (e.g. water) droplet and the outside surface of the membrane. As the membrane material is more hydrophobic the larger the angle of contact. Moreover, the membrane can be slightly modified if it is hydrophobic to improve the produced permeate (Pezeshk and Narbaitz, 2012).

Cellulose acetate (CA) was the first standard material used in fabricating the membrane. Currently, the polymeric materials are widely utilised like polyamide, polypropylene, and many other polymers since they are chemical and physically stable and long-lasting. Table 4 shows a list of a conventional polymeric material and their hydrophobicity. The limitations of cellulose acetate membranes are the fouling problems since it collects more organic materials creating biological degeneration and its stability over a wide pH range. Accordingly, polyamide (PA) membrane was developed to overcome those obstacles. Moreover, PA is less hydrophilic than CA (Ren and Wang, 2011).

*Table 4. A list of a membrane material and their hydrophobicity (Ren and Wang, 2011).*

| Membrane material | Hydrophobicity | Operating pH Range |
|---|---|---|
| Cellulose acetate | Hydrophilic | 5...8 |
| Polyamide | Slight hydrophobic | 2..13 |
| Polypropylene | Hydrophobic | 2...13 |
| Polyvinylidene fluoride | Slight hydrophobic | 2…11 |
| Polysulfone | Slight hydrophobic | 2...13 |
| Polyethersulfone | Slight hydrophobic | 2...13 |
| Polyetherimide | Hydrophilic | 2…11 |

# 4. Membrane fouling

Membrane fouling is the major contribute restriction to the efficient operation of reverse osmosis and nanofiltration facilities. It is the accumulation of foulant and contaminants on the membrane surface causing poor salt rejection efficiency, decreasing in the quality of the water produced, increasing the operating cost and membrane layer damage. In the last decade, the research has been focusing on studying the nature of foulant, understanding fouling mechanisms, and learning the relation between different types of foulant and the factor affecting the membrane performance. The fouling causes increase in the operating pressure and usually 10% decrease in the production of water (Avlonitis et al., 2003).

Commonly, the feed water has high TDS and carries suspended solids. The dissolved materials mainly consist of partially soluble salts like carbonates and sulphates. Also, the suspended solids include inorganic, biological bodies, and colloids. In the membrane processing, the feed water concentration increases resulting in increasing the concentration of the dissolved materials and suspending of solids following by blocking the flow through the membrane and decreasing the flow rate of permeate (El-Dessouky and Ettouney, 2002c). The fouling is considered as a combined irreversible phenomenon. It can be classified into several mechanisms: (1) narrowing the membrane pores, (2) adsorption of small particles into the membrane pores, and (3) blocking the pores. The foulants are categorised into four different classes: (1) colloidal/particulate foulants, (2) inorganic foulants, (3) organic foulants, and (4) biological foulants (Speth et al., 2000).

## 4.1 Colloidal foulants

One of the dominant fouling types is the colloidal fouling, and it mainly occurs due to less efficient pretreatment of the feed water. Colloidal particles are carrying negative charges generating accumulation on the membrane surface and leading to cake formation and increase in hydraulic resistance (Armstrong et al., 2009). However, they are reversible fouling and can be easily removed by backwashing. Aluminosilicates (Clays) are the most common known colloidal matter, and it represents 29% of the main fouling composition detected on RO membrane sheets (Peña et al., 2012).

## 4.2 Inorganic foulants

When the sparingly soluble salts concentration increase in the concentrate line and the solution reaches supersaturation conditions, the salts starts to precipitate. The formation of scale leads to a decrease in permeate flux and salt rejection efficiency. The scale formed mainly contains calcium carbonates, calcium sulphates and silica groups. The common prevention action is a proper, accurate antiscalant dose (Song and Tay, 2011). It is considered as the leading fouling on the reverse osmosis and the nanofiltration, and it represents 22% of the main fouling composition (Kennedy et al., 2008).

## 4.3 Organic foulants

Another source of fouling is the Natural Organic Matter (NOM) which are higher molecular weight organics such as humic materials and fulvic acids. As the majority of membrane material is hydrophobic, the NOM adsorbed on the surface resulting on blocking section of membrane and directly affect the permeate flow. Moreover, NOM is a source of nutrients for biological fouling. NOM can be removed by raising the pH value (>9) resulting in a negative charge NOM. Also, by conducting chemical cleaning (Fritzmann et al., 2007). They represent 8% of the main fouling composition (Peña et al., 2012).

## 4.4 Biological foulants

The biofouling appears in all the membrane processes which are defined as bacterial growth attached to the membrane surface. The bacterial growth produces a matrix of polysaccharides and protein derivatives. The extracellular polymeric substances (EPS) are usually described as the main factor for membrane biofouling (Liu and Fang, 2002). They represent 31% of the main fouling composition. Besides, it is remarkably challenging to overcome because the bacteria and algae have certain protection mechanisms against the biocides (El-Dessouky and Ettouney, 2002c).

According to the presented classification, four main categories of foulants can be identified on the membrane surface. Table 5 summarise the main foulants and characteristics of each category. Biofouling and colloidal foulants are about 60% of the total foulants composition, demonstrating the importance of optimising the pretreatment of feed water to enhance the membrane performance. The inorganic/mineral scaling was recognised as main foulant category in 22% of the

studied cases, and calcium carbonate and silica are the most commonly detected scales (Peña et al., 2012). The location of identifying the foulant type varies between each type. The biofouling mainly located at the inlet side of membrane stage, in the first section of the lead membrane module. On the other hand, mineral scale located at the tail end of membrane module because the feed water usually reaches high supersaturation state in the permeate stream (Karabelas et al., 2014). More details are presented in Section 6.3.

A study was conducted on the outcome of water source type on the characteristics of the main fouling. In this study, brackish water and sea water were utilised. Figure 4 illustrates the distribution of main fouling in both cases. It was observed that both biofilm and colloidal matter are the main two categories identified on the membrane surface regardless the water type. However, scaling was recognised as the main issue in brackish water. On the other side, organic and metal precipitates are more observed in sea water case (Peña et al., 2012).

*Table 5. Main foulants composition identified on membrane surface (Peña et al., 2012).*

| Fouling category | Chemical composition | Characteristics | Expected membrane failures |
|---|---|---|---|
| Colloidal matter, 29% | Aluminosilicates | Mix of different very small particles | Increase in hydraulic resistance |
| Inorganic/scale, 22% | Calcium carbonate, calcium sulphate, calcium phosphate, and silica | All mineral salts are detected in crystalline shapes, excluding silica is detected as amorphous | Affects membrane rejection efficiency and mainly affect the last position of the membrane elements. And it can be prevented by accurate antiscalant dosing |
| Organic, 8% | Humic and fulvic acids | Thin precipitate covering the surface of the membrane | They can be easily removed and recover the membrane performance |
| Biofilm, 31% | Polysaccharides/ Protein derivatives | Sticky brownish deposit on membrane surface | Increase in TMP, decrease in permeate flux, and fouling will mainly affect the first membrane modules in treatment station |
| Metals, 10% | Iron 67.7%<br>Manganese 12.9%<br>Aluminium 19.4% | Amorphous precipitates | Decrease in permeate flux. However, effective pretreatment of feed water minimise their deposit |

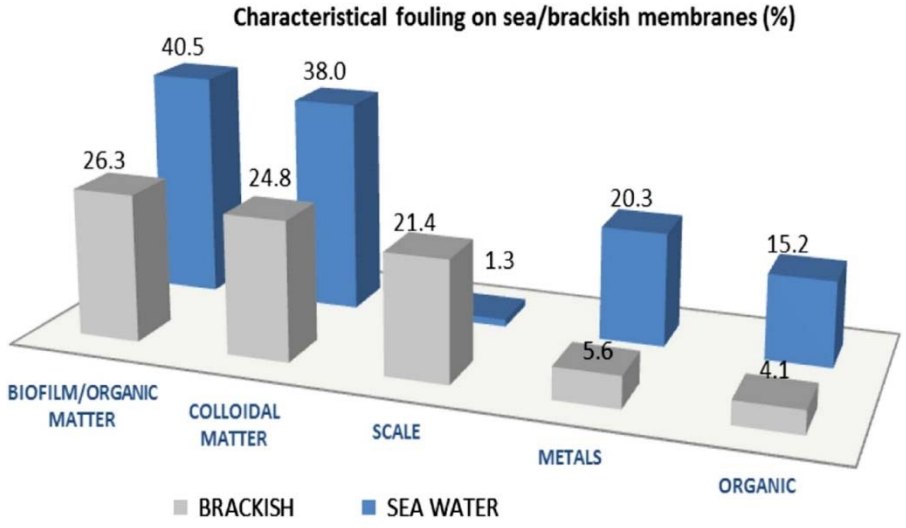


*Figure 4. Main fouling percentage identified in brackish and sea water study cases.*

## 5. Antiscalants and biocides

As outlined in the previous section, the inorganic/scale foulants are composed of carbonates, sulphates, and silica. Thermodynamically, the scaling occurs when the solution reached supersaturation leading to precipitation, and the kinetic of precipitation increases is the key factor of scaling (Lee and Lee, 2000). The growth of the crystals precipitated depend on the concentration of nucleation sites, and the crystallisation is classified into surface and bulk crystallisation (Gu et al., 2014). Therefore, the principal roles of antiscalants are to disturb the precipitation and stop the crystallisation growth. The main three mechanisms that explain the antiscalant work are precipitation threshold inhibition, dispersion, and crystal modification explained in Figure 5. Fundamentally, the inhibition is blocking the active growth sites with the impurity to freeze the crystal growth, and the dispersion mechanism is achieved by anionic dispersion which increases the repulsion charge of crystal and increases the activation energy bar to prevent crystal growth. Lastly, the crystal modification mechanism is achieved by certain antiscalants which can be adsorbed on the crystal surface resulting in slowing the crystal growth and stop the formation of hard deposits. The effectiveness of an antiscalant is determined by evaluating the three-mechanism efficiency (Chen et al., 2015).

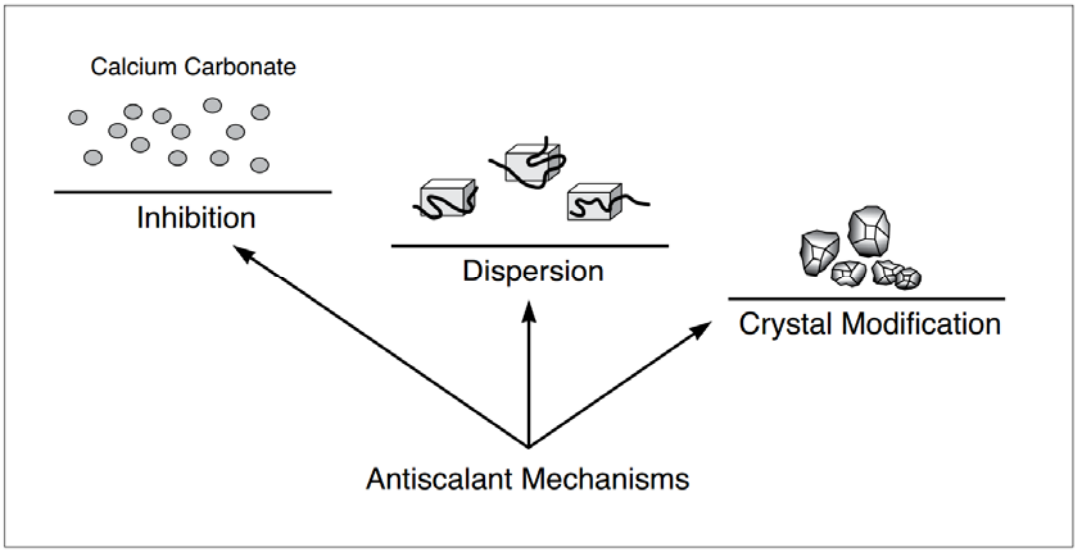


*Figure 5. The three antiscalant mechanisms (Ecolab, 2015).*

The antiscalants are classified into different categories based on what chemicals they are derived from. Antiscalants containing phosphorous are named as polymeric phosphates which are synthesised by organic monomer and phosphate monomer such as Poly-Phosphino Carboxylic Acid (PPCA), and non-polymeric phosphonate antiscalants such as the amino trimethylene phosphonic acid (ATMP) (Ghani and Al-Deffeeri, 2010). The second category is polymeric antiscalants, and polyacrylates are the most known polymer utilised as it has a high efficiently ability for inhibiting the nucleation. An inventor has claimed that a copolymer of acrylic acid and 2-acrylanmido-2-methylpropanesulfonic acid (AA-AMPS) has a powerful calcium carbonate and calcium phosphate tolerance when sufficient dose is introduced to membrane system. Moreover, the antiscalant is effective when the temperature is controlled between 5 to 40 $^{o}$C and pH between 7 to 8.2 (Musale, 2010). However, most of the current antiscalant employed in the industry acts as nutrients in the eutrophication process (Camargo and Alonso, 2006) and due to the current regulation regarding the discharge of chemicals, the industry starts focusing on adopting efficient phosphorus-free polymers and environmentally friendly chemicals. The term green antiscalant is described as nontoxicity and biodegradation. Currently, the common green antiscalants are poly aspartic acid (PASP), polyepoxysuccinic acid (PESA), and polyacrylic acid sodium salt (PAAS) (Liu et al., 2011).

The biocides are the solution to destroy the bacteria cells and the microorganisms. It had been reported that free chlorine is an effective biocidal agent which can basis prevent biofilm (Yu et al., 2013). However, free chlorides ($OCl^-$, $HOCl^-$) are not able to remove the old dead biofilm cells, and it only kills the new bacterial cells entering the membrane unit. Further, it has an adverse effect on the membrane surface since it might attack the amide group in the polyamide membrane surface (Kang et al., 2007). Chlorine dioxide ($ClO_2$) and mono-chloramine ($NH_2Cl$) are alternative options to replace the free chlorine (da Silva et al., 2006).

## 5.1 Antiscalants and biocides supplier products review

Companies worldwide are competing to produce antiscalants, biocides and cleaning chemicals with the best cost to performance ratio. Antiscalants are categorised according to their specific performance towards particular potential scale.

The methodology of determining the effectiveness of commercial antiscalants against different scale potential is based on measurements of homogeneous crystallisation induction time of $CaCO_3$, gypsum, silica, and other scales versus different antiscalant dosage. The study is carried out by utilising online turbidity probe, and through studying the onset of rapid crystallisation, a turbidity-time curve can be obtained to estimate induction time (Shih et al., 2005). This approach is considered as a quick assessment of antiscalant, and the final ranking is based on studying the impact of antiscalant dose on the membrane surface as described in chapter 8. Commonly, the supplier's recommendation regarding the antiscalant dose is volume or mass basis without revealing the actual content of active ingredients.

Avista Inc. produces and distributes water treatment chemicals. They have offices in the United States, United Kingdom, and regional distribution offices in Europe and the Middle East. Avista's portfolio has various antiscalants products (mostly in the liquid form) effective for common potential scale with wide pH range (i.e. acidic and basic products) (See Appendix A, Table A-1). However, no available antiscalant to tolerate calcium phosphate and the deposit iron and manganese. Vitec is the antiscalant brand name of Avista (Avista Technologies, 2016). Besides, the biocide brand name is RoCide (See Appendix B) and cleaning chemical product name is AvistaClean (See Appendix C) (Avista Technologies, 2017). Genesys provides antiscalants to tolerate calcium phosphate, iron and manganese, and most of their products are basic chemicals in liquid form (See Appendix A, Table A-2). Genesys is antiscalant brand name, and Genesol is the biocide and membrane cleaning brand name. They manufacture their chemical in the United Kingdom, and they have 40 distributors globally covering Africa, Asia, Europe, the Middle East and North and South America (Genesys International, 2016).

American water Chemicals (See Appendix A, Table A-3) have only acidic antiscalants. Their colourless antiscalant tolerates most of the mineral scales except iron and manganese. The antiscalants, biocides, and cleaner brand names are AWC (American Water Chemicals, 2013). Accepta has fewer variety antiscalants, their antiscalants have high pH value and cannot tolerate barium sulphate and strontium sulphate (Accepta, 2016). Likewise, Italmatch Chemicals antiscalants cannot treat barium and strontium

sulphate scale as well as silica scale (See Appendix A, Table A-4) (Dequest Italmatch chemicals, 2016).

Kemira Oyj develops and distributes water treatment chemicals. They have Research centres in Finland, United States, and China. Moreover, distributors globally covering Europe, Asia, Middle East and North and South America. Kemira's membrane program portfolio has a broad range of antiscalant for scale control. Their antiscalants are efficient towards all common scale types except Calcium phosphate (See Appendix A, Table A-5). KemGuard is the antiscalant brand name of Kemira. Furthermore, the biocide brand name is Fennocide and cleaning chemical product name is KemClear (Kemira Oyj, 2016a). Moreover, Kemira has effective antiscalant towards inhibiting silica scale formation in the case of high silica content in the feed water (Kemira Oyj, 2016b). Appendix B and Appendix C listed various biocide and cleaning agents and their chemical properties for RO applications from different suppliers.

## 6. Membrane monitoring techniques review

The membrane fouling and flux decline remain the primary difficulties facing the membrane filtration processes despite the many improvements done on development and design of new high-efficient membranes modules, utilising various chemical additives, and determining the optimum operating conditions. Evaluating the characteristic of the feed water is the conventional technique to monitor the membrane fouling, and it is widely implemented in the industry. However, this method is expensive which lead the researchers to develop novel methods to monitor the membrane surface online to observe the growth of fouling layers. The *in-situ* and non-destructive monitoring methods are the most reliable ways to describe the growth of the fouling layer on the membrane surface without the need to stop the process and analyse membrane offline. Performing a successful monitoring method requires analysis of the membrane processes and particularly the bulk fluid stream, at the membrane-fluid interface. Most the non-invasive techniques have been implemented to analyse the membrane-fluid interface. The *in-situ* monitoring techniques can be categorised into two divisions, concentration polarisation and fouling phenomena analysis. Further, the techniques can be classified into optical and non-optical techniques (Chen et al., 2004).

Flemming has developed a classification of the monitoring devices by separating them into three levels (as listed in Table 6). The first level combines the devices which can detect the change in thickness of fouling layer without providing any information related to the composition of the foulant (i.e. the category of devices could not distinguish between fouling and scaling). The second level of devices can differentiate between the organic and inorganic form of foulant. Lastly, the third level provides comprehensive information regarding the microorganisms and the chemical composition of foulant (Flemming, 2003). Level 1 monitoring devices are more mature and can be used for the *in-situ*, on-line, full-scale process. On the other hand, level 2 and 3 are usually time-consuming, and fundamentally, they are usually applied for laboratory and research level for realistic monitoring biofilm formation. The next sections listed various optical and non-optical techniques in level 1, and the recently employed monitoring devices in full-scale RO stations from both classifications.

The approach of level 2 monitoring devices is to recognise signals from biomolecules in the interest of distinguishing between fouling classes. FTIR-ATR-spectroscopy particular for amide bands is a successful approach to identify organic and inorganic materials. Moreover, the method of utilising auto-fluorescence of biomolecules such as amino acids (e.g., tryptophane) is recognised as a proper way to detect biofouling (Zinn et al., 1999). Additionally, microscopic detection of biofilm formation is considered an accurate method. However, it is challenging to differentiate between the microorganisms and agglomerated abiotic bodies unless a dye is applied to the system (Nivens et al., 1995). Level 3 devices are in the laboratory level operation. However, an alternative way was developed to collect all the information about the nature of foulant. The method is employing in a predictive approach by using all the collected information and utilised then in chemical addition plan. Membrane biopsy is a method to monitor normalised permeate flow and pressure drop and utilised the information collected to apply it in a predictive approach (Fazel and Chesters, 2015).

*Table 6. Three categories of the monitoring device (Flemming, 2003).*

| Monitoring level | Explanation |
|---|---|
| Level 1 devices | The devices which can detect the change in thickness of fouling layer without providing any information related to the composition of the foulant. |
| Level 2 devices | Devices which can differentiate between the organic and inorganic form of foulant. |
| Level 3 devices | Devices provide comprehensive information regarding the microorganisms and the chemical structure of foulant. |

## 6.1 Optical techniques

The optical techniques use a video recorder and cameras associated with a microscope to record the particles near the membrane surface. The advantage is that it gives a very precise realistic observation. Furthermore, laser lenses can be used to provide high-resolution images. However, the majority of optical techniques requires a particularly designed membrane module. One of the conventional optical techniques is the direct observation through the membrane (DOTM). The DOTM is an active, efficient method to study the particulate and colloidal matter deposition on the membrane surface. Several studies implement DOTM technique by changing the cross flow speed, the transmembrane pressure, the permeate flux, and running below and above the critical flux to examine the response of the depositing of particles (Bacchin, 2004;Bacchin et al., 2006;Bhattacharya and Hwang, 1997). Figure 6 illustrates the system used for this detection technique; the setup includes a video camera recorder and a monitor. DOTM techniques can examine the biofouling by using fluorescence so the smaller particles can be imagined. Still, there is one disadvantage that the images captured by the video camera are limited in top or side position and directing to the membrane surface. Therefore, it is difficult to monitor the cake thickness and to apply it to large industrial-scale experiment (Chen et al., 2004;Li et al., 1998).

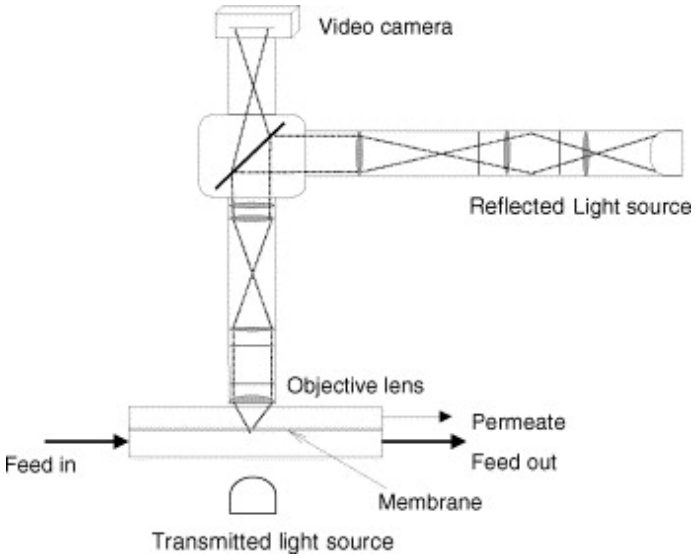


*Figure 6. The DOTM technique components (Chen et al., 2004)*

Direct Microscopic Observation (DMO) technique can be implemented by manipulating several operating parameters as crossflow velocity during the experimental work to have a clear view of all the phenomena happened such as membrane characteristics, the surface roughness, and the free energy adhesion. Figure 7 shows the elevation and side view of the setup of DMO experiment.

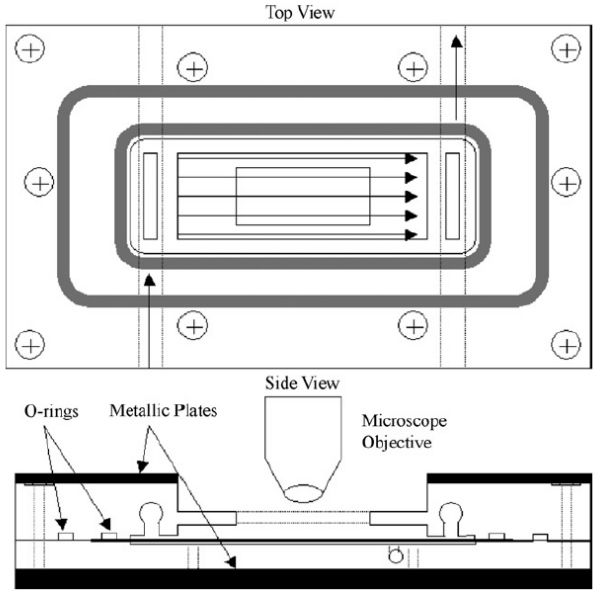


*Figure 7. The top and side view of the setup of DMO (Subramani and Hoek, 2008)*

Another method is the Laser triangulometry, which applies the laser reflections and the length of the reflected light, as the deposit is developed over the membrane surface, the reflected beam shifted allowing the calculation of the depth of the formed cake layer (Altmann and Ripperger, 1997). Figure 8 shows the height of the cake formed and the shift of the light reflected.

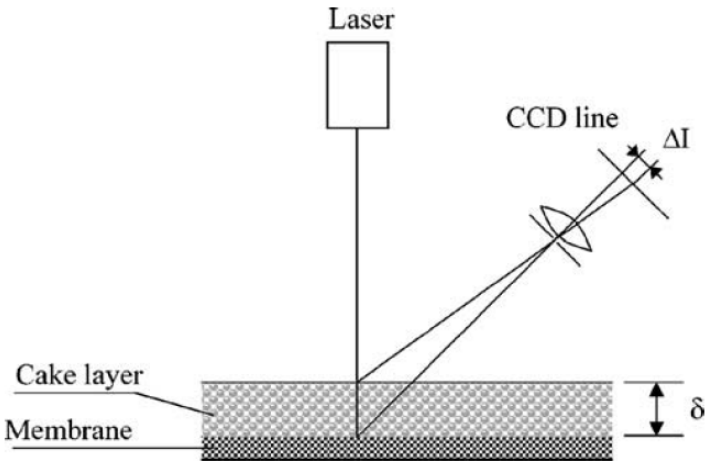


*Figure 8. The Laser triangulometry experimental setup (Chen et al., 2004).*

Optical shadowgraph is a technique to get a concentration characterization at the membrane surface from the measurements of the refractive index. Primarily, this technique uses the deflection of the light beam. Figure 9 illustrate the track of light beam through the membrane module. Difficulty in the procedures and processing the obtained data are the disadvantages of this technology. Moreover, at low concentration, the profiles cannot be estimated directly rather than extrapolating the concentration profile to determine the values at low levels (Vilker et al., 1981). Additional laser source can be appropriated in this technique as He-Ne laser to get more accurate measurements by directing the laser vertically to the membrane surface (Zhang and Ethier, 2001). An electromagnetic wave can be applied as a source for measure the concentration profile based on the aspects that it propagates perpendicular to the refractive index angle (Chen et al., 2004).

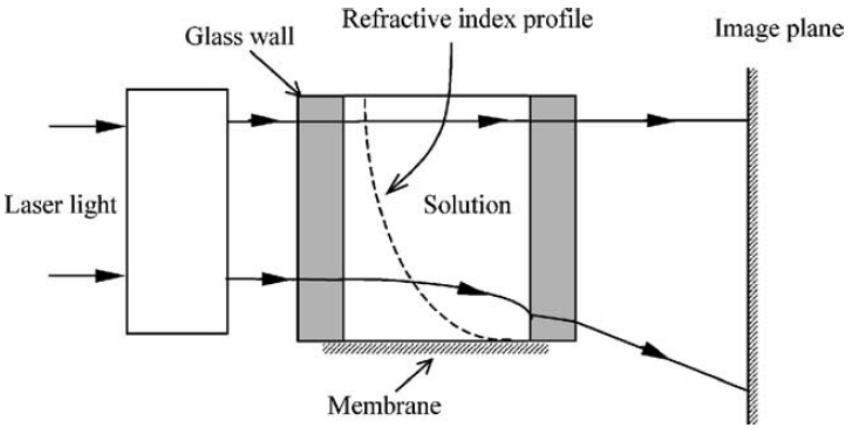


*Figure 9. The track of light beam through the membrane module (Chen et al., 2004).*

Photo-interrupt sensors as the Electronic Diode Array Microscope (EDAM) determine the distance between the membrane surface and the cake layer formed to estimates the concentration profile. Figure 10 shows the EDAM microscope. Additionally, particles can be utilised as a tracer in different techniques. Those particles must be extremely reflective so the recorded camera can capture the particles movements and get their concentration profile. This technique is termed as Particle Image Velocimetry (PIV) (Gaucher et al., 2002).

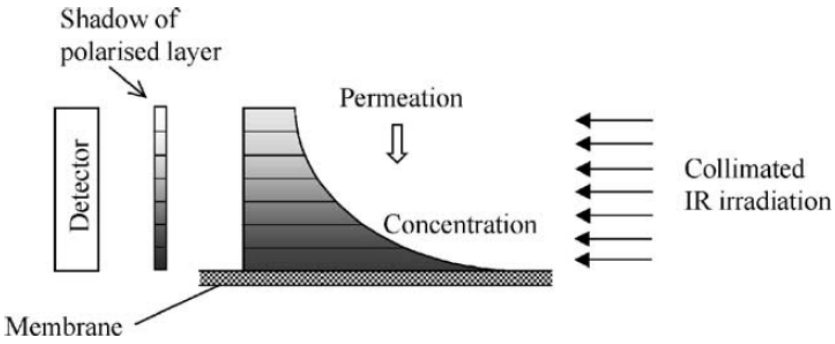


*Figure 10. The EDAM microscope (Chen et al., 2004).*

All the presented optical techniques in this section are an *in-situ* visual observation of the membrane surface, and they are restricted to flat membrane modules. Recently, the latest trend in research is to utilise optical sensor in an *ex-situ* mode. *Ex-situ* refers to taking side stream from the full-scale operation and employ optical sensors as early detection of fouling potential. RO *EX-situ* Scale Observation Detector (EXSOD) is the latest high-resolution optical sensor. It has been applied to full-scale RO membrane to observe the first stage crystals nucleation and propagation via optical microscope

associated with illumination to improve the recognition of transparent mineral scale (Uchymiak et al., 2009). In the research studies of EXSOD, low-pressure plate-and-frame RO cell was utilised, and the system was located at the tail of RO element. Moreover, it is mainly concentrating on brackish water RO pilot plant and gypsum scaling (Uchymiak et al., 2007).

Inventories have claimed development of a monitoring device comparable to EXSOD. The device can be operated with seawater at a high pressure similar to full-scale seawater desalination system. Besides, the device was successfully detecting mixed scale types (Hoek and Tanuwidjaja, 2011).

## 6.2 Non-optical techniques

The second group in level 1 monitoring device is non-optical methods. Those methods are more advanced considering they used modified signals to enhance the captured images to angstrom level using techniques as ultrasounds and small-angle neutron scattering (SANS). The blocking of the membrane pores can only be examined using SANS techniques through manipulating the intensity of neutron scattering to observe the pores of the membrane. Although SANS is a powerful technique, it is only limited to laboratory research because of high-priced and complicated operation (Chen et al., 2004).

Ultrasonic time-domain refractometry (UTDR) is monitoring device to observe the rate of the cake formation. It utilised sound waves to determine the fouling thickness on the membrane surface by transmitting the sound wave through the membrane module to fouling layer, and calculating the taken time for returning the reflected wave. The wave transmits through the membrane module without affecting or ruining the flow or fouling development. The results are reported in term of amplitude versus time. Moreover, linking different measurement techniques can be used to provide us with an accurate analysis. On-Line Feed Fouling Monitoring (FFM) can be combined to UTDR to provide a realistic prediction (Taheri et al., 2013).

Several investigations have been carried out by employing UTDR in full-scale flat-sheet RO membrane modules for *in-situ* real-time scale monitoring. Chai et al. (2007) monitored $CaSO_4$ scaling and the UTDR's signal response, and it was well corresponding to scaling formation and flux decline. Chong et al. (2007) observed the

silica scale formation in RO module and the resulting amplitude vs. time data was accurately compared to membrane fouling development. Sanderson et al. (2002) examined the $CaCO_3$ scaling phases starting from initiation phase to growth and removal. It was done by monitoring the echo of amplitude signal against time which mirrors the state of fouling layer. Moreover, the UTDR's output signal can clearly distinguish between different flows modes in membrane module whether it is a dead end or cross flow (Li et al., 2005). Figure 11 represent an ultrasonic transducer installed on the top of a membrane cell.

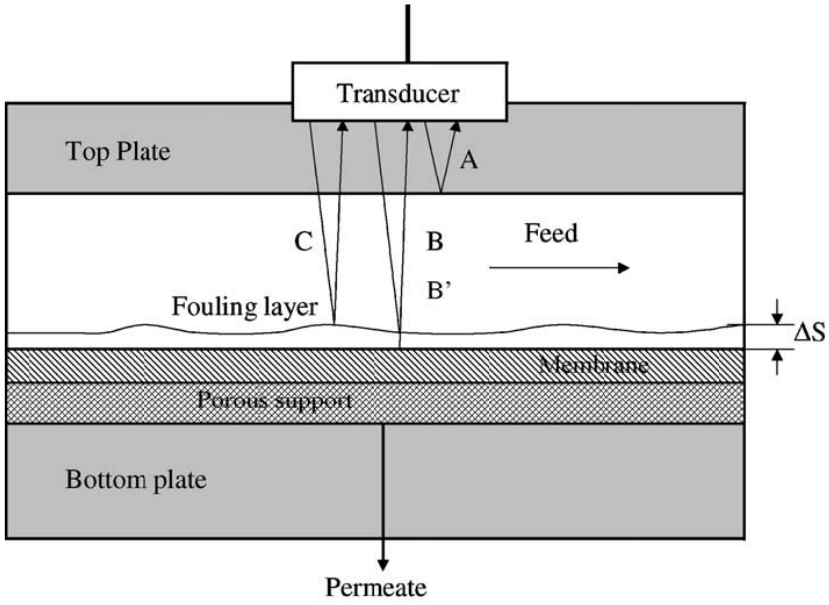


*Figure 11. The ultrasonic transducer installed on the top of a membrane cell (Sanderson et al., 2002).*

Electrical Impedance Spectroscopy (EIS) is a sensitive method for monitoring and observing the buildup of the layers and the thickness of fouling at early stages (Bannwarth et al., 2015;Sim et al., 2013). EIS operates by introducing various preidentified frequencies into RO module and monitor the voltage difference output change across the membrane (Kavanagh et al., 2009). Inventors have claimed that using a modified EIS method was successfully applied to real-time detection of membrane fouling degree and assists in water pretreatment strategies (Lee et al., 2011;Oh et al., 2013).

Moreover, Nuclear Magnetic Resonance (NMR) is a technique for examing the biofouling distribution, evolution, and the arrangement of molecules over the membrane surface (Çulfaz et al., 2011;Graf von der Schulenburg D. A. et al., 2008).

The NMR is based on the proton excitation by using a magnetic field, as the proton get excited, it changes its arrangement, and through radio frequency pulse it shows data about the surrounding system. NMR can achieve a high-resolution field scene. It is applicable for dynamic systems and not only gives information about the cake thickness and concentration profile, but it also provides data on the local concentration (Airey et al., 1998). Besides, NMR gives early detection of biofouling, evaluation of the impact of chemical addition (Fridjonsson et al., 2015), and the impact of the flow velocity on the biofilm formation and the arrangement of particles. (Valladares Linares R. et al., 2016). Moreover, time-domain low-field nuclear magnetic resonance (TD-NMR) is an alternative way to monitor the fouling progress and provides quantitative results. It can be utilised to measure the crystal content of fouling by sending and receiving magnetic pulses (DeJong and Hartel, 2016).

The vital difficulties are based on determining methods for on-line monitoring the membranes with a quick and accurate analysis of the data. Additionally, the suitable methods are applied to various applications including research investigations and full-scale processes. A summary list of level 1 optical and non-optical methods reviewed in this chapter and their suitable processes are documented in Table 7.

*Table 7. List of optical and non-optical monitoring techniques.*

| Category | Technique | Technology utilized | Measurement quality (Output resolution) | Suitable process* | Fouling characterisation/Distinguish |
|---|---|---|---|---|---|
| Optical | DOTM | Direct observation using camera and video recorder | >0.5 μm | MF, UF | Biofouling and Scaling/ does distinguish |
| | DMO | Direct observation using microscope | - | NF, MF | Biofouling and Scaling/ does distinguish |
| | Laser triangulometry | Application of the laser reflections | 5 μm | MF, UF | Fouling thickness/ does not distinguish |
| | Shadowgraph | The index of refraction | >200 μm above membrane | MF, UF, NF, RO | Fouling thickness/ does not distinguish |
| | EDAM | Electronic Diode Array Microscope | - | NF, MF | Fouling thickness / does not distinguish |
| Non-optical | SANS | Neutron scattering | 0.1 nm | MF, UF, NF, RO | Biofouling and Scaling/ does distinguish |
| | UTDR | Ultrasonic waves | 0.75 μm | MF, UF, NF, RO | Biofouling and Scaling/ does distinguish |
| | EIS | Electrical spectroscopy | - | MF, UF | Biofouling and Scaling/ does distinguish |
| | NMR | Proton excitation by using magnetic field | 10 μm | MF, UF | Biofouling and Scaling/ does distinguish |

*MF=microfiltration; UF=ultrafiltration; NF=nanofiltration; RO=reverse osmosis.

## 6.3 The suitable tool for prediction of membrane fouling

According to all the documented monitoring techniques, a particularly designed membrane module has been developed for most of the methods. On the other hand, few methods can be applied to the commercial modules study. One of the most widely used methods to overcome the difficulty in installing the monitoring device to the commercial module is to have a by-pass flow system *ex-situ* (similar to EXSOD reviewed in the optical techniques section). The membrane fouling simulator (MFS) is a functional tool to predict the fouling potential in a non-destructive observation mode by utilising a bypass module. The MFS unit consists of transparent membrane cells connected to a pressure transmitter sensor. The fouling buildup is determined via monitoring pressure difference, and the fouling nature is recognised by visual observation. The location of MFS installation point affects what is being monitored.

MFS is installed at the inlet sides to monitor the biofilm build up, and it is installed at the tail position for monitoring scaling. Moreover, it is commonly used for early warning of fouling and investigating the characterization of the fouling potential (Vrouwenvelder et al., 2006).

As reviewed previously, the biofilm/colloidal matter contribute by 60% as main fouling, and they mainly affect the first membrane module. Therefore, the MFS is usually installed on the inlet side of lead membrane module (see Figure 12). Moreover, feed spacers must be installed in MFS unit, considering it is clearly representative for biofouling studies in RO system and with the absence of feed spacer, different flow profile and different amount of biomass growth on the membrane surface will be obtained. Besides, it underestimates the effect of fluid flow channelling over the concentration polarisation (Vrouwenvelder et al., 2010a).

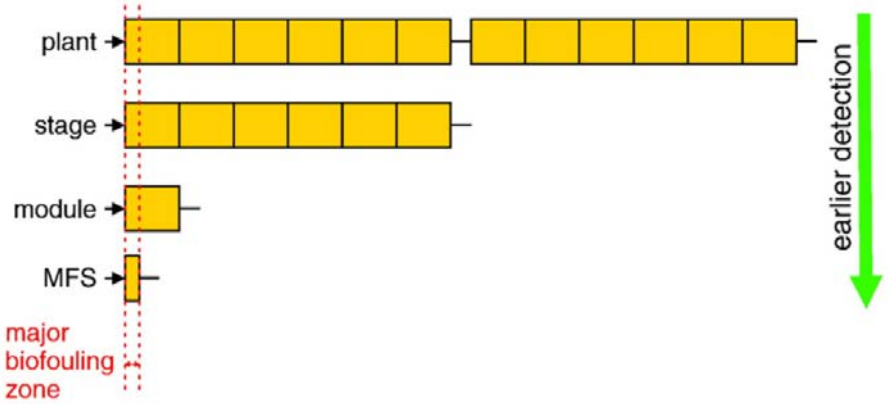


*Figure 12. MFS location as early fouling detector (Vrouwenvelder et al., 2010a).*

The industrial strategy guideline has recommended taking corrective action on total 15 % increase pressure drop in RO desalination stage. However, this approach is not practical since the pressure drop happens in the first membrane module and by monitoring the overall pressure drop of the whole train, the pressure drop in the lead module will be higher than 15% and other elements will be lower (Vrouwenvelder et al., 2009c). Accordingly, monitoring the pressure difference with a sensitive pressure transmitter (shown in Figure 13 A) is essential to measure the percentage increase in the feed spacer channel pressure drop (FCP). According to Figure 13 B, higher linear

velocity across membrane module increases the pressure drop range and increase the rate of biofilm development. Therefore, in the full-scale RO station, the linear velocity in lead modules is usually controlled between 0.07 to 0.2 m/s. However, as the MFS primary objective is an early warning, MFS is commonly operated at higher linear velocity (0.33 m/s) to have more precious pressure drop measurements (Vrouwenvelder et al., 2009a).

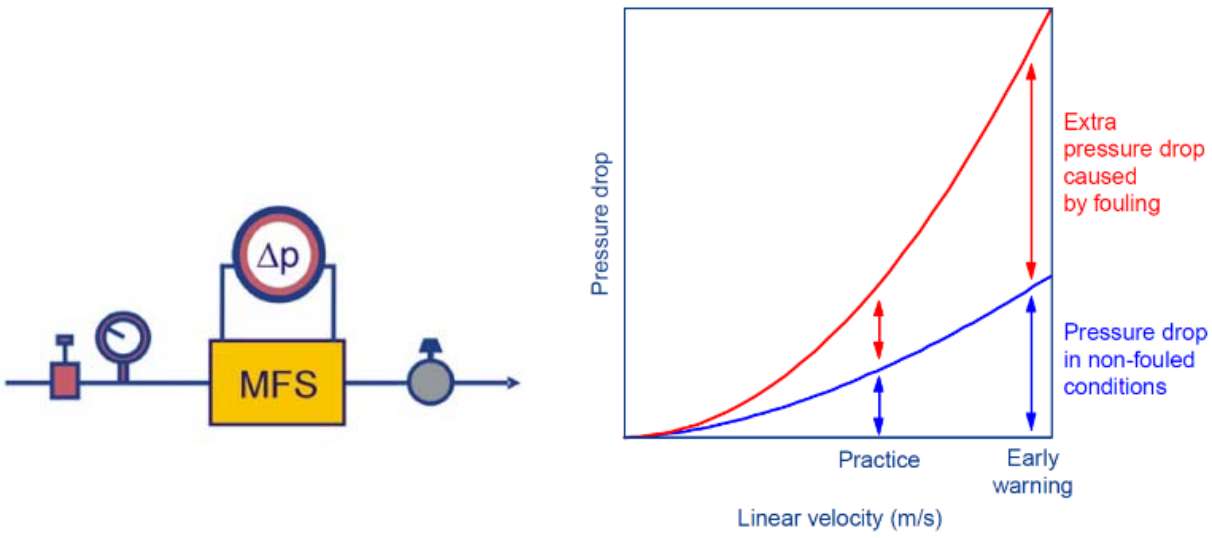


*(A)* *(B)*

*Figure 13. The MFS system setup for early biofouling warning monitoring (A) Pressure transmitter and flow controller configuration. (B) The relation between pressure drop and linear velocity and the impact of fouling on the pressure increase (Vrouwenvelder et al., 2010b).*

Scaling has been identified as leading fouling in brackish water reverse osmosis (BWRO), and mainly affect the last position of the membrane elements. Investigating the mineral scaling is done by monitoring the supersaturation level and the surface scale coverage percentage of concentrate line (Gu et al., 2013). Therefore, the MFS unit is usually installed at the end position (Vrouwenvelder et al., 2008).

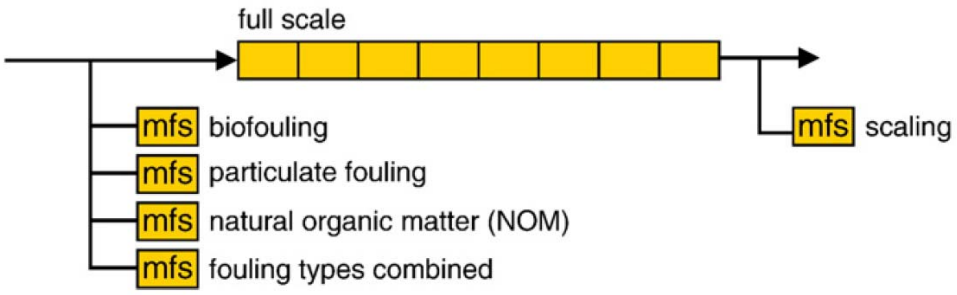


*Figure 14. The position of MFS units to monitor different fouling types (Vrouwenvelder et al., 2011).*

The potential annual saving in case of installing MFS units as an early fouling indicator are estimated to be about 10% of replacing the membrane modules, cleaning chemicals, and the labour required for cleaning and replacing the membrane modules, and 2 to 5% energy savings (Creber et al., 2010). Table 8 presents a study on the potential annual savings in two different cases: (1) Brackish water reverse osmosis (BWRO) with average capacity 1000 $m^3$/h, and (2) Sea water reverse osmosis (SWRO) with an average capacity 10,000 $m^3$/h.

*Table 8. The potential annual savings in BWRO and SWRO (Vrouwenvelder et al., 2011).*

| | Energy (kWh/$m^3$) | Membranes (€ /$m^3$) | Chemicals (€ /$m^3$) | Average capacity ($m^3$ /h) | Potential annual savings (€) |
|---|---|---|---|---|---|
| BWRO | 0.5–1.0 | 0.0133–0.0266 | 0.0285 | 1000 | 66 500 |
| SWRO | 3.5–4.2 | 0.0475–0.095 | 0.0475-0.057 | 10000 | 1 900 000 |

# EXPERIMENTAL PART

## 7. Research Objectives

The previous chapters have shown the principles of RO membrane filtration and its role in desalination, the adverse effects of fouling and biofouling on the hydrodynamic performance of RO membrane, and the role of antiscalants and biocide in controlling the scaling and biofouling respectively. Additionally, a review of past and current real-time monitoring techniques for membrane surface monitoring in both *in-situ* and *ex-situ* systems. Due to the wide variety of water sources (e.g. Brackish and sea water) in RO desalination processes, the membrane research major objective is to develop complementary approaches to control fouling. The approach is based on two sides: (1) development of new chemicals to control fouling and biofouling. (2) A useful tool for quantitative monitoring of fouling and evaluation of cleaning steps, in order to keep the produced water quality over long operating periods. The main research objectives of the thesis are presented as following:

*Objective 1: To evaluate antiscalant on a single stage RO membrane (Chapter 8)*
Three antiscalants were assessed in this study to investigate the promotion of the RO desalination recovery percentage despite the presence of higher concentrations of the scale-forming components as silica, calcium carbonate, and calcium sulphate. Two crossflow RO membrane units were utilised in the test, and the assessment was based on the permeate flux decline and the normalised pressure drop. Additionally, at the end of each scaling run, the membrane coupons were analysed and quantified by optical imaging scanning electron microscopy (SEM) equipped with energy dispersive X-ray spectrometry analysis (EDS), powder X-ray diffraction (XRD), and X-ray fluorescence spectrometry (XRF) to provide quantitative and quantified analysis.

*Objective 2: To investigate biocides to control the accumulation of biofilm on a single stage RO membrane (Chapter 9)*
Two biocides were evaluated, Biocide1 was used as a reference to assess the performance of slowly released biocide (Biocide2). The study was focusing on simulating fouling accumulation in the cross-flow RO filtration units by utilising fresh bacterial inoculum and nutrients and exposing the system to biocide dose for cleaning. Accordingly, the permeate flux and normalised pressure (NP) were continuously

monitored to verify the ability of biocide to control biofouling on RO membrane. Further, at the end of the test, the membrane coupons were examined to determine the effect of biocide on the biofilm accumulation.

*Objective 3: To develop a membrane fouling simulator prototype device (Chapter 10)*
The research objectives were: (1) Verification of equipment accuracy/sharpness for detecting fouling of the spacer grids surface and membrane surface. (2) Benchmarking results to the standard MFS system. (3) The device response to chemical addition (Biocide and Antiscalants). (4) The device capability to classify and distinguish between organic and inorganic fouling type in combined fouling cases.

## 8. Evaluation of antiscalants on a single stage RO membrane

This section summarises the experimental work to investigate and rank the performance efficiency of three antiscalants by comparing to a blank reference run and evaluating the normalised permeate flux decline associated with transmembrane pressure (TMP). At the end of each scaling run, the membrane coupons were analysed and quantified by optical imaging scanning electron microscopy (SEM) equipped with energy dispersive X-ray spectrometry analysis (EDS), powder X-ray diffraction (XRD), and X-ray fluorescence spectrometry (XRF) to provide quantitative and quantified analysis.

### 8.1 Overview

The acceptable recovery percentage of brackish water reverse osmosis (BWRO) is between 65-85%, and the remaining percentage RO rejects were considered as wastewater. Commonly, the BWRO reject stream is discharged without further water recovery. The reject stream discharge is considered as energy loss because of initial pumping to reach the operating pressure, and chemical losses since the chemical involved in the process are not recovered. Moreover, the RO reject has high salt contents, so it must be suitably managed to avoid environmental pollution. Still, high recovery leads to more membrane fouling challenges and reduction in membrane hydraulic performance and ultimately reduce the membrane life (M. Gamal Khedr, 2012). The present work investigates the promotion of the RO desalination efficiency by the evaluation of a high-tolerance antiscalant which enables safe operation of RO at high recoveries despite the presence of high concentrations of the scale-forming components as silica, calcium carbonate, and calcium sulphate. Figure 15 illustrates the recovery percentages when primary RO desalination reject stream is treated by secondary RO unit. The RO reject is pressurised to optimum operating pressure before introducing to secondary RO unit.

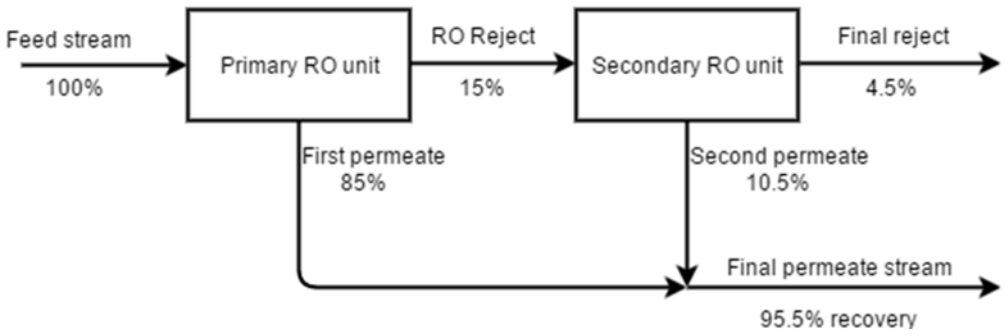


*Figure 15. Treatment of RO rejects stream by secondary RO unit.*

## 8.2 Materials and methods

The study was carried out on a model reject brine from a reverse osmosis station (mimic reject water characteristics from an industrial brackish water RO). The model solution was prepared using reagent grade mineral salts of $NaHCO_3$, $Na_2SO_4$, $Na_2SiO_3 \cdot 5H_2O$, $CaCl_2 \cdot 2H_2O$ and $MgCl_2 \cdot 6H_2O$. A study of the model solution was done to determine the scale forming potential. The scale potential of $CaCO_3$, $CaSO_4$, and $SiO_2$ was quantified by the supersaturation index (SI) as Equation (1):

$$SI_x = \frac{IAP}{K_{sp,x}} \quad (1)$$

Where IAP is the ion activity product and $K_{sp,x}$ is the solubility product. SI value greater than unity indicates that the mineral salt solubility limit is exceeded and this is a sign for scaling possibility. The SI was calculated using the hyd-RO-dose® software (French creek software, 2017). Moreover, PHREEQC software (Parkhurst and Appelo, 2013) was used to determine Calcium Carbonate Precipitation Potential (CCPP) which is the amount of $CaCO_3$ that would precipitate to achieve calcium carbonate equilibrium. Furthermore, an initial test was performed with the original composition of model reject brine, resulting in instant membrane blockage, showing the model solution is strongly concentrated brine. As the ions concentration at the boundary layer of membrane surface is typically 12 to 40 % higher than the bulk water (Ferguson et al., 2011), the model solution compositions were decreased by 40 % to reduce the ion concentrations level in the boundary layer at the membrane surface and minimise the concentration polarisation. The modified composition of the ions concentrations, conductivity, and the calculated saturation indices and CCPP of the model solution are listed in Table 9. The saturation indices express that the model solution exceeded the solubility limit with respect to $CaCO_3$, $CaSO_4$, and $SiO_2$.

Membrane coupons were cut from a commercial RO membrane (DOW FILMTEC™ BW30-4040 membrane, polyamide thin-film composite membrane with 99.5 % salt rejection). The list of antiscalants utilised in the test and their dry solid content percentage are presented in Table 10.

*Table 9. The composition of the model solution.*

| Ions | | Concentration, mg/l |
|---|---|---|
| Sodium | $Na^+$ | 2058.6 |
| Bicarbonate | $HCO_3^-$ | 533.2 |
| Sulphate | $SO_4^{2-}$ | 3666.8 |
| Silica | $SiO_2$ | 134.1 |
| Calcium | $Ca^{2+}$ | 1200 |
| Magnesium | $Mg^{2+}$ | 300 |
| Chlorides | $Cl^-$ | 2998.3 |
| Conductivity | | 27.1 (mS/cm) |
| Calculated T.D.S. | | 16268 (mg/L) |
| Saturation Levels (dimensionless) | | |
| $CaCO_3$ (calcite) | | 32 |
| $CaSO_4 \cdot 2H_2O$ (gypsum) | | 3.3 |
| $SiO_2$ (silica) | | 1.2 |
| CCPP ($gCaCO_3$/L water) | | 21.8 |

*Table 10. List of Antiscalants.*

| Antiscalants | Dry solid, % |
|---|---|
| AS1 | 40.3 |
| AS2 | 32.1 |
| AS3 | 37.0 |

Membrane scaling experiments were conducting in a membrane bench unit, where both concentrate and permeate recirculated into feed tank. The unit consists of two lines; one line (Figure 16) consists of four test cells (Sterlitech module CF042 Cell), each cell with active membrane surface area of 42 $cm^2$. Moreover, the other line consists of A5 one plate-and-frame membrane cell with active membrane surface 218 $cm^2$ (Figure 17 shows the details of the single A5 cell). The feed reservoir was an electrically stirred (Agitators 509, Grundfos Alldos Electric agitator) polyethylene tank (Dosing tank 502,

Grundfos Alldos). A cooling water recirculator (Lauda Alpha, Lauda-Brinkmann,) served to maintain constant reservoir temperature. A pH meter to constantly monitor the pH value in the tank. A positive displacement pump (Model G-13, INC Hydra-cell industrial pump, Wanner Engineering) was used to deliver constant feed solution to membrane modules. The pressure difference was monitored using differential pressure transmitter (DPharp EJX 910A pressure transmitter, Yokogawa). A digital flow meter (ADMAG AXF025H integral flows meter, Yokogawa) connected to a monitoring platform, provided continuous monitoring of permeate flow rate. Feed and permeate conductivities were monitored with conductivity meters (Hach Lange 3400 SC digital conductivity).

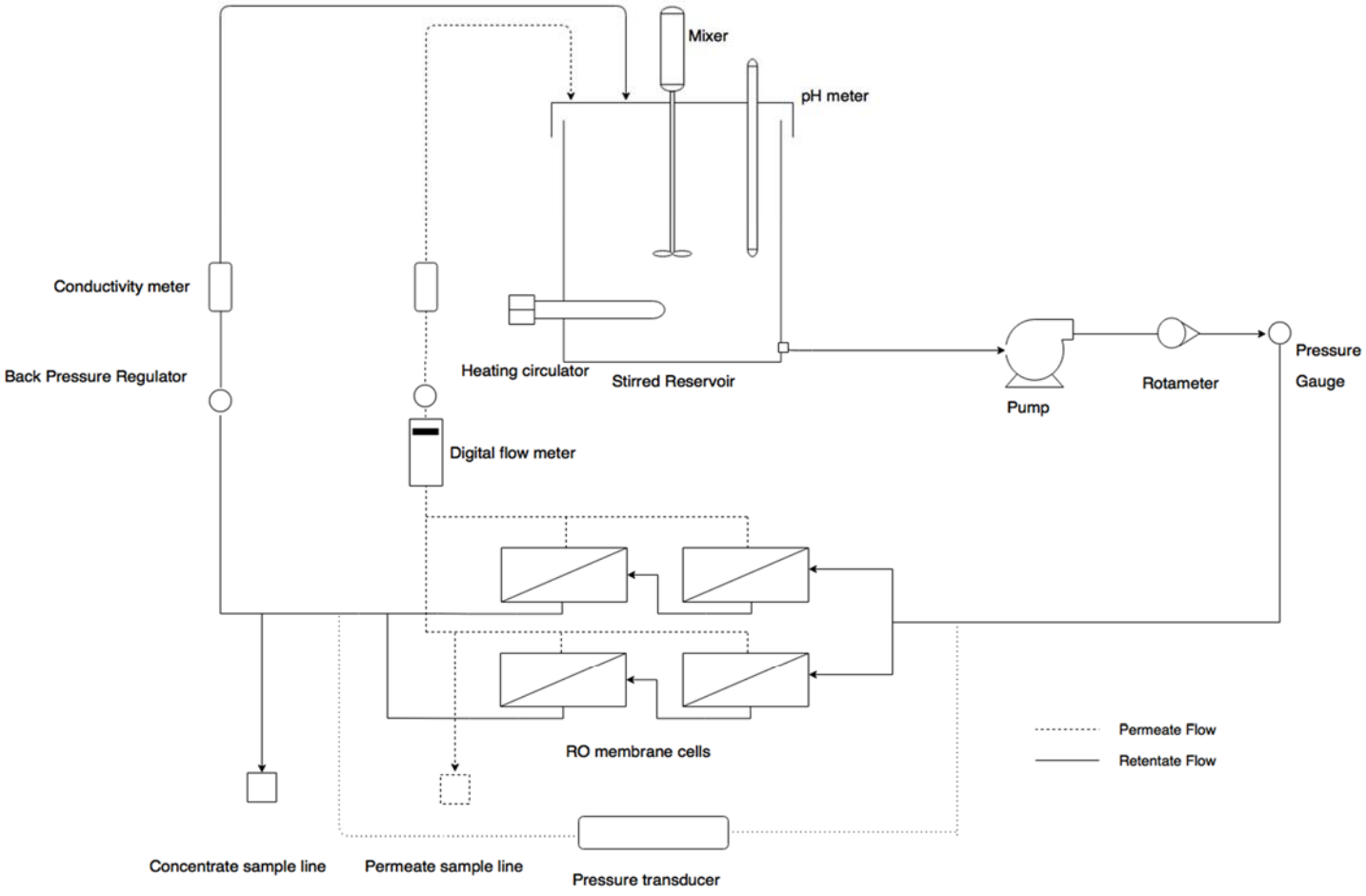


*Figure 16. RO membrane diagnostic system.*

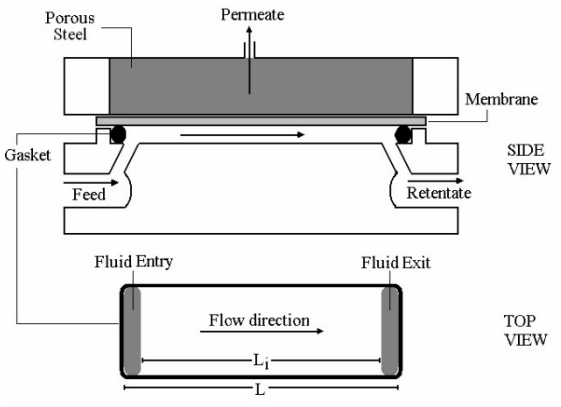


*Figure 17. The details of a single A5 membrane cell.*

## 8.3 Scaling experiment

As shown in Table 9, the values of saturation index indicate that the model solution is supersaturated with respect to calcite, gypsum and silica. The scaling experiments were carried by circulating the feed solution through membrane modules for a five days period in a total recycle mode (i.e., permeate and concentrate lines were continuously recirculated to the feed tank). Before starting each experiment, membrane coupons were soaked in deionised water (DI) for one day then placed inside the membrane cells without using membrane spacer. This was followed by filling the feed tank with 37 litres DI water from WaterMan RO unit (the total volume is 40 litres after adding the model stock solutions). The DI water was recirculated through the system at a flow rate of 48 L/h followed by the addition of the anion quantity of the model solution (sodium sulphate and sodium hydrogen carbonate) as a stock solution for 22 hours to establish a baseline. The remaining of the model solution was added, starting with the Sodium metasilicate pentahydrate then rapidly the antiscalant dose followed by the cation stock solution (calcium chloride dihydrate and magnesium chloride hexahydrate) to initiate the membrane scaling experiment. Because of the $CO_2$ degassing to the atmosphere and the mineral crystallisation, the pH was shifting up and downward. Accordingly, the pH value of the solution was maintained at value eight by adjusting with NaOH and HCl (Hydrochloric was preferred over sulphuric acid due to the potential of sulphuric acid to form sulphate scales). The tank temperature was kept between 20 to 25 ºC. Moreover, the operating pressure was controlled manually at 10 bars.

The monitored permeate flow was normalised to the baseline to compare the antiscalants performance to blank run (No antiscalant dose). The normalised permeate flow (NPF) calculation followed Equation (2) (Dow chemicals, 2011). The Normalised

calculated permeate was reported as flux and expressed in litres of water per membrane area $m^2$ per hour (LMH).

$$NPF = Permeate\ flow\ \left(\frac{L}{h}\right) \times \left(\frac{Baseline\ aNDP}{aNDP}\right) \times \left(\frac{Baseline\ TCF}{TCF}\right) \quad (2)$$

Where aNDP (Average net driving force) was calculated using Equation (3). The Baseline aNDP was calculated from the first 22 hours experimental run (Baseline flux).

$$\begin{aligned} aNDP(Average\ Net\ Driving\ Force) \\ = \left(\left(\frac{Feed\ pressure\ (bar) + Concentrate\ pressure\ (bar)}{2}\right)\right. \\ \left. - \left(\frac{Feed\ TDS + Concentrate\ TDS}{200}\right)\right) \\ - Permerate\ pressure\ (bar) \end{aligned} \quad (3)$$

Where feed, concentrate, and permeate pressures were recorded during the test runs, and concentrate TDS was calculated by multiplying the feed TDS by a correction factor using Equation (4).

$$Concentrate\ TDS = Feed\ TDS \times \frac{Feed\ Flow\ \left(\frac{L}{h}\right)}{Concentrate\ Flow\ \left(\frac{L}{h}\right)} \quad (4)$$

The TCF (Temperature correction factor) was calculated using Equation (5), and similar to Baseline aNDP, the Baseline TCP was calculated during the first 22 hours of experimental run.

$$\begin{aligned} TCF(Temperature\ correction\ factor) \\ = EXP\left\{2640 \times \left(\left(\frac{1}{298}\right) - \left(\frac{1}{273 + Feed\ Temp\ C}\right)\right)\right\} \end{aligned} \quad (5)$$

## 8.4 Results and discussion

The experimental work started with a reference run to monitor the permeate flux decline without antiscalant dose. Next, the same experimental work was done with an antiscalant dose of 2, 10, and 20 mg/L (based on dry solid content) to examine the

degree of effectiveness retardation of homogeneous crystallisation and slow growth of scale crystals. Figure 18 represents the comparison of the three antiscalants performance at 2 mg/L dose. After the addition of cation stock solution in AS3 run, the permeate flux increased because the operating pressure failed to be controlled at 10 bars. Overall, the system was not operated successfully at antiscalant doses below 10 mg/L, and the salts precipitated in the feed, permeate and concentrate streams. Moreover, the pump could not provide a constant feed flow rate. Figure 19 A shows the concentrate conductivity probe and its chamber (Figure 19 B) situation using 2 mg/L antiscalant dose. Clearly, the dose was not sufficient for inhibiting the sparingly soluble salts from precipitation. 10 mg/L dose was the next proposed treatment based on the high calcite saturation index of the model solution and comparing related publication and several inhibitors dosage profiles (Ferguson et al., 2011).

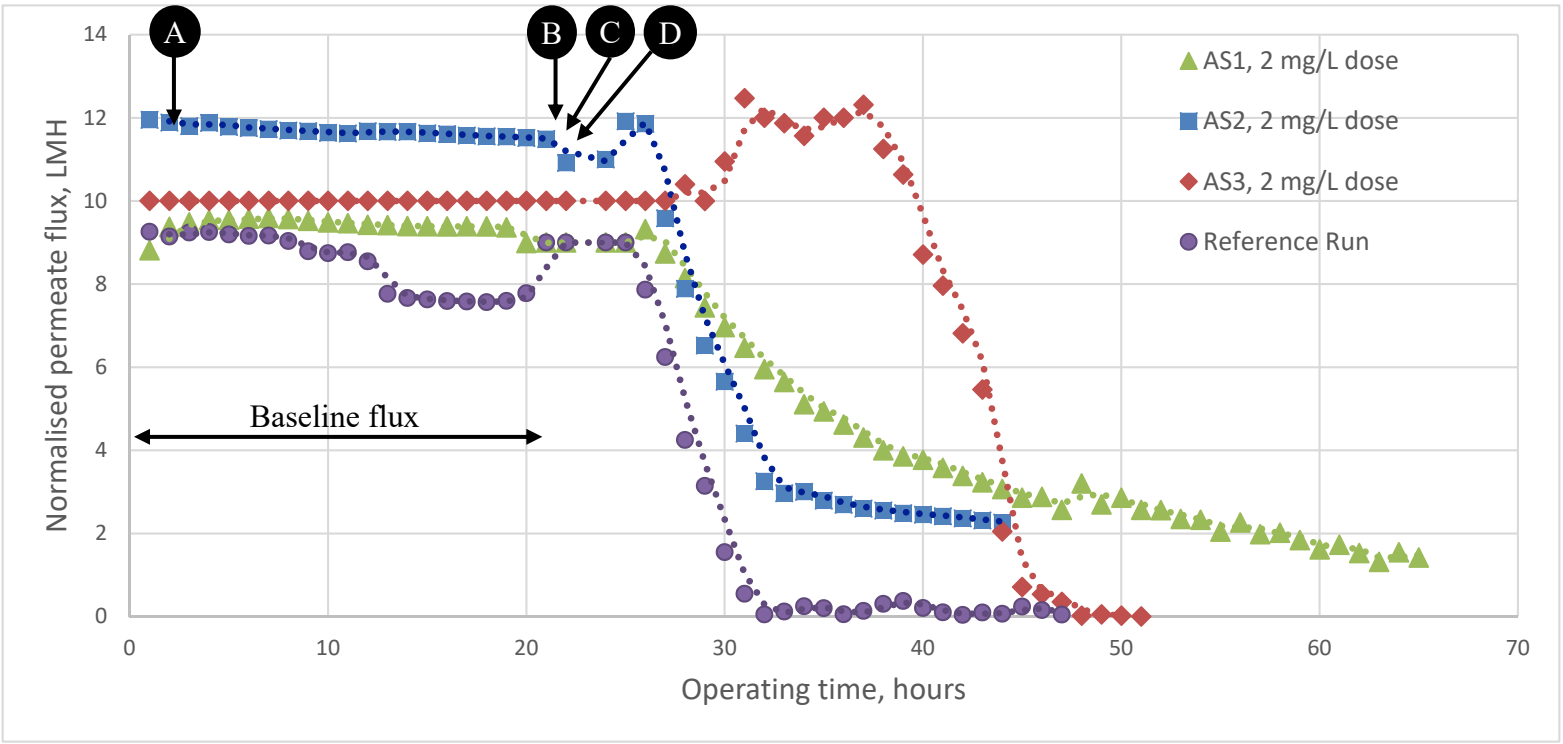


*Figure 18. Normalised permeate flux decline for a 2 mg/L antiscalant dose. Point(A)Anion stock solution addition, Point(B)Antiscalant addition, Point(C)$Na_2SiO_3.5H_2O$ addition. Point (D) Cation stock solution addition.*

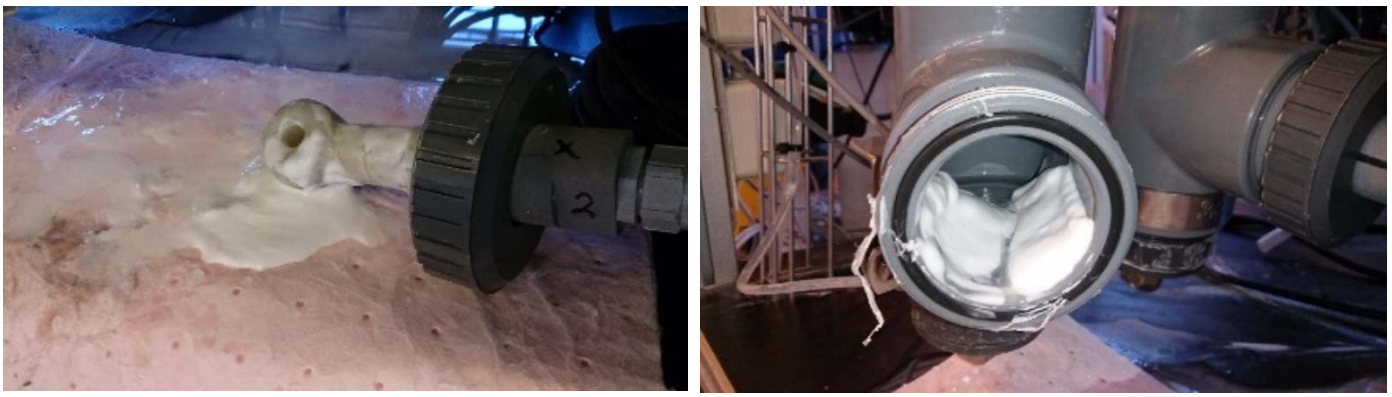

*(A)* *(B)*

*Figure 19. The precipitated salts in the system during the 2 mg/L dose of antiscalant. (A) Concentrate conductivity probe. (B) Its chamber.*

The 10 mg/L experimental work presented a clear difference in term of permeate decline duration (Figure 20). Moreover, the higher dose was able to delay the crystallisation growth of supersaturated solutions (i.e. the three inhibitors act as strong threshold inhibition). AS3 has shown the highest baseline, and its relative permeate flux took more than 43 hours to decline to 2 LMH, and AS2 took 55 hours. Additionally, by comparing the fluxes at 35 operating hours, AS2 recorded the highest flux 6 LMH.

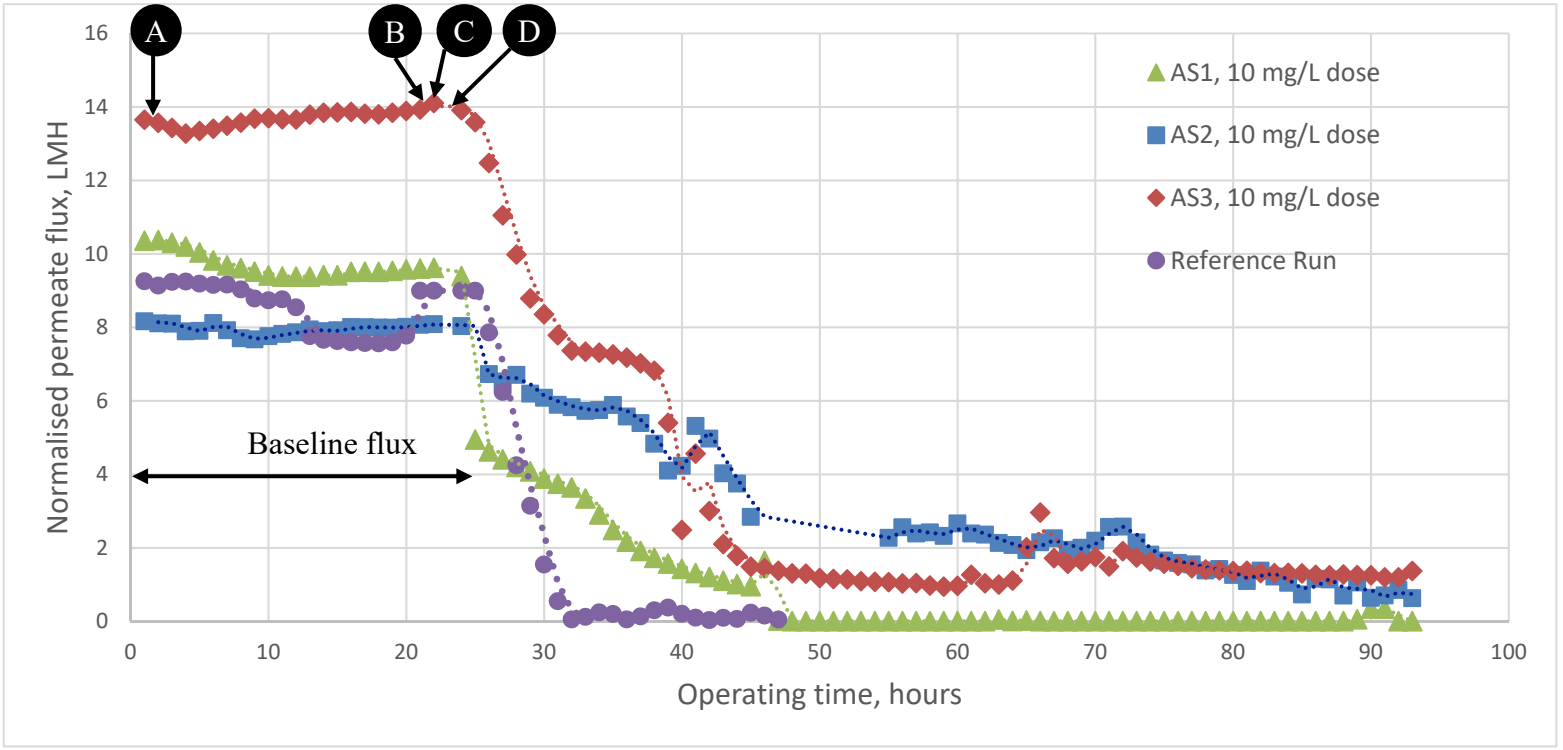


*Figure 20. Normalized permeate flux decline for a 10 mg/L antiscalant dose. Point(A)Anion stock solution addition, Point(B)Antiscalant addition, Point(C)$Na_2SiO_3.5H_2O$ addition. Point (D)Cation stock solution addition.*

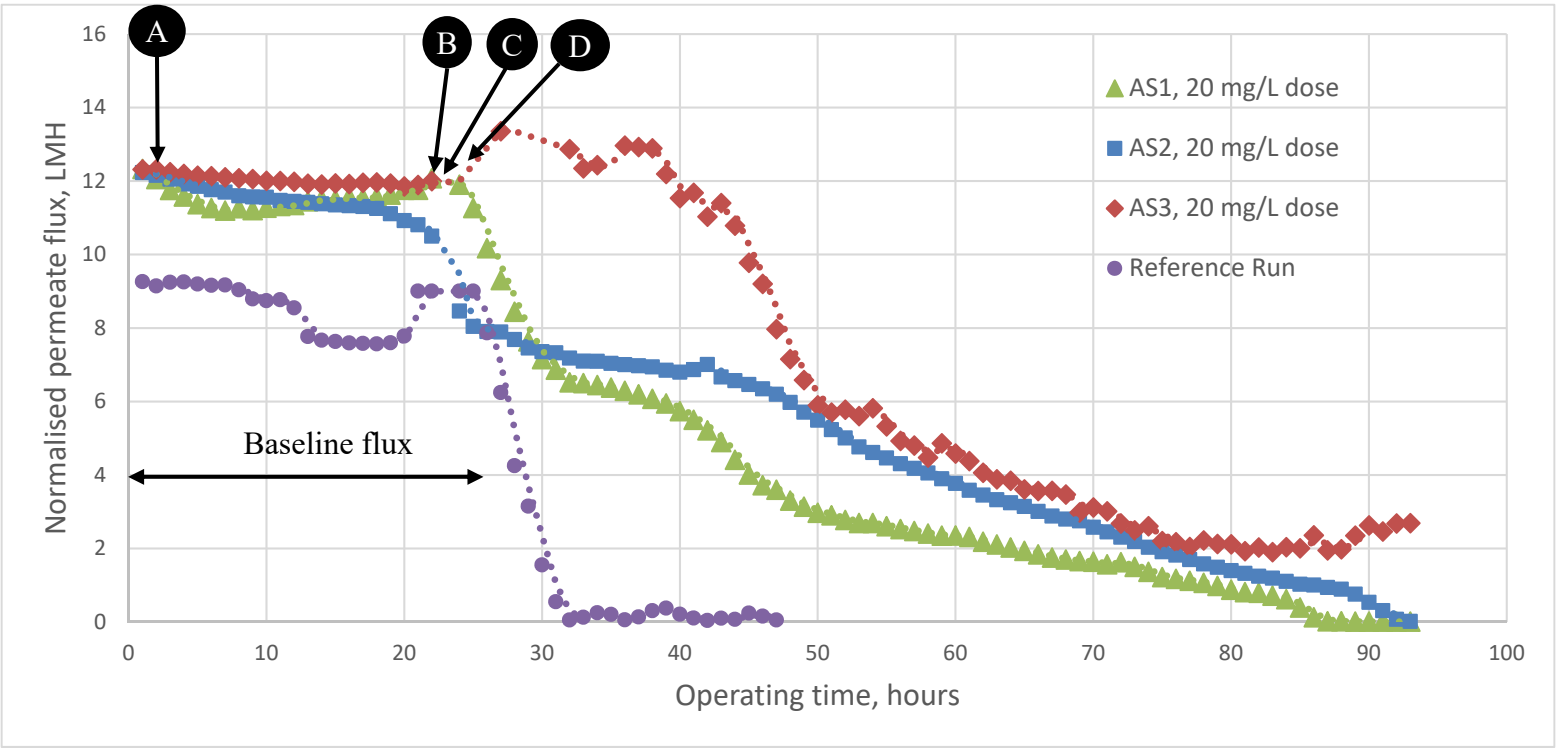


*Figure 21. Normalised permeate flux decline for 90 hours operating time with 20 mg/l antiscalant dose. Point (A) Anion stock solution addition, Point (B) Antiscalant addition, Point(C) $Na_2SiO_3.5H_2O$ addition. Point (D) Cation stock solution addition.*

Above the 10 mg/L (20 mg/L dose) more permeate was successfully recovered, the system was stably operated, and there were permeate flows in case of AS2 and AS3 after 90 hours operating time. Figure 21 illustrate the permeate decline profiles over 90 hours operating time. The AS3 case had the biggest impact on the delaying the decline rate of normalised permeate flux decline to reach 2 LMH. In other words, the higher dose has shown much extended time compared to a lower dose.

A summary of the normalised permeate flux decline period extent (operating time) until it reached 2 LMH (A selected point for assessment) is presented in Table 11. The duration of the normalised permeate flux to reach 2 LMH in the reference run was about 30 hours. On the other hand, AS1 (2 mg/L) took the longest duration, about 53 hours. Furthermore, the AS2 (2 mg/L) experimental run had shown a high baseline compared to other antiscalants, and after 39 hours operation time, it recorded the least flux. A similar baseline flux should be considred in order to compare the different run, it should be mentioned AS2 run at 2 mg/L had a different baseline flux. Therefore, a correction factor was implemented in calculations based on the difference in baseline flux (i.e. relative approach), the same concept was applied to AS3 at 10 mg/L dose. Based on the

three different doses, it seems AS1 is the less efficient antiscalant in terms of delaying the normalised permeate flux decline, and retardation of homogeneous crystallisation. However, it is not sufficient to build the comparison on the decline permeate flux. A more comprehensive picture will be available after including the membrane analysis and identifying the different mineral scale deposits on the membrane surface.

*Table 11. 2 LMH duration (in hours) comparison.*

| Antiscalant / Dose | AS1 | AS2 | AS3 |
|---|---|---|---|
| 2 mg/L | 53 | 39* | 44 |
| 10 mg/L | 35 | 55 | 43* |
| 20 mg/L | 57 | 71 | 73 |

*Relative approach values.

It was observed in all the test runs that after the addition of the cation portion and initiating the membrane scaling experiment, the scaling occurs instantaneously meaning that the induction period for membrane scaling is practically nonexistent. The induction time is defined as the duration between the onset of supersaturating and the formation of critical nuclei. This time primarily depends on the saturation indices with respect to gypsum, calcite, and silica, also the Calcium Carbonate Precipitation Potential (CCPP) value. Therefore, an alternative method was tested by gradual addition of cation portion of the model solution (In seven hours period) to examine the effect of nonexisting induction time on the permeate flux, and the permeate flux decline against the increase of saturation indices and CCPP. Two different cases were evaluated (AS3 at 10 mg/L and AS2 at 20 mg/L dose) to observe the effect of antiscalant. Based on the obtained results (presented in Figure 22 and Figure 23), the normalised permeate flux versus the saturation index declined linearly in both cases until the slope of normalised permeate flux around SI of 20 for calcite and 2 for gypsum started to decrease, this indicates that high saturation indices have a direct impact on the permeate flux decline. The reduction in the permeate flux was about 40 percent independent of the antiscalant nature and dosage quantity. Experimental work shown in Figure 22 and Figure 23 was done in A5 membrane cell, and in CF042 Cell respectively. Therefore,

the pressure drop reading range was different. However, the pressure drop increases by 15 percent after the addition of the entire cation stock solution in both cells.

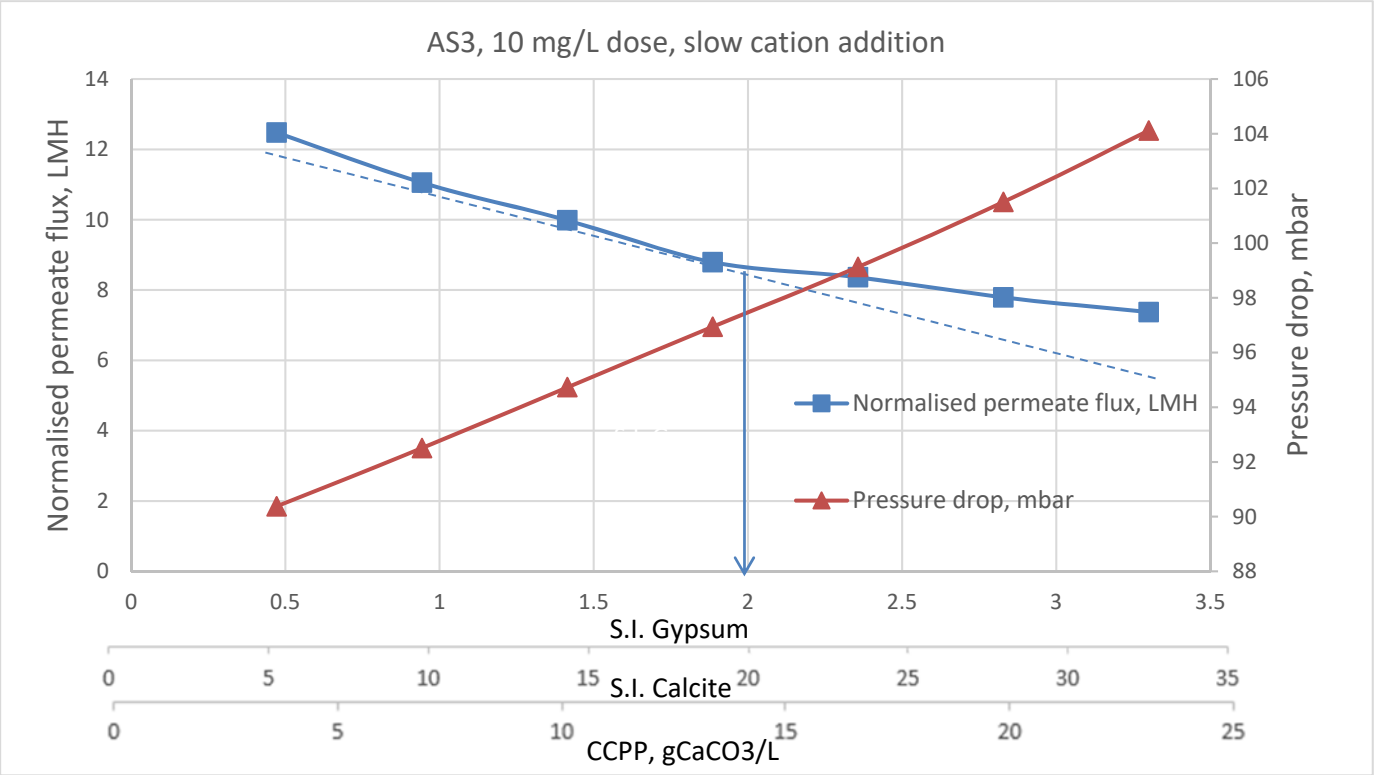


*Figure 22. The effect of saturation indices and CCPP on the permeate flux and pressure drop with AS3 10 mg/L dose.*

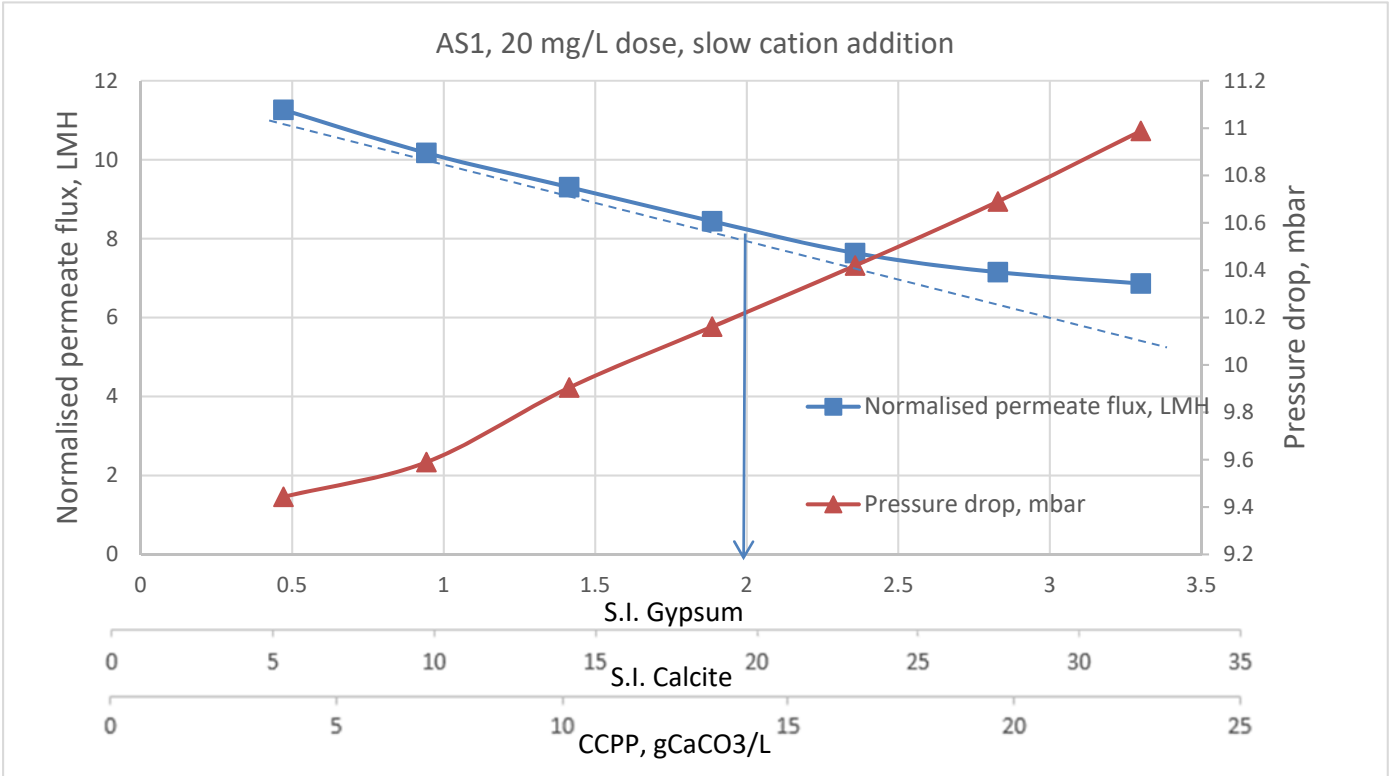


*Figure 23. The effect of saturation indices and CCPP on the permeate flux and pressure drop with AS1 20 mg/L dose.*

The pressure drop across the membrane module was used for evaluating the performance and gives an indication about the propagation of both bulk and surface crystallisation. A variation was observed when pressure drop starts to increase after adding the antiscalant dosage. In other words, theoretically, certain antiscalants were able to delay the propagation of mineral crystals on the membrane surface and to adsorb on crystals particles and impart a high anionic charge, tending to retain the crystals separated. Figure 24, Figure 25, and Figure 26 illustrates the variation in the pressure difference response with different antiscalants. Each antiscalant case has taken different duration for the TMP to increase 0.3 bars. AS1 has taken 12 hours, and AS3 has taken 17 hours. AS2 obtained the longest duration by 21 hours (i.e. AS2 has the most efficient impact in term of delaying the TMP rise, reflecting it has anionic dispersant).

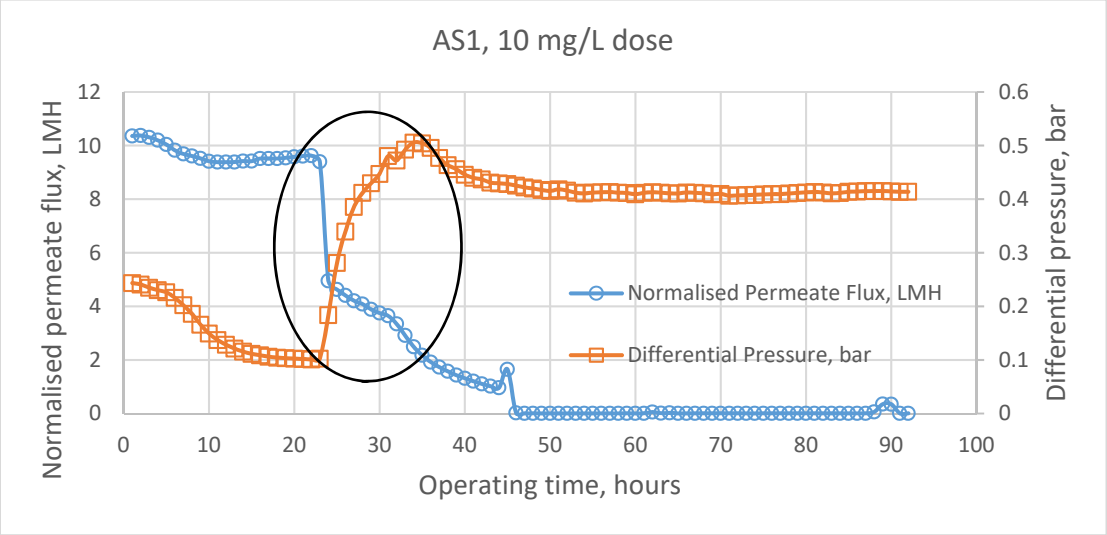


*Figure 24. Pressure difference profile at AS1 10 mg/L dose.*

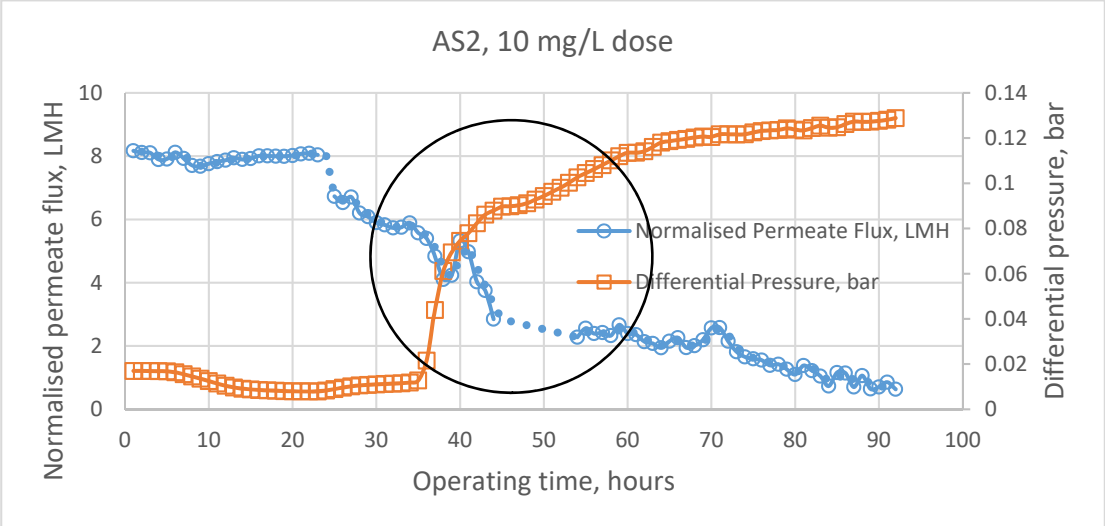


*Figure 25. Pressure difference profile at AS2 10 mg/L dose.*

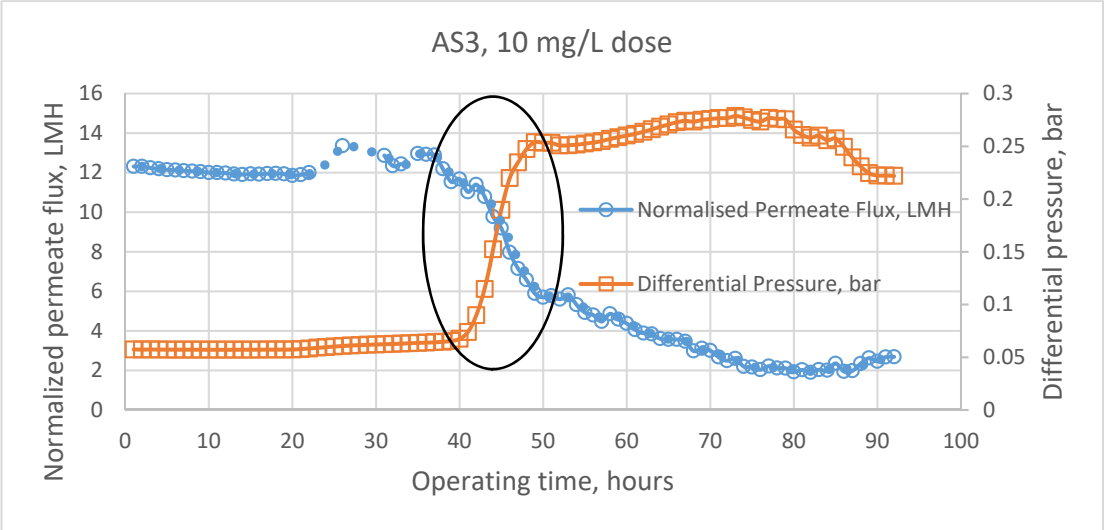


*Figure 26. Pressure difference profile at AS3 10 mg/L dose.*

The experimental results have proven that the increase in the antiscalant dosage has a positive influence on the permeate flux. The below Figure 27, Figure 28, and Figure 29) illustrate each antiscalant type separately.

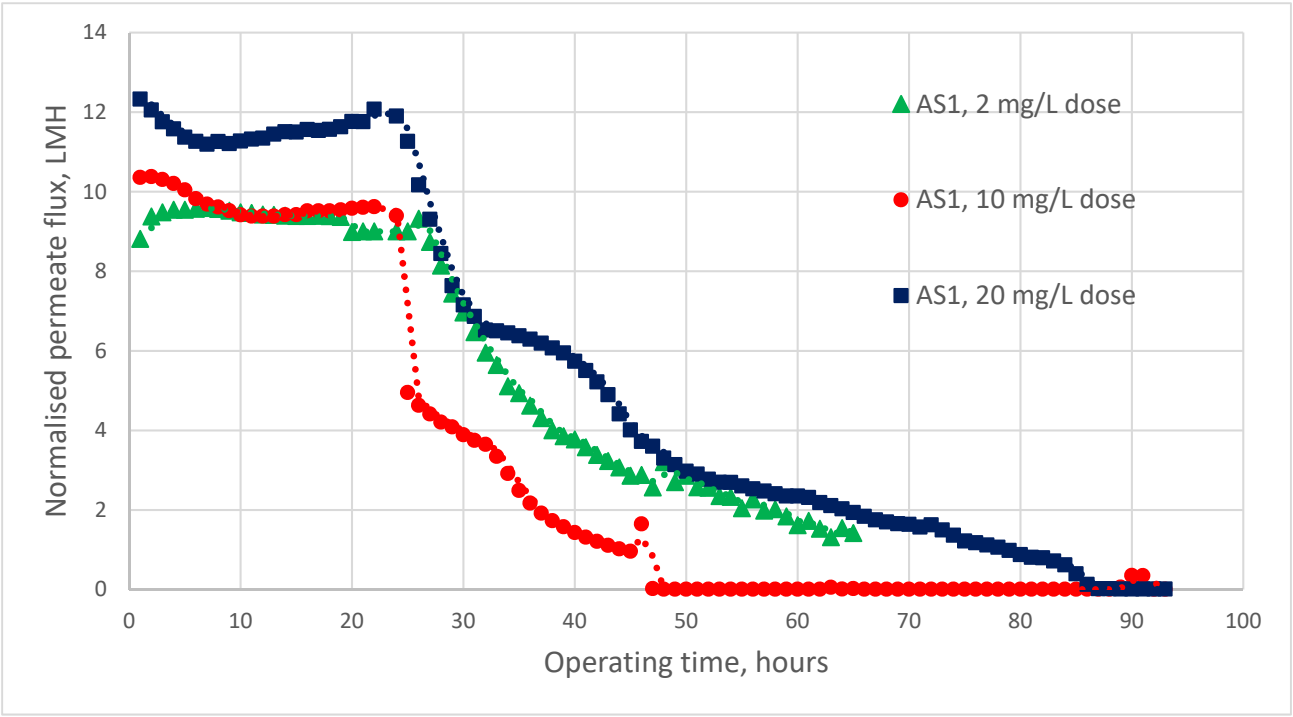


*Figure 27. Normalised permeate flux at different AS1 doses.*

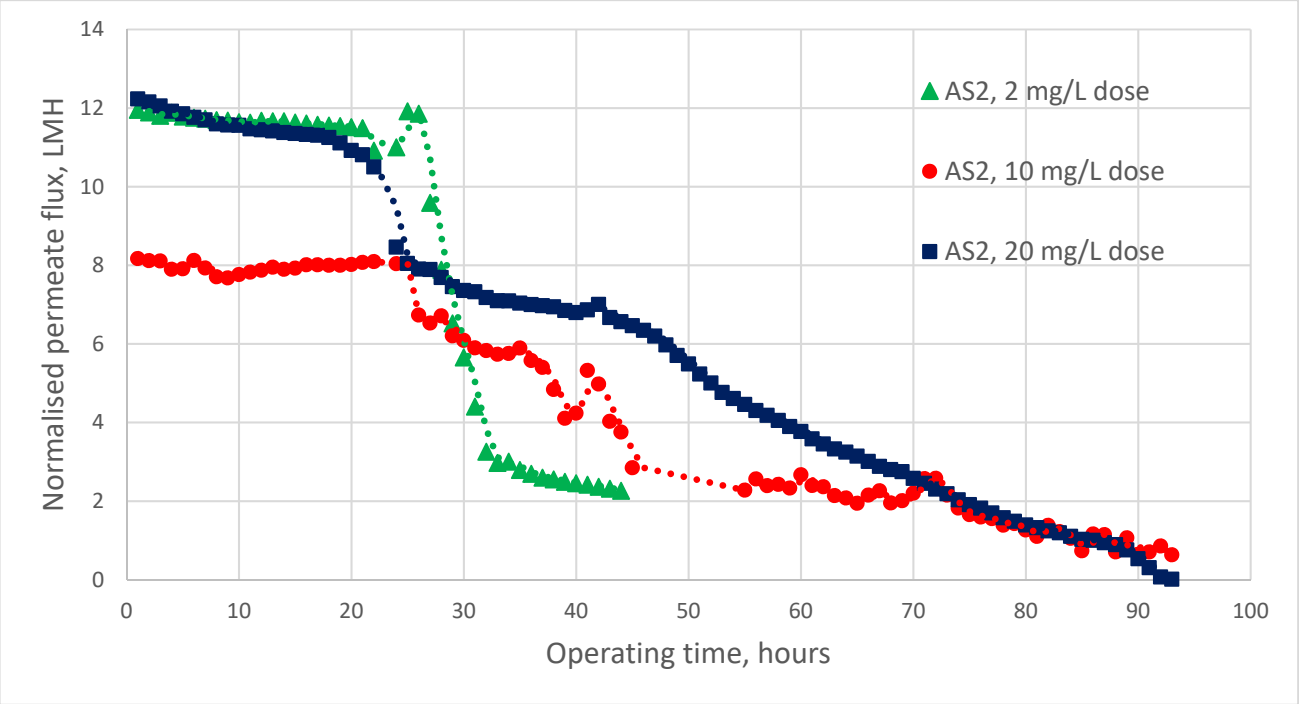


*Figure 28. Normalised permeate flux at various AS2 doses.*

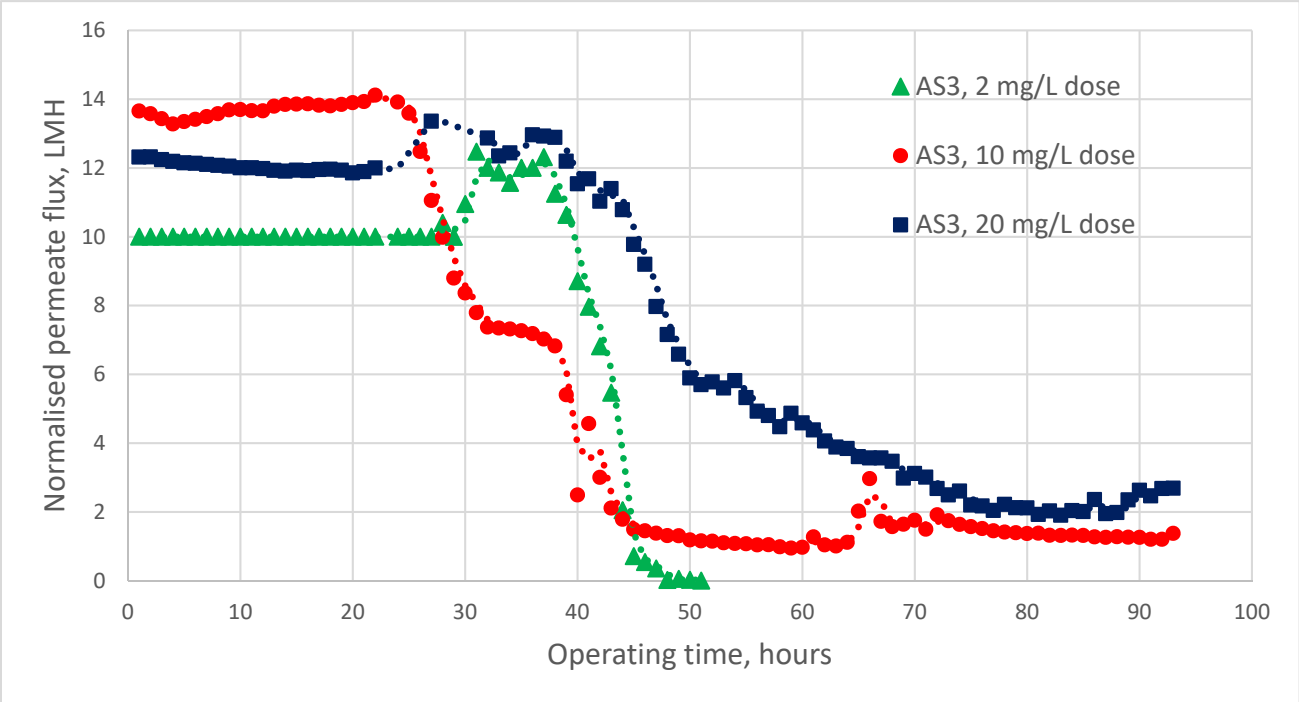


*Figure 29. Normalised permeate flux at different AS3 doses.*

The salt rejection curves were not reported during the experimental study since the induction period for membrane scaling was practically nonexistent. Consequently, all the salt rejection curves follow the same trend (Figure 30), thus it was not adopted as evaluation criteria. The main outcomes are: (1) AS1 was the least efficient antiscalant in terms of declination of normalised permeate flux. (2) Both AS2 and AS3 were showing similar related results in term of declination of normalised permeate flux. On the other hand, AS2 has the most effective impact in terms of delaying the TMP rise.

The next section will present the membrane analysis, and the identity of different mineral scale to obtain a comprehensive evaluation.

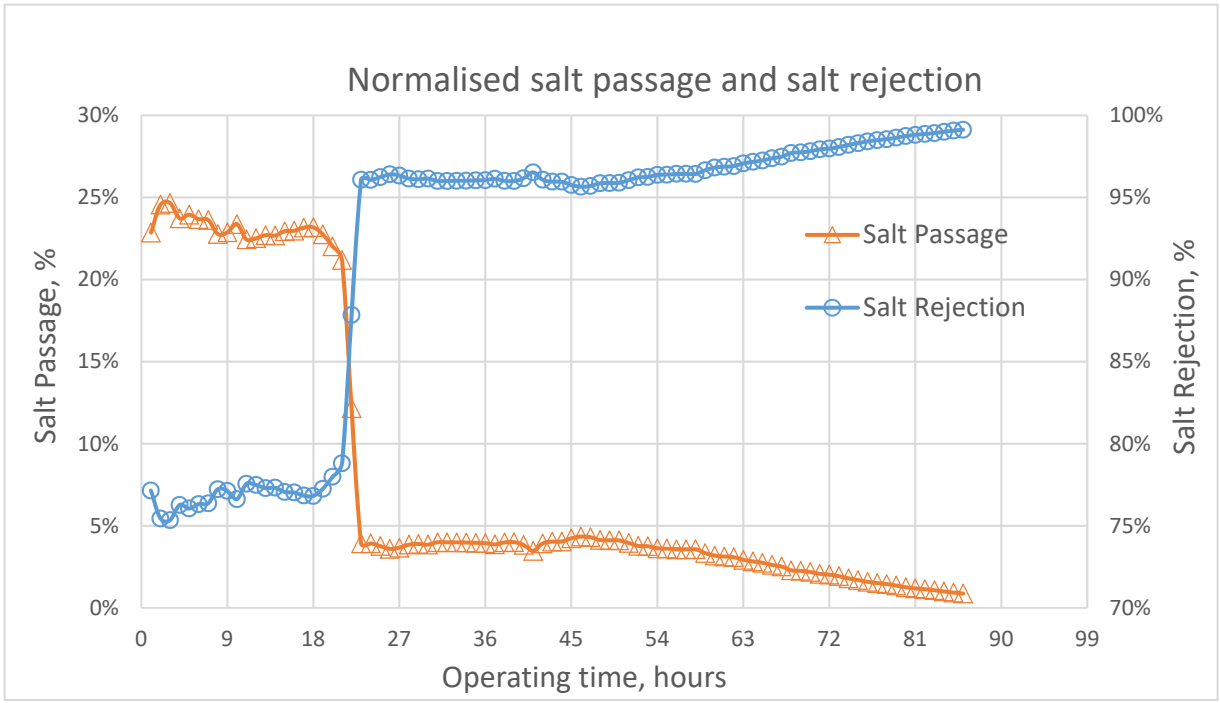


*Figure 30. The trend of normalised salt passage and salt rejection in inhibitor evaluation.*

## 8.5 Analysis of membrane samples

Previously, it was mentioned that surface crystallisation, and bulk crystallisation mechanisms explain the reason behind the permeate flux decline (Figure 31). In bulk crystallisation, the mineral ions of the supersaturated solution are joined in random sequence to form large combined mineral ions and then deposited on the surface. On the other hand, in the surface crystallisation the crystals precipitate directly on the surface then all the precipitated particles start to propagate along the membrane surface (Lee and Lee, 2000). In the entire conducted experimental work, the membrane coupons were analysed after the surface scale coverage reached 100% (i.e. when the permeate flux reached zero).

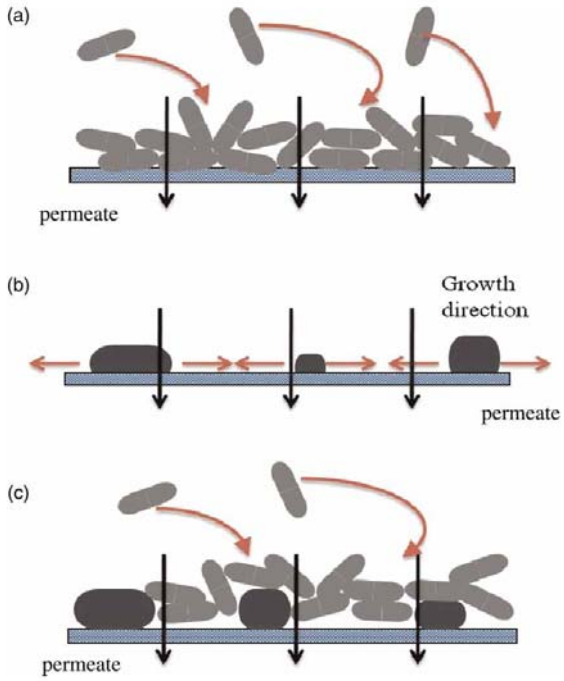


*Figure 31. The two mechanisms for scale crystallisation (a) Bulk crystallisation (b) Surface crystallisation (c) The two mechanisms combined (Lee and Lee, 2000)*

The fouled membrane coupons were analysed at Kemira's Espoo Research Centre by Analytics team. Several analytical tools were used for identifying the deposit mineral scale on the membrane surfaces. Scanning electron microscopy (SEM) (Philips XL 30 Feg FESEM) was used to make a quantitative assessment of deposit type, and energy dispersive x-ray spectrometry analysis (EDS) (Oxford Instruments EDS with AZtec software) was used to obtain the compositional information of deposits. Powder X-ray diffraction (XRD) (PANalytical X'Pert PRO MPD, Co Tube) for determining the chemical nature and phases of mineral foulant (i.e. if calcium sulphate was found as anhydride $CaSO_4$ or as gypsum $CaSO_4 \cdot 2H_2O$). Lately, x-ray fluorescence spectrometry (XRF) (PANalytical AXIOS 2, 4 kW, Rh tube, SuperQ software) for determining the elemental composition of solid particles, and the results were expressed as percentages of the major element oxides. SEM micrographs were captured from the middle section of membrane coupons. XRD/XRF samples were collected by scrapping the entire surface and through measuring 2 grams of sample in a liquid cup then grounding it by hand in a mortar.

The calculated saturation index indicates that the model solution was supersaturated with respect to calcium carbonate, calcium sulphate and amorphous silica. Therefore, the main expected mineral scale to be found are the calcite, argonite crystals, and the third most common polymorph (Vaterite). Moreover, calcium sulphate anhydrite,

calcium sulphate dihydrate, magnesium carbonate (Magnesite), magnesium silicate, and amorphous silica are expected to be the main scaling sources.

The analysis of reference run coupons (i.e. run without antiscalant) has unveiled some interesting results. SEM images (Figure 32 B) showed spherical shape particles which contain 23% calcium and 18% sulphur, and Figure 32 A presents the sharp straight edges needle calcite crystals, and platelets type structure gypsum crystals. Moreover, XRD showed high quartz and argonite crystals which apparently was built on calcite faces. Vaterite was not identified, reflecting the presence of a significant quantity of magnesium (Antony et al., 2011). In page 31, it was mentioned that the model solution compositions were decreased by 40 % to minimise the concentration polarisation. By comparing the initial composition membrane coupones to reference run (modified composition), the main difference was less calcite and aragonite in reference run.

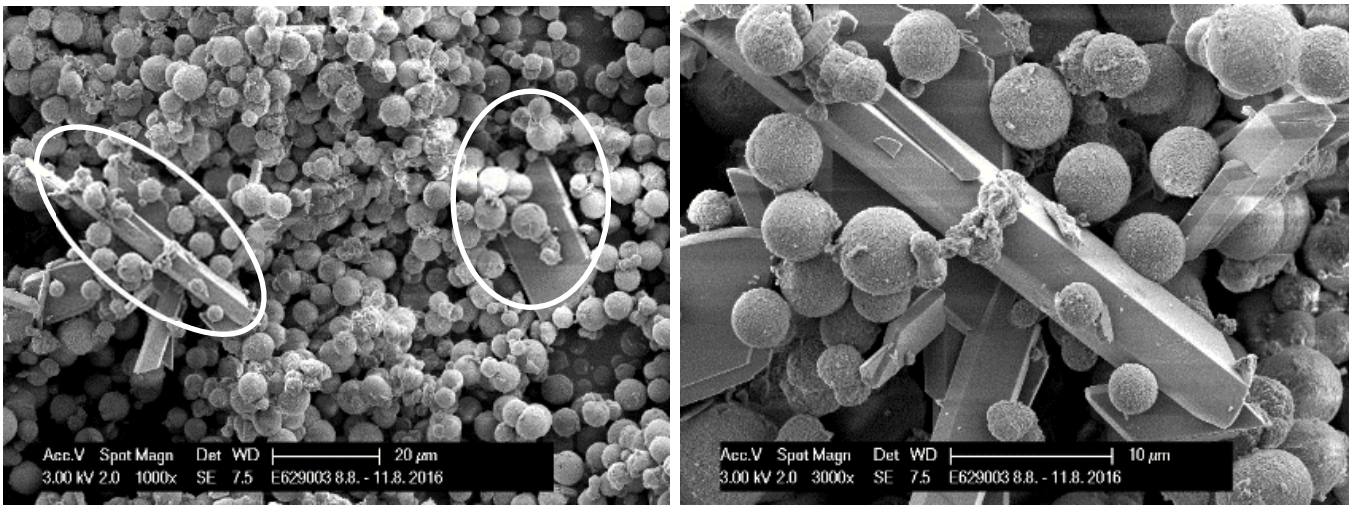


*(A)* *(B)*

*Figure 32. SEM micrographs of a reference run. (A) Shows the calcite and gypsum crystals. (B) Shows spherical shape particles*

The next analysis was identifying the morphology of deposit crystals of the three inhibitors based on 2 mg/L dose. SEM micrographs from AS1 showed a clear difference compared to reference run. The rounded spherical shape particles (Figure 33 B) were deformed indicating that AS1 function via crystal modification mechanism and XRD has not identified argonite crystals. Additionally, XRD revealed gypsum and calcite crystals although they were not seen in SEM images (middle section of membrane coupons) indicating that the scaling was not evenly distributed over the surface.

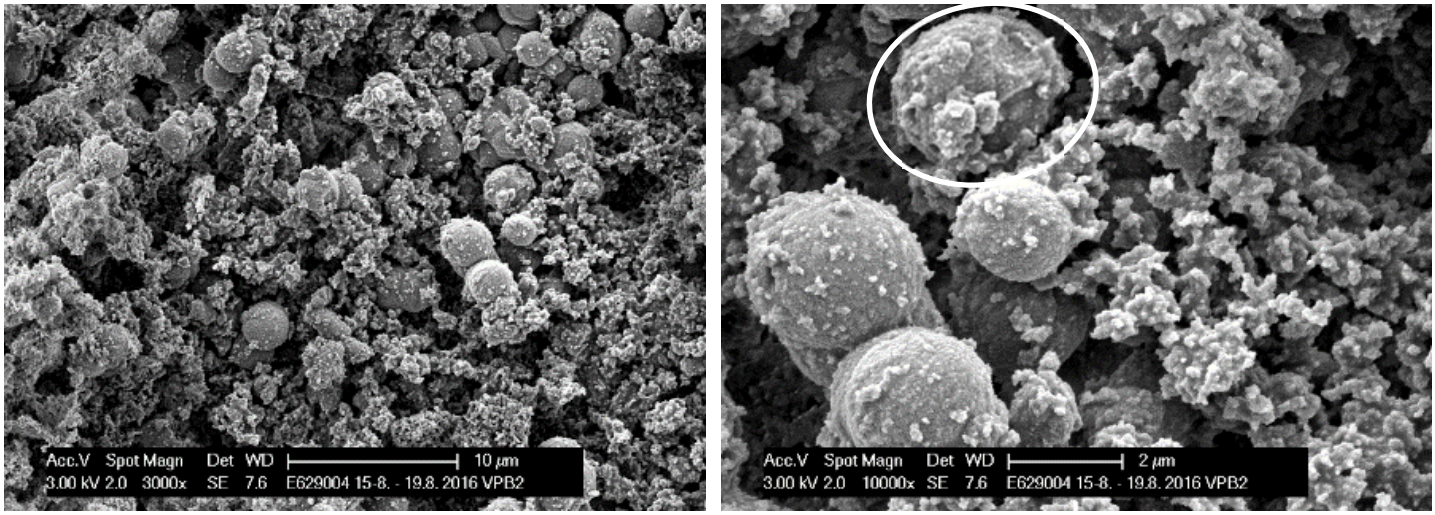


*(A)* *(B)*

*Figure 33. SEM micrographs of AS1 (2mg/L). (A) Shows the deformed spherical shape particles. (B) Shows a single deformed spherical particle.*

The AS2 and AS3's SEM micrographs (Figure 34 and Figure 35) have shown fewer signs of the spherical shape particles, which indicates that those two antiscalants function via crystal modification mechanism. However, the straight edges needle calcite crystals, platelets type structure gypsum, and crystal rods gypsum crystals were clearly recognised from the SEM images. Furthermore, XRF studies indicated a lower content of quartz in the three antiscalants cases. Moreover, the least quartz content was in AS2 case, showing its effectiveness towards silica.

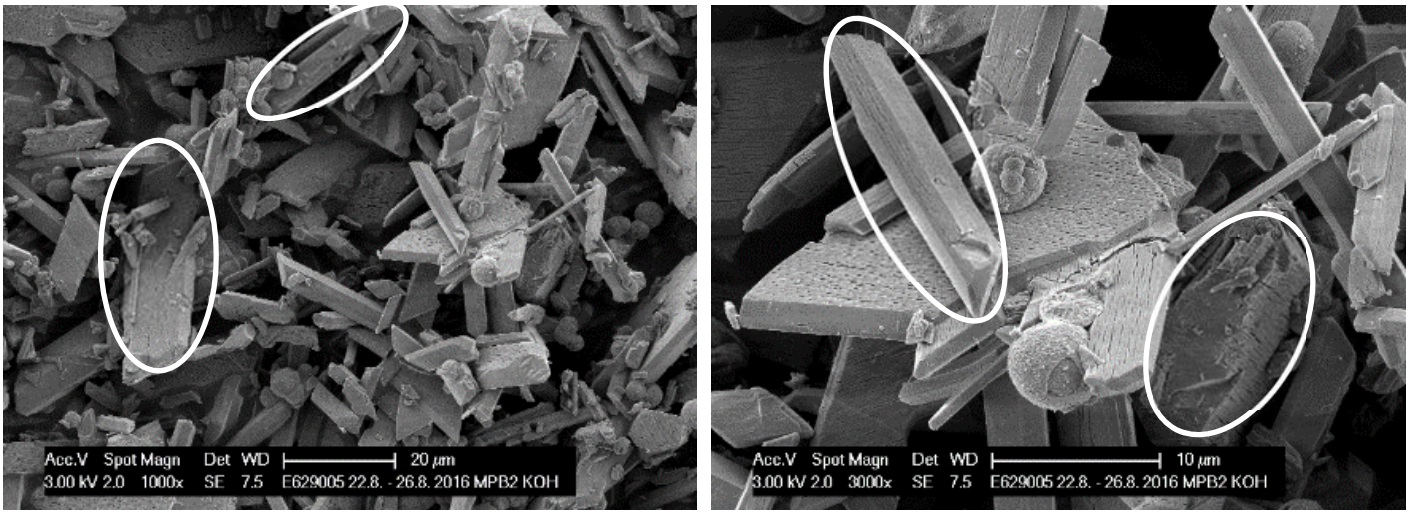


*(A)* *(B)*

*Figure 34. SEM micrographs of AS2 (2mg/L). (A) Shows different crystal form of calcite and gypsum. (B) Shows needle calcite crystals, platelets type structure gypsum.*

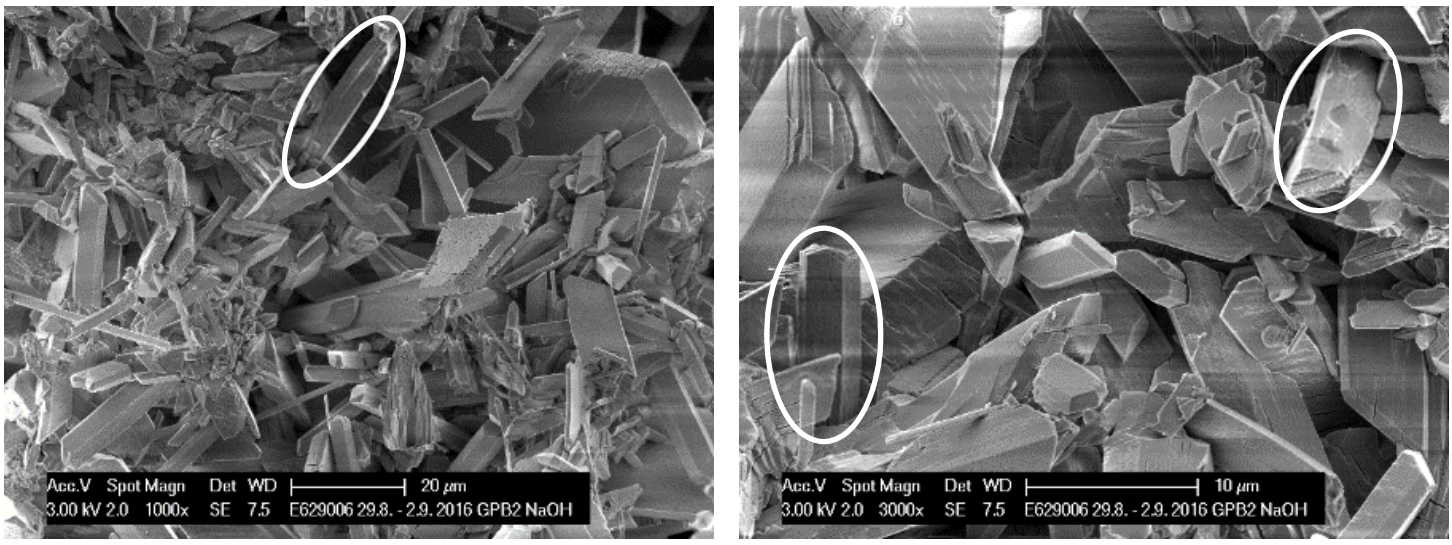


*(A)* *(B)*

*Figure 35. SEM micrographs of AS3 (2mg/L). (A) Shows needle-like gypsum. (B) Shows oriented needles calcite crystals, platelets type structure gypsum.*

Several outcomes were collected after analysis the 10 mg/L antiscalants dose membrane coupons. AS1 SEM micrographs (Figure 36 A) reveal interesting results. The mineral deposits have formed a clay-like precipitate, and XRD shows argonite and calcite crystal. SEM micrographs of AS3 (Figure 36 B) showed distorted and plate-like morphology gypsum and its effect to modify the calcite cubic shape crystals. SEM micrographs of AS2 reveal a clay-like precipitate with calcite crystals in block-shape with modified edges (Figure 37). Moreover, the XRF results indicate that weight percentage of calcium element is the lowest in AS2 case.

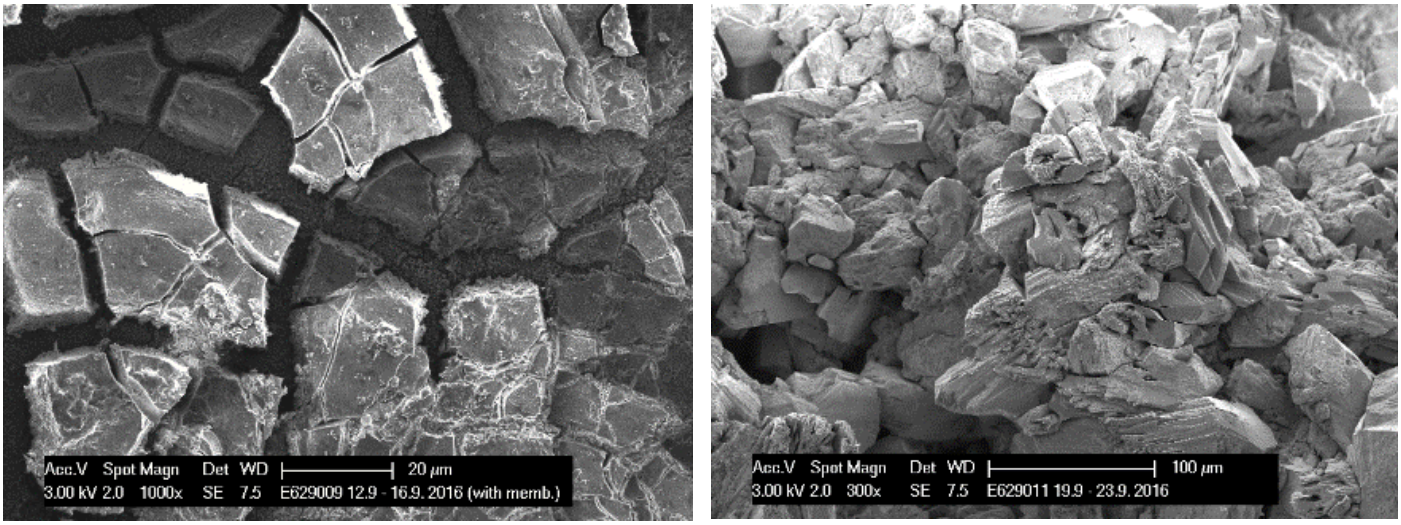


*(A)* *(B)*

*Figure 36. SEM micrographs of (A) AS2 (10mg/L) clay-like precipitate and (B) AS3 (10mg/L) distorted calcite and gypsum crystals.*

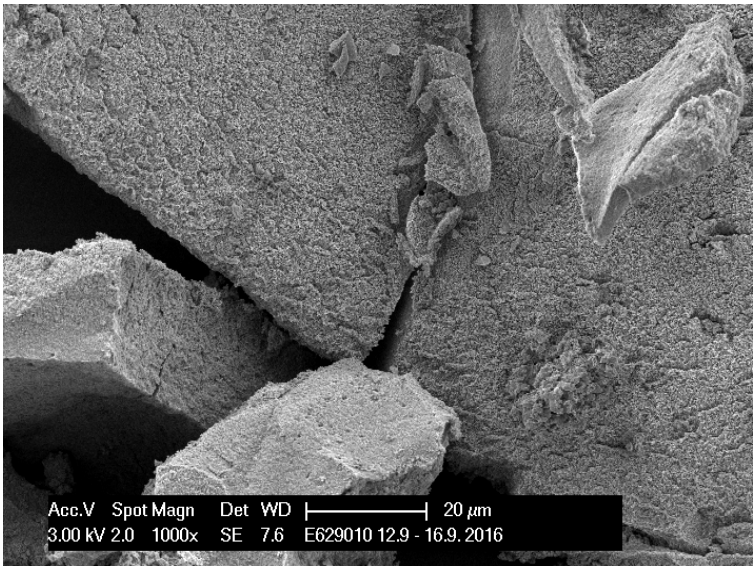


*Figure 37. SEM micrographs of AS2 (10mg/L) shows calcite crystals in block-shape with modified edges.*

At the highest dose (20 mg/L), all the deposit was clay-like precipitate blended with calcite and gypsum crystals (Figure 38). EDS analysis has shown less Ca compared to 10 mg/L cases, and it was challenging to collect the minimum mass for XRD/XRF analysis.

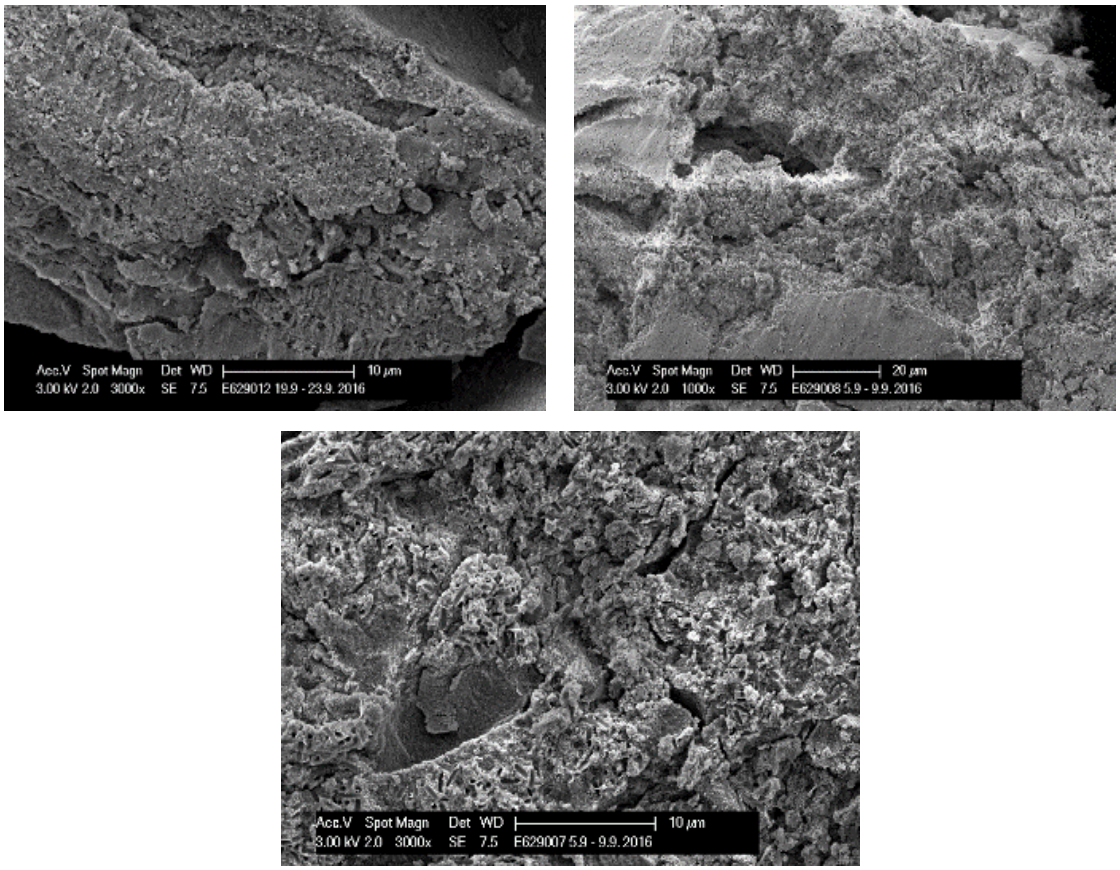


*Figure 38. SEM micrographs of AS1 (Top left), AS3 (Top right), and AS2 (bottom) (20 mg/L) case.*

## 8.6 Ranking the antiscalant effectiveness

Based on the rate of permeate flux decline and the amount of water recovered, AS1 had the least performance, and both AS2 and AS3 has revealed a similar rate of flux decline. However, by including the rate of TMP increase, AS2 has presented the most efficient impact in term of delaying the TMP rise. Lastly, from the membrane coupons autopsy results, AS2 has the most effective impact on changing the crystal formation and crystal morphology, and its mechanism to tolerate the calcium carbonate, gypsum, and silica via crystal modification mechanism. Table 12 illustrate the evaluation and the ranking of the three inhibitors.

*Table 12. Ranking the three antiscalants involved in experimental work.*

| Evaluation criteria | AS1 | AS2 | AS3 |
|---|---|---|---|
| Efficiency of decreasing rate of permeate flux decline | 3rd position | 2nd position | 1st position |
| Delaying the TMP rise | | 1st position | 2nd position |
| Silica content on membrane surface | | 1st position | 2nd position |
| Distorting calcite crystals structures | | 1st position | 2nd position |
| Distorting gypsum crystal structures | | 2nd position | 1st position |

# 9. Evaluation biocides for controlling biofouling in RO systems

The primary objective of this chapter is to investigate the ability of biocides to prevent biofouling on a single stage RO membrane; the same RO system used in antiscalant evaluation. Commonly, the biofouling control is divided into two groups, prevention and cleaning. However, the ideal condition for biofouling control is to prevent the initial attachment of fouling material on the membrane surface. Therefore, the efficiency of biocides for biofouling prevention was preliminarily investigated in this study. The study was focusing on simulating fouling accumulation in the cross-flow RO filtration units by utilising fresh bacterial inoculum (Meiothermus bacteria) and nutrients and exposing the system to biocide dose for cleaning. As previously reviewed, biofouling is the main reason causing losses in the hydraulic performance of RO membrane. Therefore, the permeate flux and normalised pressure drop (NP) were continuously monitored to verify the ability of biocide to control biofouling on RO membrane.

## 9.1 Overview

The membrane surface offers the water a surface for the biofilm to grow on. Feed water usually contains salt ions and organic matters which are a primary source of nutrients for the growth of microorganisms. Therefore, the development of biofilm is unavoidable. Furthermore, the hydrodynamic operating conditions, such as feed water flow rate and permeate flux has a significant impact on biofilm formation. Dreszer et al. (2014) reported that the high flow rate increases the shear stress and consequently reduces the rate of biofilm growth, but other studies indicated that higher shear rate attribute in the formation of thinner high-density biofilm layer (Suwarno et al., 2014).

An illustrative diagram of the main phases occurring during biofilm development is given in Figure 39. Initially, the organic molecules started to form a film on the membrane surface resulting in creating a conditioning film. The film acts as a foundation to attract the free moving bacterial cells from the feed water. At the following stage, all the polysaccharides, lipids, and proteins reached a mature stage and started to attach cells irreversibly. All the attached polysaccharides and lipids are defined as Extracellular polymeric substances (EPS). EPS primary function is to assist the growth of biofilm by connecting new nutrients and microbes to the existing biofilm matrix. Moreover, it helps in the formation of complex biofilm by forming a cross-

linking network matrix to protect the biofilm against shear force and cleaning attacks (Flemming et al., 2007). The majority of micro-organisms in all water systems are capable of adhering and grow on the membrane surface. Commonly, *Arthrobacter*, *Corynebacterium*, *Flavobacterium*, and other bacterial species colonised the membrane surfaces (Matin et al., 2011).

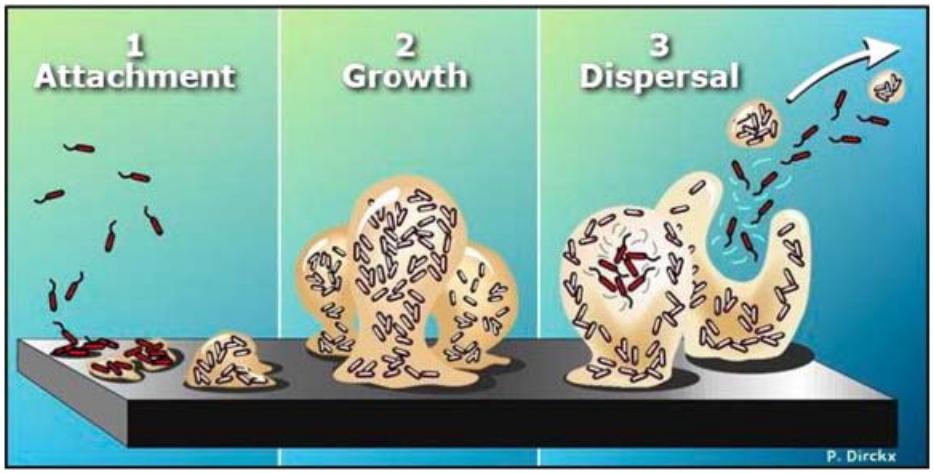


*Figure 39. Biofilm development phases (Matin et al., 2011).*

## 9.2 Materials and methods

The experimental investigation was performed in an extreme biofilm conditions by using tap water, fresh bacterial inoculum (Meiothermus bacteria), and nutrients to rapidly build a biofilm over the membrane surface. Two biocides were evaluated: Biocide1 and Biocide2. Biocide1 was used as a reference biocide to evaluate the performance of slow released biocide (Biocide2). Commerical thin-film composite polyamide DOW FILMTEC™ BW30-4040 membrane sheets and feed Spacer-Diamond type 34mil (0.864 mm) were utilised for the test. The membrane spacer is clearly representative for biofouling studies since it prevents flow channelling inside the membrane modules and develop actual amount biomass growth on spacer grid and membrane surface.

The experiments were conducted by filling the feed tank with 40 litres feed water and circulate through membrane modules in a total recycle mode for two weeks (i.e. permeate and concentrate lines were continuously recirculated to the feed tank). Before each experiment, membrane coupons were soaked in deionized water (DI) for one day and then placed inside the membrane modules including membrane spacer. Line 1

consists of four test cells (Sterlitech module CF042 Cell), each cell with active membrane surface area of 42 $cm^2$, and line 2 consists of A5 one plate-and-frame membrane cell with active membrane surface 218 $cm^2$. The feed water was recirculated through the system at flow rate 18 L/h. The tank temperature was kept at 40 ºC to keep the bacteria growing. Moreover, the operating pressure was controlled at 10 bars. After creating a baseline with tap water for 4-5 hours, meiothermus bacteria and nutrients were added to the system to initiate the biofilm formation. The permeate flux and normalised pressure drop (NP) were continuously monitored. The biocide was added stepwise when the permeate flux dropped by 10-15 % of initial values. The biocide dosage was calculated based on the final product.

Water samples were collected from both permeate and concentrate line on a daily basis (typically before the biocidal dosage) to monitor the microbiological quality by measuring Adenosine tri-phosphate (ATP). ATP is the energy compound present in every living microorganism. The measurement was analysed using LumiKem®, 2nd generation ATP measurement kit by Kemira. The kit includes: (1) KemiZyme™ Lite (2) KemiCal™1 (3) KemiLyse™ Lite.

The ATP test has involved two steps: (1) Two drops (100 µL) of KemiCal™1, and 400µL KemiZyme™ Lite were added in a test tube to record $RLU_{KC1}$ for the KemiCal™1 calibration to convert the luminometer RLU value to actual ATP. (2) 100µL of the well-mixed water sample and two drops (100 µL) of KemiLyse™ Lite were added in a test tube for at least a minute for incubation then 400µL KemiZyme™ Lite was added to record $RLU_{tATP}$. Equation (6) were used to calculate the total ATP (tATP) by converting RLU values to ATP concentration (pg ATP/mL). Total ATP measured the entire ATP within the sample, including the ATP release from dead cell plus the ATP of living cells.

$$tATP\ \left(pg\frac{ATP}{mL}\right) = \frac{RLU_{tATP}}{RLU_{KC1}} \times 2{,}000\ \left(pg\frac{ATP}{mL}\right) \qquad (6)$$

Bucs et al. (2014) method was adopted to characterise the accumulated biofouling material on the membrane coupons. (2x2 cm) sections of membrane and spacer were collected from inlet and outlet side of membrane cells and placed separately in capped tubes filled with 90 mL of autoclaved tap water or DI water. Then the capped test tubes were mixed on a vortex for two- minutes followed by placing in an ultrasonic cleaning

bath for another two minutes. This process was repeated three times. The biomass-water suspension from the tubes was utilised to determine the active biomass by measuring the tATP (pg ATP/cm$^2$). Another membrane samples were collected for microscopic fluorescence images to capture any live cells on the surface of the membrane.

## 9.3 Results and discussion

The experimental tests started by operating the two lines at the similar operating condition. After introducing the fresh bacterial inoculum (Meiothermus bacteria) and nutrients, the permeate flux began to decline. The biocidal dosage process started after one day of operating the system. Figure 40 and Figure 41 displays the monitored permeate fluxes decline rates, cumulative biocide dose and the recorded tATP values from both concentrate and permeate lines for the two biocides cases. It was observed that both biocides were effective towards decreasing the tATP values. Moreover, at 5 ml/L cumulative dose of biocide 2, the permeate flux significantly dropped from 25 to 20 LMH. And by comparing the two biocides performance (See Figure 42), biocide 2 had higher flux at a dose lower than 5 ml/L. Still, the instant drop in permeate flux at 5 ml/L biocide 2 indicating there could be an adverse effect from either biocide 2 dose or line 1 membrane cell (Sterlitech module CF042 Cell).

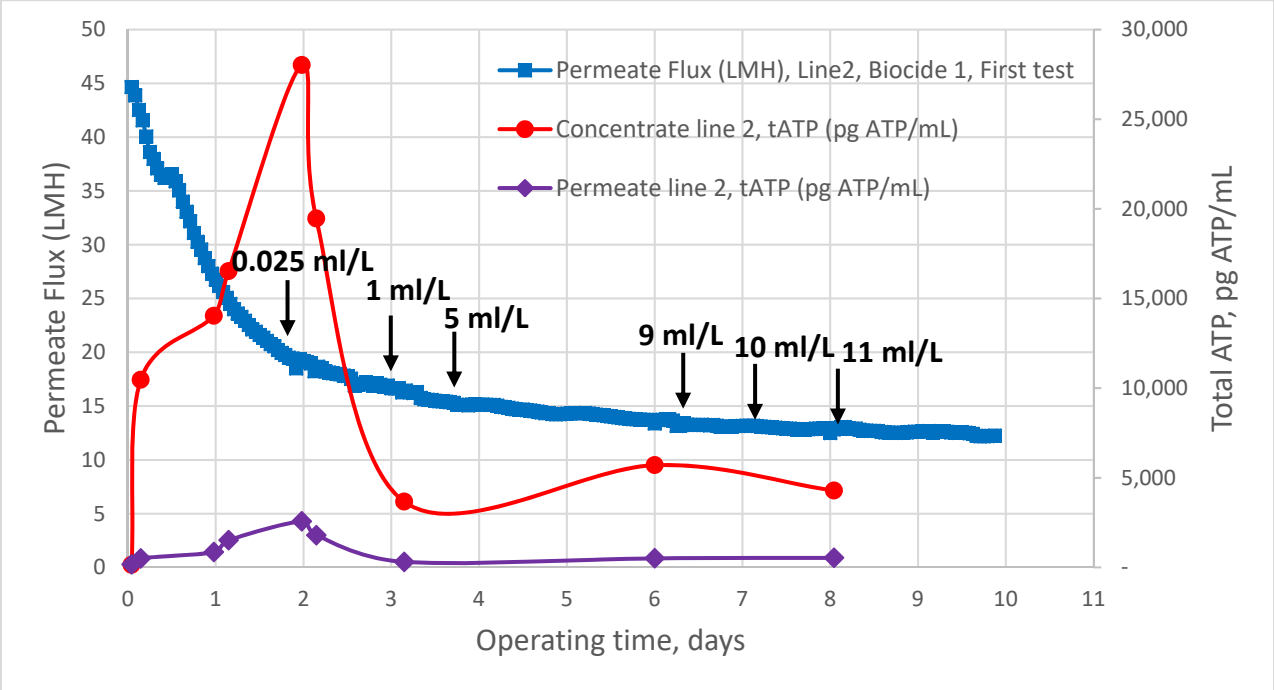


*Figure 40. Monitored and measured parameters of the first test (biocide 1).*

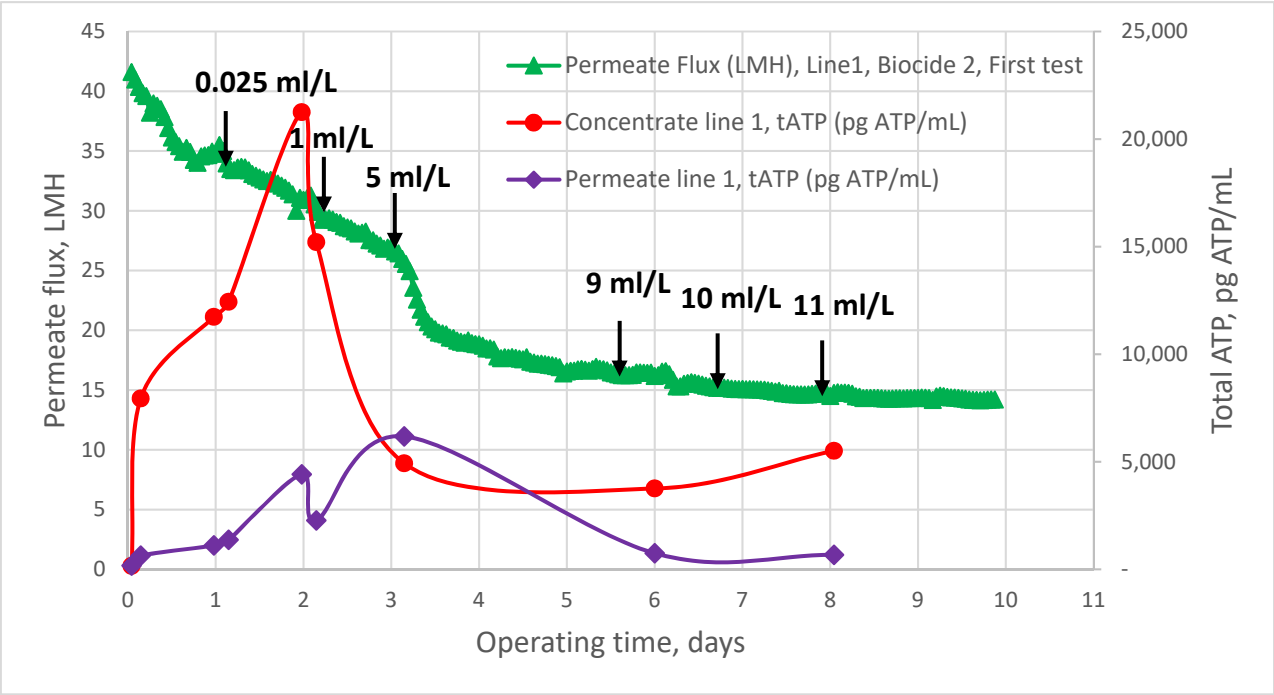


*Figure 41. Monitored and measured parameters of the first test (biocide 2).*

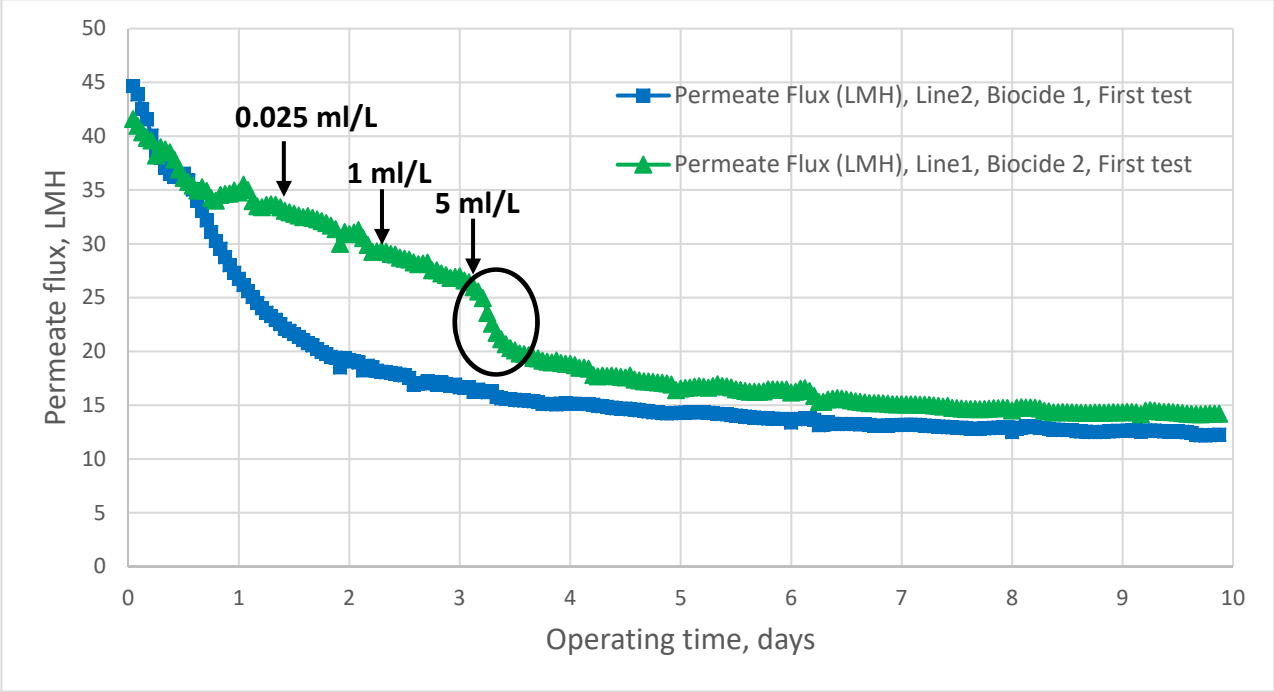


*Figure 42. Comparison between two biocides permeates fluxes performance in the first test.*

The following experiment was continued by repeat the same procedure with shifting the biocide dosage between lines, to check if the negative effect is from the biocidal dose or the different membrane cells. The biocide dosage started with 5 ml/L. Figure 43 displays the comparison between two biocides performance. It was observed that

the same permeate flux drop occurred at 5 ml/L and 15 ml/L biocide 2 dosage, demonstrating that biocide 2 dose is the cause of the negative impact.

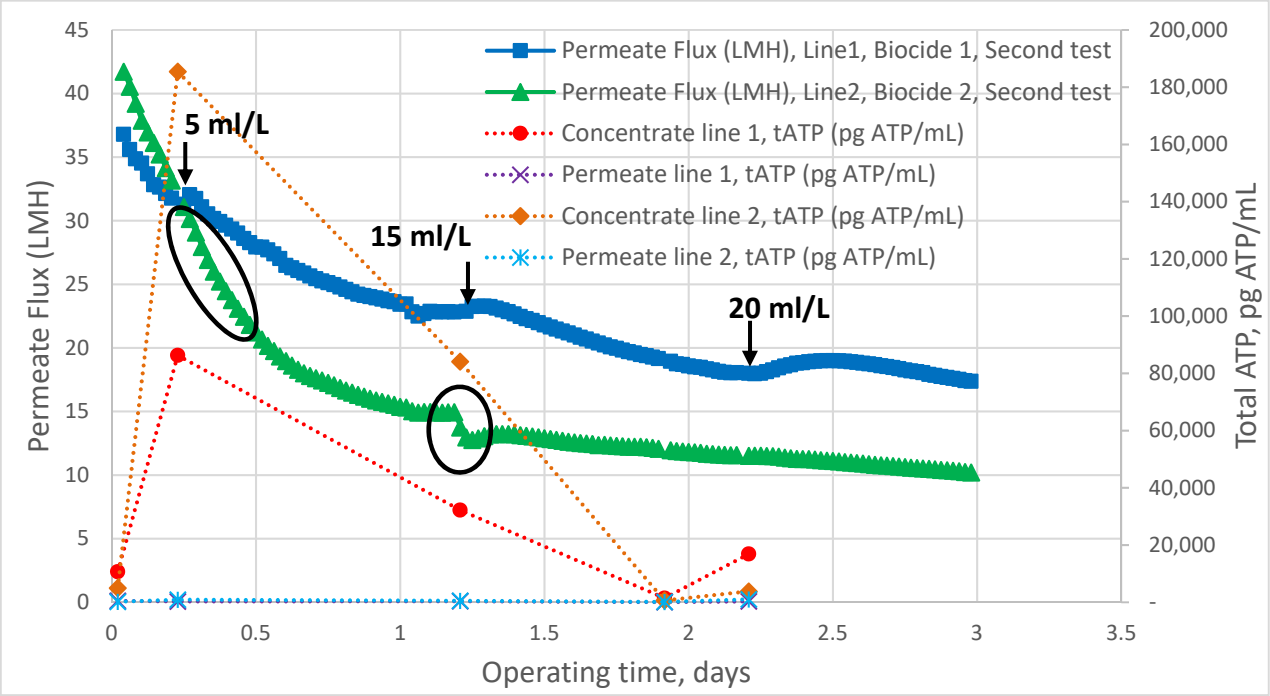


*Figure 43. Comparison between two biocides permeates fluxes performance in the second test.*

Comparing the normalised pressure difference of line 1 which consists of four test cells (Sterlitech module CF042 Cell), indicated that Biocide 2 was more effective in term on preventing the pressure difference rise. Figure 44 shows the normalised pressure drop trend of two biocides. Although in the second test 20 ml/L cumulative dose of biocide 1 were added, the normalised pressure was not prevented from increasing. On the other hand, 5 ml/L Biocide 2 was sufficient to maintain the pressure difference at a low level.

Despite the fact that Biocide 2 (Slow released biocide) has a negative impact on membrane permeate flux, it showed a positive result in term maintaining pressure difference from increasing by controlling the growth of biofilm. Besides, it has less biomass accumulation on the membrane surface (mg ATP/cm$^2$). Therefore, a chemical compatibility test was performed to classify and confirm whether or not this biocide is compatible with the polyamide thin-film-composite membrane.

The membrane autopsy has revealed that the biomass accumulated on the outlet side of membrane module was higher than inlet side in both membrane and spacer grid

samples. Moreover, Biocide 2 (Slow released biocide) membrane samples had less biomass fouling (pg ATP/cm$^2$) compared to Biocide 1. (See Figure 45).

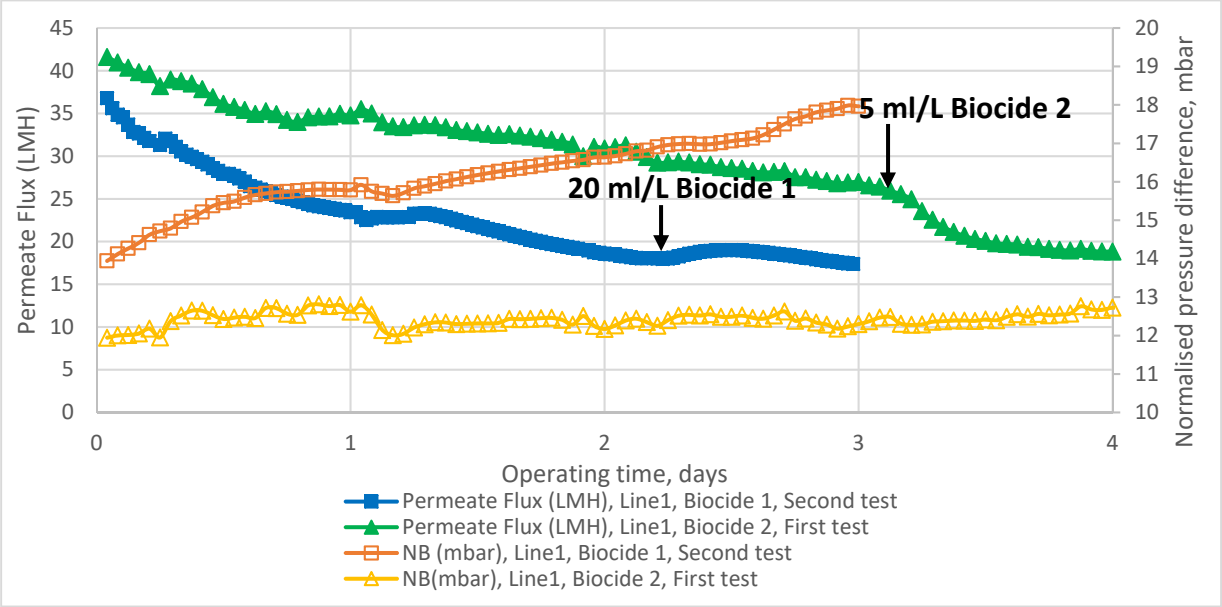


*Figure 44. Comparison between two biocides normalised pressure differences and permeate fluxes performance.*

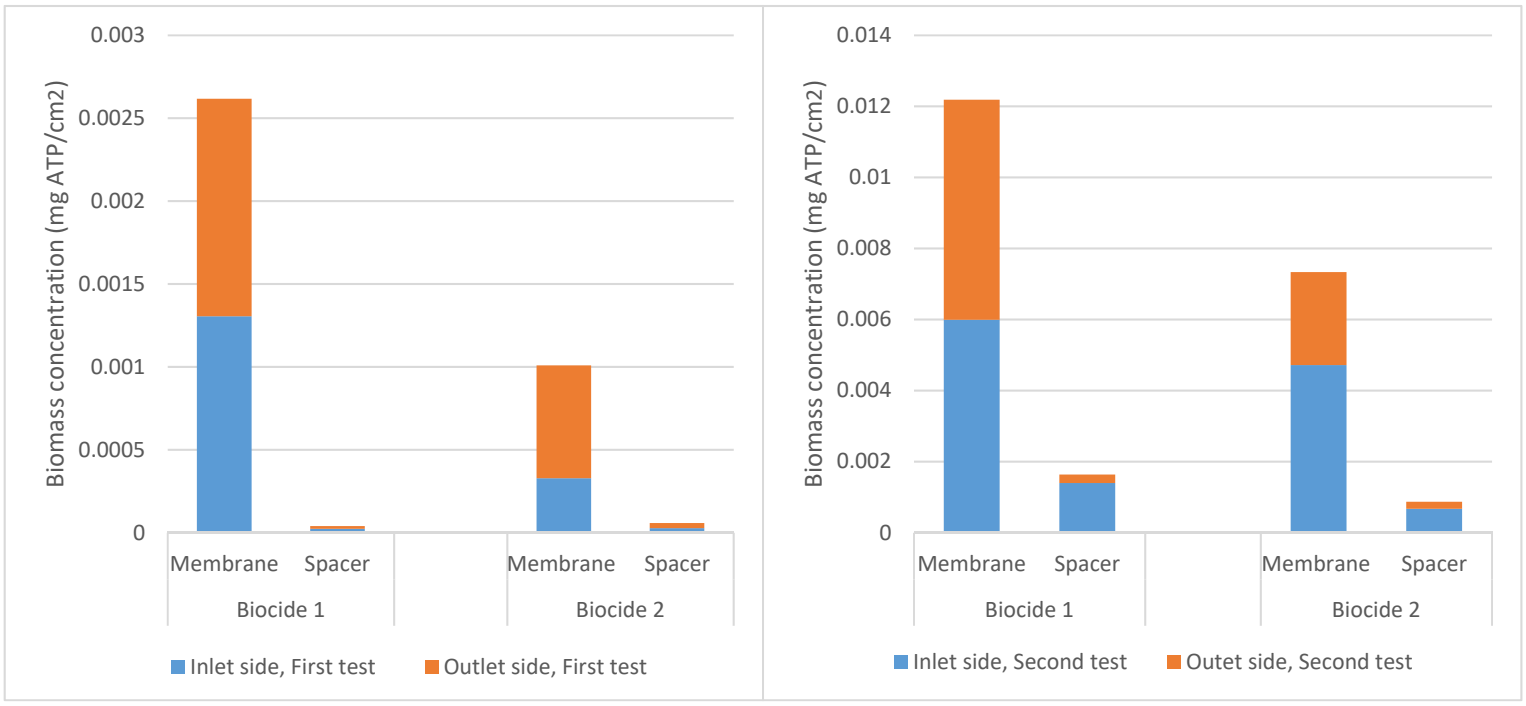


*Figure 45. Biomass accumulation on the membrane coupons and spacer grids.*

## 9.4 Evaluation the biocide Compatibility with polyamide membrane

A chemical evaluation test was conducted to verify the Biocide 2 compatibility with polyamide thin-film-composite membrane. A 3.5 weight% sea salt test solution was prepared, and the system was continuously operated for 20 hours to establish a baseline. The pH value was controlled between 6.5 to 7.5 Later a high dose (120 ml/L) of the active component of Biocide 2 plus (100 ml/L) Biocide 1 was added to line 1 (which is connected to four Sterlitech module CF042 Cell). And (100 ml/L) Biocide 1 to line 2 (which is connected to A5 one plate-and-frame membrane) for comparison. The normalised permeate flux and salt passage were calculated. Figure 46 shows the significant decrease in permeate flux in the case of a mixture of Biocide 1 and Biocide 2 active component. The active component of biocide 2 is cationically-charged biocide which explains the reason behind the incompatibility. The membrane and chemical charge play an influential role in the salt passage and salt rejection, Figure 47 illustrate the impact of cationically-charged Biocide 2 high dose during the compatibility test run. The salt passage decrease significantly and salt rejection reached 100%.

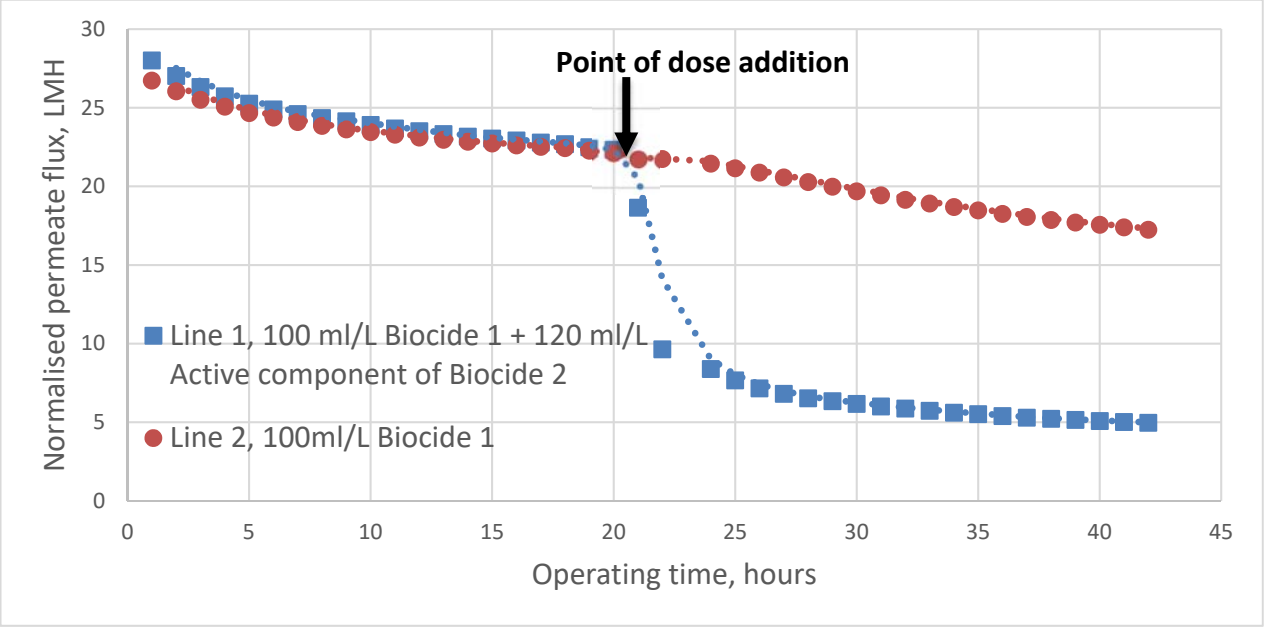


*Figure 46. Normalised permeate flux response to high biocide dosage.*

The polyamide thin-film-composite membrane is a negatively charged membrane, and when positively charged ions (The active component of Biocide 2) come in contact with it, the concentration of cation ions at membrane boundary layer became higher than in the bulk solution. Moreover, at the same time, the membrane repelled the negatively

charged ions (See Figure 48). Subsequently, the overall salt rejection depends directly on anions and cations attraction force (Bartels et al., 2005).

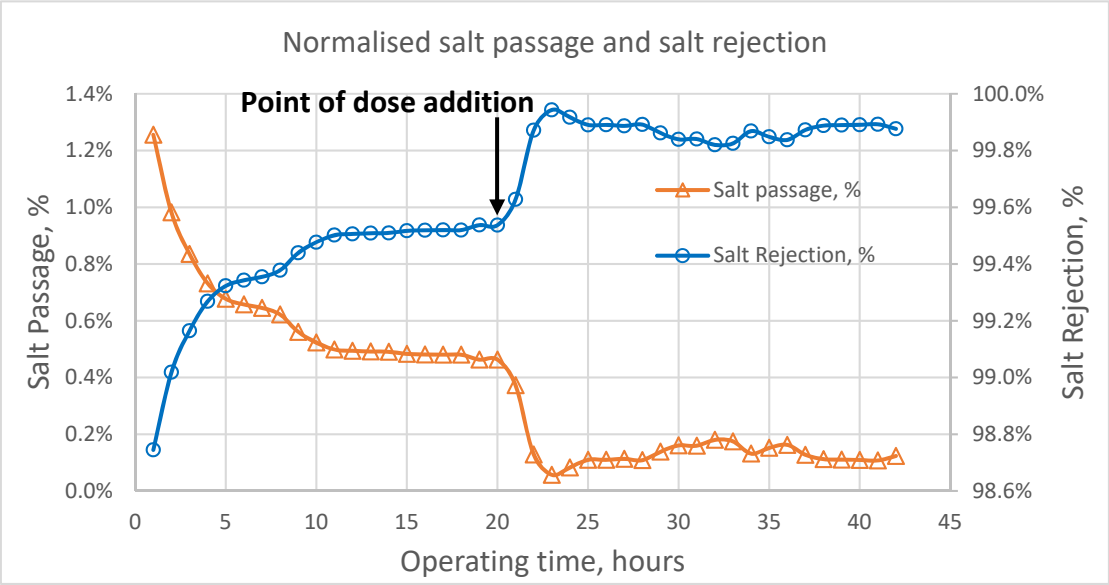


*Figure 47. The impact of a mixture of Biocide 1 and Biocide 2 active component on the salt passage percentage.*

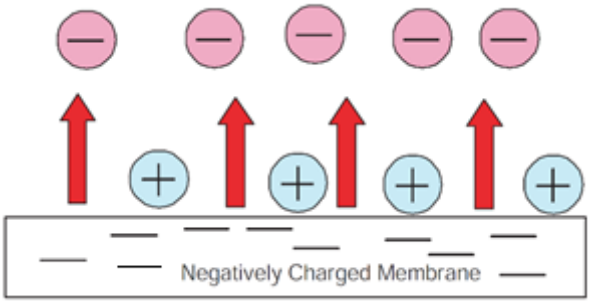


*Figure 48. The negatively charged membrane attracting the cations.*

# 10. Development of membrane fouling simulator prototype

The general research objective of this chapter is to develop and test a membrane fouling simulator (MFS) prototype device. The specific goals are:

- Verification of equipment accuracy/sharpness for detecting fouling of the spacer grids and membrane surface in the early phase.
- Benchmarking results to the standard MFS system.
- The device response to chemical addition (Biocide and Antiscalants)
- The device capability to classify and distinguish between organic and inorganic fouling type in combined fouling cases.

## 10.1 Overview

The study was primarily focused on monitoring the biofouling development and scaling. The progress of biofouling occurs at three main phases: (1) Induction, (2) Log growth rate, (3) Plateau phase (Figure 49). It is quite challenging to control the biofilm in the desalination process during the induction period. However, the biofilm is controlled below a threshold of interference (dotted curve) based on precise information of biofilm development collected directly from the process (Flemming, 2003). The early warning mechanism (as described in section 6.3) is the most suitable way to obtain detailed information about the induction phase and taking corrective actions.

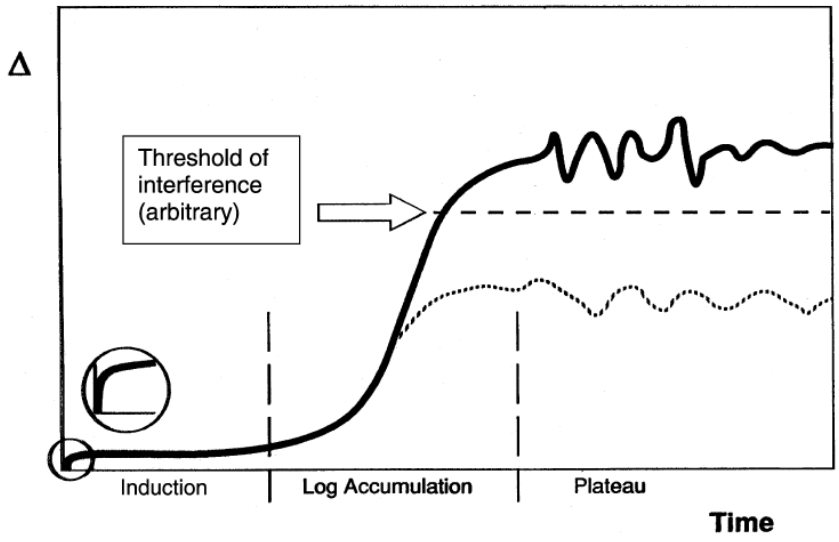


*Figure 49. Biofilm phases. Delta is referring to different monitoring parameters (thickness, accumulated cells, etc.) (Flemming, 2003)*

In membrane modules, two main types of pressure drop can be identified: (1) trans-membrane pressure (TMP) which is the differential pressure between the feed and permeate line occurs due to the friction factor over the membrane surface. (2) Feed channel pressure drop (FCP) which is the differential pressure between the feed and concentrate line (Figure 50) (Vrouwenvelder et al., 2009b). The FCP is directly indicating the fouling layer build up. On the other hand, the TMP is for evaluating the hydraulic performance of membrane module. Consequently, the prototype will monitor the FCP and observe the fouling buildup.

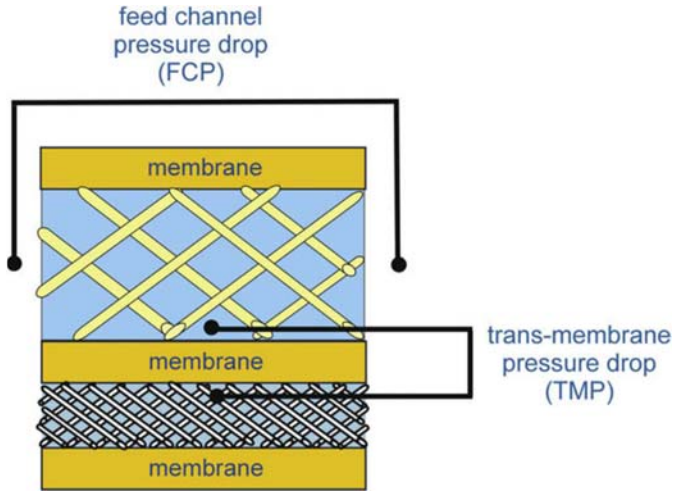


*Figure 50. TMP and FCP pressure drop in membrane modules (Vrouwenvelder et al., 2009b).*

## 10.2 Materials and methods

The prototype consists of two fouling cells with external dimensions (0.2 × 0.30 × 0.04 m) connected to separate feed tanks to compare the fouling development by operating at various flow rates. A sensitive differential pressure transmitter over each cell to monitor the FCP, and a high-resolution camera equipped with white light and UV-fluorescence spotlights to differentiate between living bacteria and dead biomass. The membrane cells have a transparent surface enabling the detecting camera to recognise the membrane and spacer fouling. The device has no permeate production. However, the FCP and biofilm buildup are not affected by the absence of permeate flux (Vrouwenvelder et al., 2006). Figure 51 shows a schematic diagram of the process.

The high-resolution camera associated with an image analysis software were processing the captured images online to calculate the membrane and spacer grid surface fouling percentage and distinguish between inorganic and organic fouling particulates. Table 13 lists the output parameters of the device.

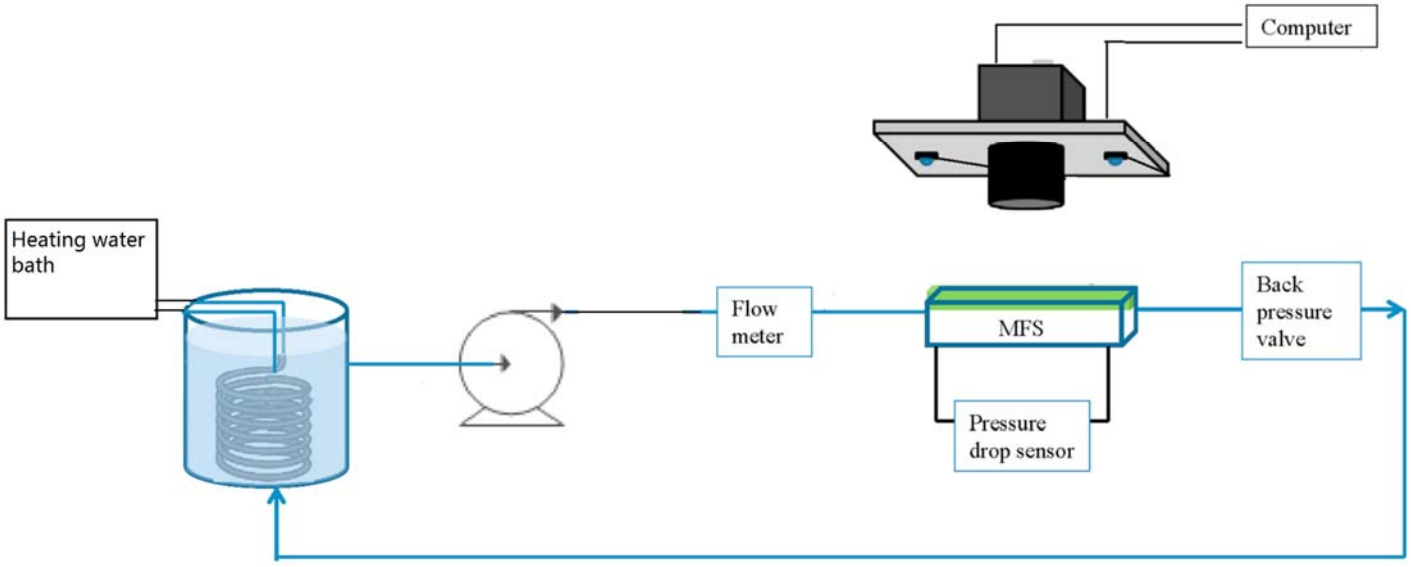


*Figure 51. A schematic diagram of the process.*

*Table 13. Prototype output parameters classification.*

| Prototype parameters | Class |
|---|---|
| Flow rate | Measured |
| Pressure difference | Measured |
| Spacer fouling % | Calculated |
| Membrane fouling % | Calculated |
| Organic fouling % | Calculated |
| Inorganic fouling % | Calculated |

The membrane and spacer coupons utilised were cut from an unused commercial membrane module (DOW FILMTEC™ BW30-4040 with feed Spacer-Diamond type

34mil (0.864 mm)) in size 0.2 by 0.04 m. (Similar to previously used membrane in antiscalant and biocide evaluation chapters).

The hydraulic characterisation of the prototype was validated by measuring the FCP through the pressure sensors across the membrane cells and comparing the results to theoretical FCP using Darcy-Weisbach pressure drop equation driven by Shock and Miguel (1987) (Equation 7).

$$\Delta P = \frac{f \rho v^2}{200} \frac{L_m}{d_h} \tag{7}$$

$$f = 6.23\, Re^{-0.3} \tag{8}$$

$$d_h = \frac{4\varepsilon}{2\frac{w+h}{wh} + (1-\varepsilon)S} \tag{9}$$

$$Re = \frac{\rho v d_h}{\eta} \tag{10}$$

$where$:

$\Delta P = pressure\ drop\ across\ the\ membrane\ cell, mbar$

$f = friction\ coefficient$

$v = cross - flow\ velocity, \frac{m}{sec.}$

$\rho = fluid\ denisty, water, 1000 \frac{kg}{m3}$

$L_m = membrane\ cell\ lenght, 0.02\ m$

$d_h = hydraulic\ diameter, m$

$\varepsilon = spacer\ porosity, 0.89$ (Vrouwenvelder et al., 2009b)

$S = specific\ surface\ of\ membrane, 11600\ m2/m3$

(Vrouwenvelder et al., 2009b)

$w = spacer\ width, m$

$h = height\ of\ spacer, 0.00076m$

$Re = Reynolds\ number$

$\eta = dynamic\ viscosity, 0.001002\ Pa.s$

The study was focusing on excessive biofouling as it is the dominant fouling type and studying the attribute of feed spacer on fouling development and the feed channel

pressure drop. The experimental investigation was performed in an extreme biofilm conditions by using tap water, fresh bacterial inoculum (Meiothermus bacteria), and nutrients. The temperature of the two feed tanks connected to the device was controlled at 45 $^{o}$C (Similar to biocide investigation chapter). Membrane fouling simulator prototype was monitoring the FCP increase, the membrane fouling, and spacer grid fouling percentage. Water samples were collected from feed tanks daily to monitor the microbiological quality by measuring ATP (similar as described in section 9.2). Moreover, the prototype response to dosing biocide 1.

Additionally, a scaling case study was conducted to evaluate the prototype image processing correctness to detect mineral scale fouling. A supersaturation $CaCO_3$ model solution was prepared using reagent grade mineral salts of $NaHCO_3$ and $CaCl_2{\bullet}2H_2O$. The model has 2.8 calcite S.I and the Calcium Carbonate Precipitation Potential (CCPP) was 1.478 grams $CaCO_3$/L water. The operating flow rate was maintained at 12 L/h. The feed tanks temperature was controlled at 25 $^{o}$C, and pH between 7.2 to 8.1. AS2 antiscalant was added in one line before starting the run to evaluate the scaling rate with and in the absence of antiscalant. Lastly, a combined fouling case study (Biofouling and scaling) similar to a real desalination station scenario was carried out to investigate the device capability to classify and distinguish between organic and inorganic fouling type. The study was initiated by tap water, fresh bacterial inoculum (Meiothermus bacteria), and nutrients. After one day opf operation, a supersaturated $CaCO_3$ model solution (Similar model solution in scaling case study) was introduced to feed tank. The temperature of feed tank connected to the device was controlled at 45 $^{o}$C, and pH between 6.4 to 7.6.

## 10.3 Results and discussion

Matching the measured and calculated pressure drop showed a similar trend between measured and calculated data at three different cross-linear velocities (Figure 52). However, the percent error was high at lower cross linear velocity (0.4 m/s). Therefore, the prototype was operated at 12 L/h (0.12 m/s) to increase the pressure drop range and obtain accurate measurements.

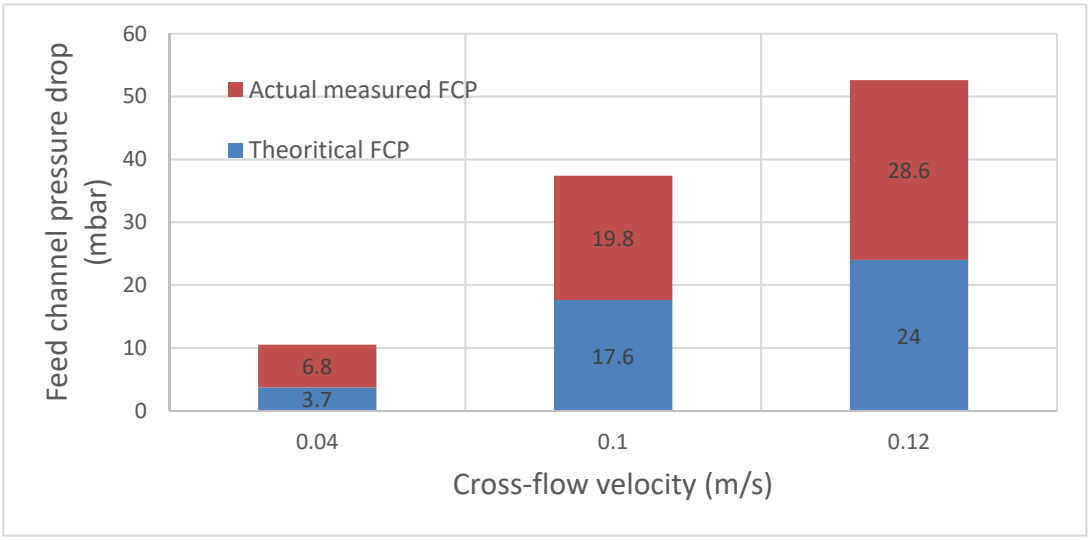


*Figure 52. The calculated and measured FCP against linear flow velocity.*

The first biofouling scenario was operated at 12 L/h (0.12 m/s). It has shown the unreliable detection of both spacer and membrane fouling. Additionally, the calculated fouling % was not directly connected to monitored FCP rise, especially when the fouling has reached log accumulation growth rate. Though, the image processing has correctly considered more than 80% of the fouling as organic particles. Figure 53 shows the inexact matching between FCP and fouling percentage (i.e. the FCP increase was not corresponding to the spacer fouling increase) in the first four days of the campaign, and delay detection of spacer fouling when the biofouling reached the log accumulation growth on the 9th operating day. Based on the obtained results, the image analysis algorithm was modified to detect the biofilm on spacer grid and membrane surface precisely.

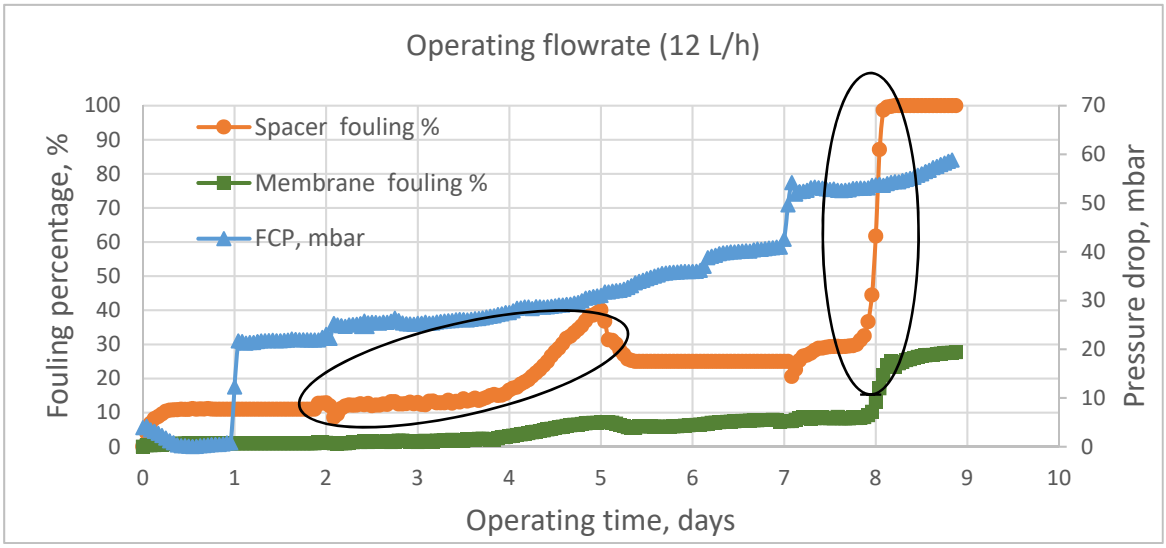


*Figure 53. The propagation of fouling percentage in the first campaign.*

In the second campaign, similar biofouling scenario was carried out, and the image analysis algorism was modified to correctly recognise and classify the fouling objects on the spacer net and membrane surface. Figure 54 illustrates the biomass development on the feed spacer channel and the spacer fouling percentage based on image analysis. Evidently, visual observation plays an important part to get closer attention on induction period of biofilm.

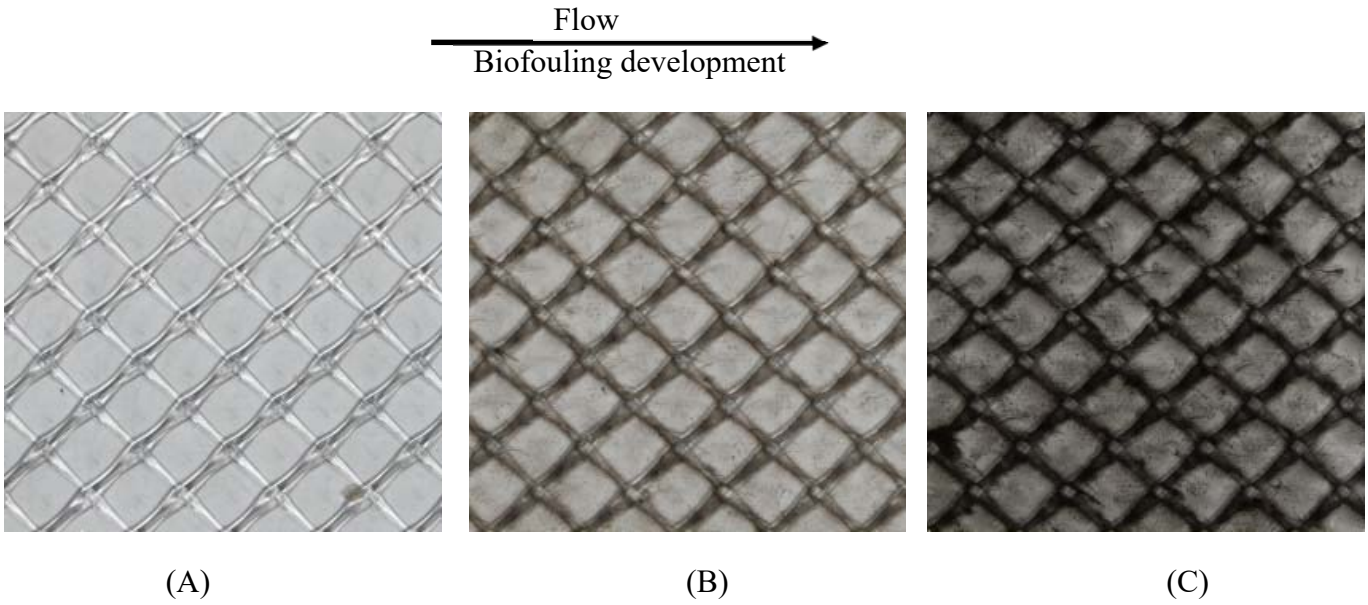


*Figure 54. Captured images from prototype transparent membrane cell (A) Initial images with clean spacer and membrane, (B) 60% spacer fouling, (C) 100% spacer fouling.*

The second primary objective was benchmarking the prototype results to standard MFS device. As described in section 6.3, conventional MFS device mainly monitored the FCP, to obtain an indication of biofilm buildup. On the other side, the prototype's high-resolution camera provides a continuous detection of biofilm induction phase besides monitoring the FCP. Accordingly, the third campaign's objective was to obtain a relation between FCP and biofilm development. It was carried out similar to previous two campaigns at flow rate 12 L/h. The results have shown that biofilm development started earlier than the FCP increased. Figure 55 shows the spacer fouling % increase and the FCP rise. As reviewed in section 6.3, the membrane operators recommended a corrective action based on 15 % increase in pressure drop as it indicated a biofilm growth. However, through visual observation and image analysis of spacer grid surface,

the prototype was able to detect the spacer fouling before the FCP increased 15% by 24 hours. In Figure 55, the black triangle represents 15 % FCP increase.

At the end of the test, a high dose of Biocide 1 was injected (5 ml/L) into the feed tank to determine the response of the system. The device detected a decrease in the spacer fouling by 9% and membrane fouling by 4% (Figure 55). Besides, the decline in the measured FCP. Consequently, the device is accurately responding to biocide addition.

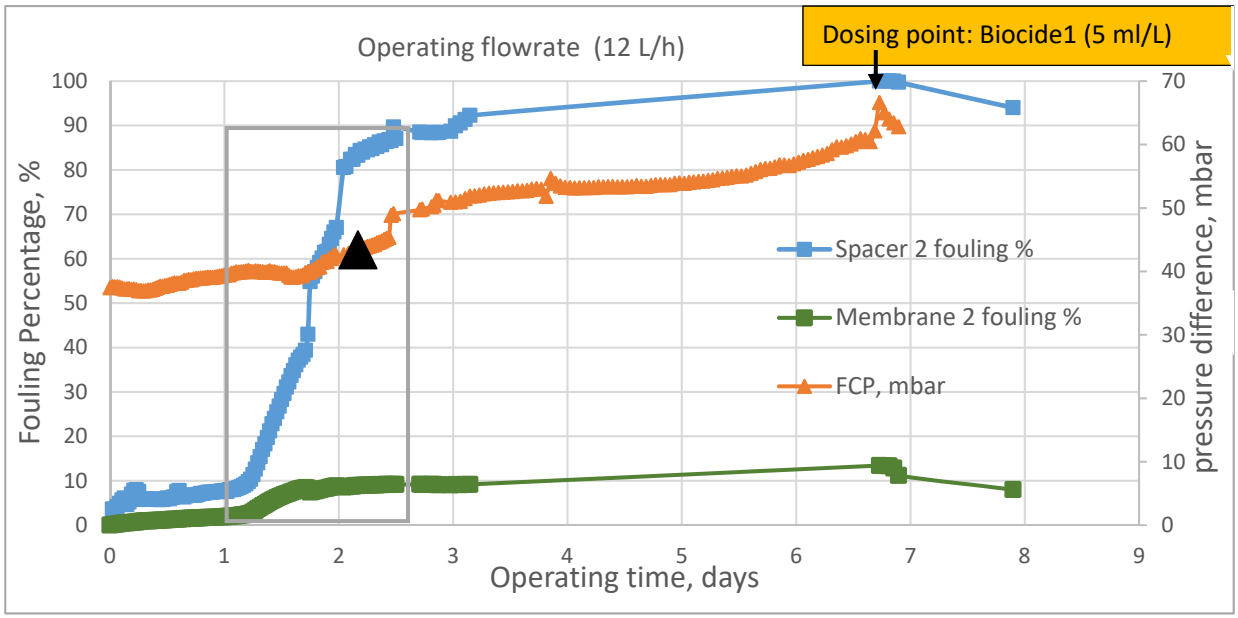


*Figure 55. The prototype third campaign output results.*

The scaling campaign was conducted to determine the system response to antiscalants addition and the detection of mineral scale nucleation and crystal growth on the spacer surface. The campaign showed positive results in term of online image processing to detect the scale formation (Figure 56). Besides, the prototype categorised the fouling as 70% inorganic fouling. Figure 57 A illustrates the mineral scaling on spacer grid in the initial state, Figure 57 B shows a captured image at the end of the test in the absence of antiscalant dose, and Figure 57 C is a captured image of antiscalant case.

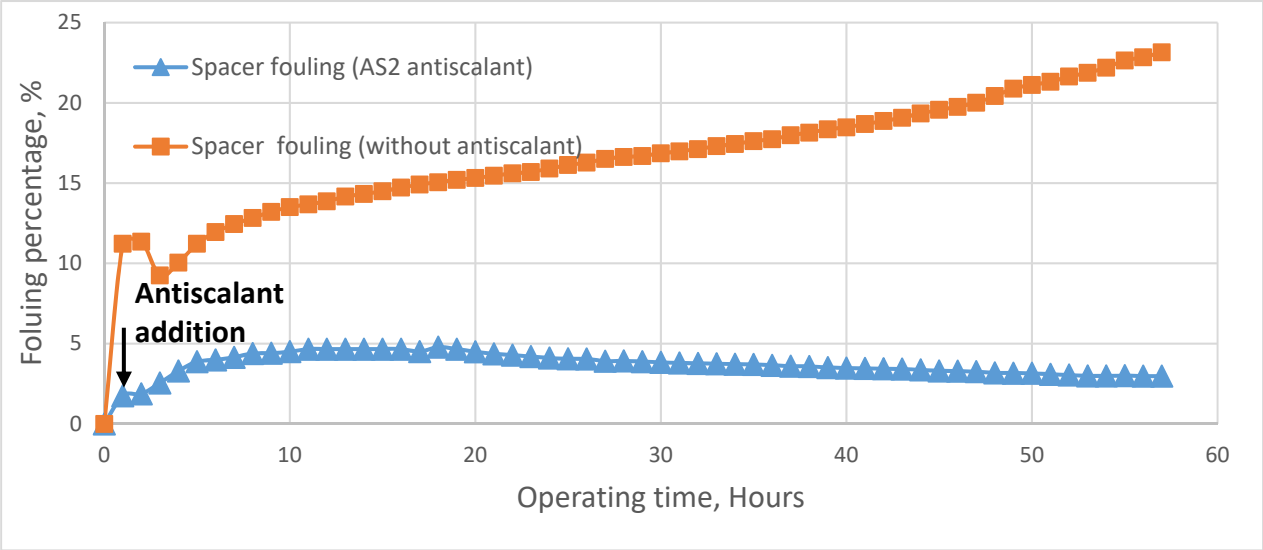


*Figure 56. The spacer fouling development in scaling campaign.*

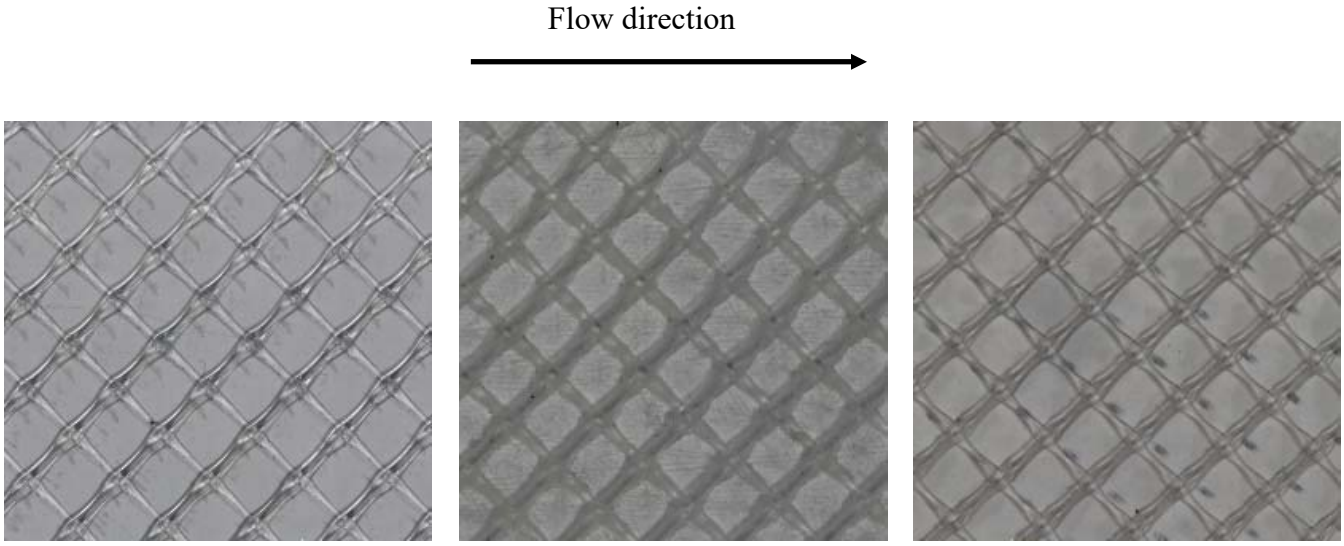


*Figure 57. Captured images from prototype transparent membrane cell (A) Initial images with clean spacer and membrane, (B) No antiscalant dose, (C) AS2 antiscalant case.*

The combined fouling has shown the device capabilities to distinguish between organic and inorganic fouling particulates. However, when the fouling reached a high fouling phase, it becomes challenging for the image processing algorithm to detect and classify the fouling nature correctly. Figure 58 illustrate the identified organic and inorganic fouling percentage and the high fouling region where the detection was inaccurate, and

Figure 59 shows a captured image on the fourth day of operation. Based on the experimental studies carried out and the achieved research objectives, the device can be classified as Level 2 device based on Flemming classification (described on page 15).

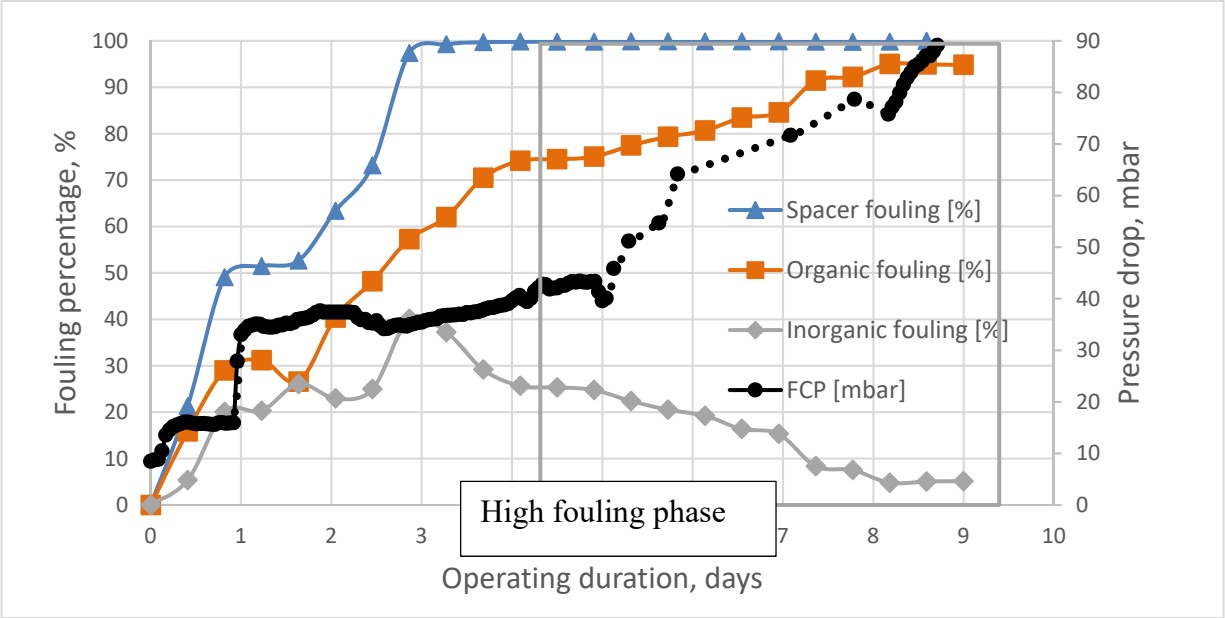


*Figure 58. The inorganic and organic fouling percentage in the combined fouling test.*

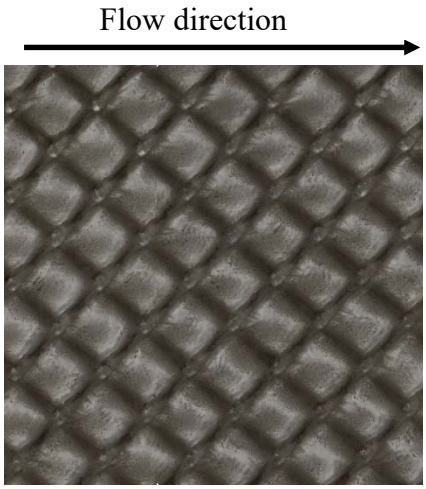


*Figure 59. Captured image at the fourth day of mixed case test.*

# 11.Conclusions and Recommendations

In this thesis, a study was conducted for increasing the permeate water recovery of membrane reverse osmosis (RO) desalination of brackish water. The research has assessed antiscalant efficiency against complex water chemistries (i.e. real feed water) instead of an individual component where there is the possibility of co-precipitation. Moreover, the formulation of antiscalant consisted of the mixture of different antiscalants selected for specific scale type and taking into account the selectivity of antiscalant mechanism. The study included ranking overall antiscalants effectiveness via the combination of bulk crystallisation studies and membrane scaling experiments. The results have shown that assessing antiscalant efficiency with model solutions have advantages over the antiscalant software models in terms of providing a full understanding of actual scale propensity (as calcite, gypsum, and silica scale formation) and effective antiscalant dose. In the last few years, the antiscalant research and development have engaged several studies to develop effective green scale inhibitors to substitute traditional antiscalants since water's eutrophic phenomenon became more serious. At present, novel green antiscalants are being developed for calcite and gypsum scale type.

The biofouling control study has shown that certain cationic biocide has a negative effect on the permeate production despite its positive impact on controlling biofouling. Therefore, membrane compatibility should be considered in advance. Moreover, the study has revealed that one single strategy has not been 100% successful. However, combining different approaches as operating conditions, biomass control and cleaning agents may be more effective than a single approach. The integral approach addresses the total membrane system starts from the feed water pretreatment.

The development of membrane monitoring prototype has shown positive outcomes in terms of the equipment accuracy for detecting fouling of the spacer grids and membrane surface in the early phase, the device response to chemical addition (biocide and antiscalants), and the device capability to classify and distinguish between organic and inorganic fouling type in combined fouling cases. Moreover, the protoype is suitable for ex-situ, real-time observations and requires small amounts of chemicals. However, based on operating the device, stable and accurate feed flows are needed to achieve constant biofilm growth and accurate pressure drop measurements.

## References


Accepta, 2016. Reverse Osmosis Chemicals | RO Membrane Systems,2017, http://www.accepta.com/water-treatment-chemicals-wastewater-effluent-treatment-products/reverse-osmosis-chemicals-ro-membranes.

Airey, D., Yao, S., Wu, J., Chen, V., Fane, A. G., Pope, J. M., 1998. An investigation of concentration polarization phenomena in membrane filtration of colloidal silica suspensions by NMR micro-imaging, Journal of Membrane Science 145(2), 145-158.

Altmann, J., Ripperger, S., 1997. Particle deposition and layer formation at the crossflow microfiltration, Journal of Membrane Science 124(1), 119-128.

American Water Chemicals, 2013. RO chemicals product list | American Water Chemicals,2016, http://www.membranechemicals.com/wp-content/uploads/2013/08/AWC_Chemical_Product_List.pdf.

Antony, A., Low, J. H., Gray, S., Childress, A. E., Le-Clech, P., Leslie, G., 2011. Scale formation and control in high pressure membrane water treatment systems: A review, Journal of Membrane Science 383(1–2), 1-16.

Armstrong, M. W., Gallego, S., Chesters, S. P., 2009. Cleaning clay from fouled membranes, Desalination and Water Treatment 10(1-3), 108-114.

Avista Technologies, 2017. Reverse Osmosis | Avista Technologies, Inc.2017, http://www.avistatech.com/reverse-osmosis.

Avista Technologies, I., 2016. Antiscalants | Avista Technologies, Inc.2017, http://www.avistatech.com/antiscalants.

Avlonitis, S. A., Kouroumbas, K., Vlachakis, N., 2003. Desalination and the Environment: Fresh Water for all Energy consumption and membrane replacement cost for seawater RO desalination plants, Desalination 157(1), 151-158.

Bacchin, P., 2004. A possible link between critical and limiting flux for colloidal systems: consideration of critical deposit formation along a membrane, Journal of Membrane Science 228(2), 237-241.

Bacchin, P., Aimar, P., Field, R. W., 2006. Critical and sustainable fluxes: Theory, experiments and applications, Journal of Membrane Science 281(1–2), 42-69.

Bannwarth, S., Darestani, M., Coster, H., Wessling, M., 2015. Characterization of hollow fiber membranes by impedance spectroscopy, Journal of Membrane Science 473, 318-326.

Bartels, C., Franks, R., Rybar, S., Schierach, M., Wilf, M., 2005. The effect of feed ionic strength on salt passage through reverse osmosis membranes, Desalination 184(1–3), 185-195.

Bhattacharya, S., Hwang, S., 1997. Concentration polarization, separation factor, and Peclet number in membrane processes, Journal of Membrane Science 132(1), 73-90.

Bucs, S. S., Valladares Linares, R., van Loosdrecht, M.,C.M., Kruithof, J. C., Vrouwenvelder, J. S., 2014. Impact of organic nutrient load on biomass accumulation, feed channel pressure drop increase and permeate flux decline in membrane systems, Water research 67(0), 227-242.

Camargo, J. A., Alonso, Á, 2006. Ecological and toxicological effects of inorganic nitrogen pollution in aquatic ecosystems: A global assessment, Environment international 32(6), 831-849.

Chai, G. -., Greenberg, A. R., Krantz, W. B., 2007. Ultrasound, gravimetric, and SEM studies of inorganic fouling in spiral-wound membrane modules, Desalination 208(1–3), 277-293.

Chen, J., Xu, L., Han, J., Su, M., Wu, Q., 2015. Synthesis of modified polyaspartic acid and evaluation of its scale inhibition and dispersion capacity, Desalination 358, 42-48.

Chen, V., Li, H., Fane, A. G., 2004. Non-invasive observation of synthetic membrane processes - A review of methods, Journal of Membrane Science 241(1), 23-44.

Chong, T. H., Wong, F. S., Fane, A. G., 2007. Fouling in reverse osmosis: Detection by non-invasive techniques, Desalination 204(1–3), 148-154.

Creber, S. A., Vrouwenvelder, J. S., van Loosdrecht, M.,C.M., Johns, M. L., 2010. Chemical cleaning of biofouling in reverse osmosis membranes evaluated using magnetic resonance imaging, Journal of Membrane Science 362(1-2), 202-210.

Crittenden, J. C., Trussell, R. R., Hand, D. W., 2012. MWH's Water Treatment : Principles and Design (3). Hoboken, US: Wiley.

Çulfaz, P. Z., Buetehorn, S., Utiu, L., Kueppers, M., Bluemich, B., Melin, T., Wessling, M., Lammertink, R. G. H., 2011. Fouling Behavior of Microstructured Hollow Fiber Membranes in Dead-End Filtrations: Critical Flux Determination and NMR Imaging of Particle Deposition, Langmuir 27(5), 1643-1652.

da Silva, M. K., Tessaro, I. C., Wada, K., 2006. Investigation of oxidative degradation of polyamide reverse osmosis membranes by monochloramine solutions, Journal of Membrane Science 282(1–2), 375-382.

DeJong, A. E., Hartel, R. W., 2016. Determination of sorbitol crystal content and crystallization rate using TD-NMR, Journal of Food Engineering 178, 117-123.

Dequest Italmatch chemicals, 2016. Reverse Osmosis & Thermal desalination | Welcome to Dequest,2017, http://www.dequest.com/sites/default/files/ITAL000002_Reverse-Osmosis-SPE-Antiscalant.pdf.

Dow chemicals, 2011. FILMTEC™ Reverse Osmosis Membranes Technical Manual, http://msdssearch.dow.com/PublishedLiteratureDOWCOM/dh_095b/0901b8038095b91d.pdf?filepath=/609-00071.pdf&fromPage=GetDoc 2017(9/6/2016).

Dreszer, C., Flemming, H. -., Zwijnenburg, A., Kruithof, J. C., Vrouwenvelder, J. S., 2014. Impact of biofilm accumulation on transmembrane and feed channel pressure drop: Effects of crossflow velocity, feed spacer and biodegradable nutrient, Water research 50, 200-211.

Ecolab, 2015. Scale Control Trends and Advances,2017, http://www.ecolab.com/~/media/Ecolab/Ecolab%20Home/Documents/DocumentLibrary/Brochures/Nalco%20WPS/PulpPaper/B346NW.pdf.

El-Dessouky, H. T., Ettouney, H. M., 2002a. Chapter 1 - Introduction, in: El-Dessouky, H. T., Ettouney, H. M. (Eds), Fundamentals of Salt Water Desalination. Amsterdam, Elsevier Science B.V., pp. 1-17.

El-Dessouky, H. T., Ettouney, H. M., 2002b. Chapter 7 - Reverse Osmosis, in: El-Dessouky, H. T., Ettouney, H. M. (Eds), Fundamentals of Salt Water Desalination. Amsterdam, Elsevier Science B.V., pp. 409-437.

El-Dessouky, H. T., Ettouney, H. M., 2002c. Chapter 8 - Reverse Osmosis Feed Treatment, Biofouling, and Membrane Cleaning, in: El-Dessouky, H. T., Ettouney, H. M. (Eds), Fundamentals of Salt Water Desalination. Amsterdam, Elsevier Science B.V., pp. 439-452.

Fane, A. G., Wang, R., Jia, Y., 2011. Membrane Technology: Past, Present and Future, in: Wang, L. K., Chen, J. P., Hung, Y., Shammas, N. K. (Eds), Membrane and Desalination Technologies. Totowa, NJ, Humana Press, pp. 1-45.

Fazel, M., Chesters, S., 2015. RO membrane cleaning using microbubbles at 6,800 m3/d wastewater RO plant in UAE, Desalination and Water Treatment 55(12), 3358-3366.

Ferguson, R. J., Ferguson, B. R., Stancavage, R. F., 2011. Modeling Scale Formation and Optimizing Scale Inhibitor Dosages in Membrane Systems, Conference at the AWWA Membrane Technology Conference, http://www.frenchcreeksoftware.com/awwa-2011/modeling_scale_formation_and_optimizing_scale_inhibitor_dosages_in_membrane_systems.pdf .

Flemming, H. -., 2003. Role and levels of real-time monitoring for successful anti-fouling strategies - an overview, Water Science and Technology 47(5), 1-8.

Flemming, H., Neu, T. R., Wozniak, D. J., 2007. The EPS Matrix: The “House of Biofilm Cells”, Journal of Bacteriology 189(22), 7945-7947.

French creek software, I., 2017. hyd-RO-dose® - Reverse Osmosis Scale & Inhibitor Modeling,2017, http://www.frenchcreeksoftware.com/hyd-RO-dose/#sca.

Fridjonsson, E. O., Creber, S. A., Vrouwenvelder, J. S., Johns, M. L., 2015. Magnetic resonance signal moment determination using the Earth's magnetic field, Journal of Magnetic Resonance 252, 145-150.

Fritzmann, C., Löwenberg, J., Wintgens, T., Melin, T., 2007. State-of-the-art of reverse osmosis desalination, Desalination 216(1), 1-76.

Gaucher, C., Legentilhomme, P., Jaouen, P., Comiti, J., Pruvost, J., 2002. Hydrodynamics study in a plane ultrafiltration module using an electrochemical method and particle image velocimetry visualization, Experiments in Fluids 32(3), 283-293.

Genesys International, 2016. Membrane anti-scalants antiscalant chemicals,2017(1/6/2017), http://www.genesysro.com/membrane-anti-scalants-antiscalant-chemicals.php.

Ghani, S., Al-Deffeeri, N. S., 2010. Impacts of different antiscalant dosing rates and their thermal performance in Multi Stage Flash (MSF) distiller in Kuwait, Desalination 250(1), 463-472.

Graf von der Schulenburg D. A., Vrouwenvelder, J. S., Creber, S. A., van Loosdrecht, M. C. M., Johns, M. L., 2008. Nuclear magnetic resonance microscopy studies of membrane biofouling, Journal of Membrane Science 323(1), 37-44.

Gu, H., Bartman, A. R., Uchymiak, M., Christofides, P. D., Cohen, Y., 2013. Self-adaptive feed flow reversal operation of reverse osmosis desalination, Desalination 308, 63-72.

Gu, T., Liu, X., Chai, W., Li, B., Sun, H., 2014. A preliminary research on polyvinyl alcohol hydrogel: A slowly-released anti-corrosion and scale inhibitor, Journal of Petroleum Science and Engineering 122, 453-457.

Hoek, E. M. V., Tanuwidjaja, D., 2011. High pressure sensors for detecting membrane fouling, PCT Int.Appl. (WO2011163278A2), 77pp.

Kang, G., Gao, C., Chen, W., Jie, X., Cao, Y., Yuan, Q., 2007. Study on hypochlorite degradation of aromatic polyamide reverse osmosis membrane, Journal of Membrane Science 300(1–2), 165-171.

Karabelas, A. J., Mitrouli, S., Gragopoulos, J., Karanasiou, A., Isaias, N. P., Al Rammah, A. S., 2014. Monitoring the membrane scaling propensity of retentate in reverse osmosis desalination plants, IDA Journal of Desalination and Water Reuse 6(2), 80-92.

Kavanagh, J. M., Hussain, S., Chilcott, T. C., Coster, H. G. L., 2009. Fouling of reverse osmosis membranes using electrical impedance spectroscopy: Measurements and simulations, Desalination 236(1), 187-193.

Kemira Oyj, 2016a. Kemira membrane program - Efficient water treatment with membrane protection,2017, http://www.kemira.com/Materials/Desalination-brochure-web-kemira.pdf.

Kemira Oyj, 2016b. Reducing silica scale on desalination membranes - Kemira,2017, http://www.kemira.com/SiteCollectionDocuments/newsroom/whats-new/2016/Kemira-KemGuard-Antiscalant-Membrane-Desalination.pdf.

Kennedy, M. D., Kamanyi, J., RodrÃguez, S. G. S., Lee, N. H., Schippers, J. C., Amy, G., 2008. Water Treatment by Microfiltration and Ultrafiltration, 131-170.

Lee, S. H., Choi, J. S., Oh, H. J., Choi, B. B., Kim, J. G., 2011. Method for monitoring membrane contamination potential of reverse osmosis membrane of seawater desalination apparatus in real time, Repub.Korean Kongkae Taeho Kongbo (KR2011067744A), 10pp.

Lee, S., Lee, C., 2000. Effect of operating conditions on CaSO4 scale formation mechanism in nanofiltration for water softening, Water research 34(15), 3854-3866.

Li, H., Fane, A. G., Coster, H. G. L., Vigneswaran, S., 1998. Direct observation of particle deposition on the membrane surface during crossflow microfiltration, Journal of Membrane Science 149(1), 83-97.

Li, J., Koen, L. J., Hallbauer, D. K., Lorenzen, L., Sanderson, R. D., 2005. Interpretation of calcium sulfate deposition on reverse osmosis membranes using ultrasonic measurements and a simplified model, Desalination 186(1–3), 227-241.

Liu, H., Fang, H. H. P., 2002. Extraction of extracellular polymeric substances (EPS) of sludges, Journal of Biotechnology 95(3), 249-256.

Liu, Z., Sun, Y., Zhou, X., Wu, T., Tian, Y., Wang, Y., 2011. Synthesis and scale inhibitor performance of polyaspartic acid, Journal of Environmental Sciences 23, S153-S155.

M. Gamal Khedr, 2012. Processing of Desalination Reject Brine for Optimization of Process Efficiency, Cost Effectiveness and Environmental Safety, in: Anonymous Advancing Desalination. Rijeka, InTech, pp. Ch. 0.

Matin, A., Khan, Z., Zaidi, S. M. J., Boyce, M. C., 2011. Biofouling in reverse osmosis membranes for seawater desalination: Phenomena and prevention, Desalination 281, 1-16.

Melin, T., Rautenbach, R., 2007. Membranverfahren: Grundlagen Der Modul-Und Anlagenauslegung. : Springer-Verlag.

Miller, J. E., 2003. Review of water resources and desalination technologies, Sandia National Labs Unlimited Release Report SAND-2003-0800 .

Musale, D. A., 2010. Method for inhibiting scale formation and deposition in membrane systems via the use of an aa - amps copolymer, PCT Int.Appl. (WO2010028196A1), 14pp.; Chemical Indexing Equivalent to 152:342985 (US).

Nivens, D. E., Palmer, R. J., White, D. C., 1995. Continuous nondestructive monitoring of microbial biofilms: A review of analytical techniques, Journal of industrial microbiology 15(4), 263-276.

Oh, B. S., Kim, M. J., Lee, S. H., Kye, J. I., Kim, J. D., 2013. Apparatus for monitoring fouling of reverse osmosis membrane for seawater desalination at real time, Repub.Korean Kongkae Taeho Kongbo (KR2013085220A), 17pp.

Parkhurst, D. L., Appelo, C., 2013. Description of input and examples for PHREEQC version 3—a computer program for speciation, batch-reaction, one-dimensional transport, and inverse geochemical calculations, US geological survey techniques and methods, book 6, 497.

Peña, N., Gallego, S., del Vigo, F., Chesters, S. P., 2012. Evaluating impact of fouling on reverse osmosis membranes performance, Desalination and Water Treatment 3994(April 2015), 1-11.

Pezeshk, N., Narbaitz, R. M., 2012. More fouling resistant modified PVDF ultrafiltration membranes for water treatment, Desalination 287, 247-254.

Ren, J., Wang, R., 2011. Preparation of Polymeric Membranes, in: Wang, L. K., Chen, J. P., Hung, Y., Shammas, N. K. (Eds), Membrane and Desalination Technologies. Totowa, NJ, Humana Press, pp. 47-100.

Sanderson, R., Li, J., Koen, L. J., Lorenzen, L., 2002. Ultrasonic time-domain reflectometry as a non-destructive instrumental visualization technique to monitor inorganic fouling and cleaning on reverse osmosis membranes, Journal of Membrane Science 207(1), 105-117.

Schock, G., Miquel, A., 1987. Mass transfer and pressure loss in spiral wound modules, Desalination 64, 339-352.

Shih, W., Rahardianto, A., Lee, R., Cohen, Y., 2005. Morphometric characterization of calcium sulfate dihydrate (gypsum) scale on reverse osmosis membranes, Journal of Membrane Science 252(1–2), 253-263.

Sim, L. N., Wang, Z. J., Gu, J., Coster, H. G. L., Fane, A. G., 2013. Detection of reverse osmosis membrane fouling with silica, bovine serum albumin and their mixture using in-situ electrical impedance spectroscopy, Journal of Membrane Science 443, 45-53.

Song, L., Tay, K. G., 2011. Advanced Membrane Fouling Characterization in Full-Scale Reverse Osmosis Processes, in: Wang, L. K., Chen, J. P., Hung, Y., Shammas, N. K. (Eds), Membrane and Desalination Technologies. Totowa, NJ, Humana Press, pp. 101-134.

Speth, T. F., Gusses, A. M., Scott Summers, R., 2000. Evaluation of nanofiltration pretreatments for flux loss control, Desalination 130(1), 31-44.

Strathmann, H., 2010. Electrodialysis, a mature technology with a multitude of new applications, Desalination 264(3), 268-288.

Subramani, A., Hoek, E. M. V., 2008. Direct observation of initial microbial deposition onto reverse osmosis and nanofiltration membranes, Journal of Membrane Science 319(1-2), 111-125.

Suwarno, S. R., Chen, X., Chong, T. H., McDougald, D., Cohen, Y., Rice, S. A., Fane, A. G., 2014. Biofouling in reverse osmosis processes: The roles of flux, crossflow velocity and concentration polarization in biofilm development, Journal of Membrane Science 467, 116-125.

Taheri, A. H., Sim, S. T. V., Sim, L. N., Chong, T. H., Krantz, W. B., Fane, A. G., 2013. Development of a new technique to predict reverse osmosis fouling, Journal of Membrane Science 448, 12-22.

Tsiourtis, N. X., 2001. Desalination and the environment, Desalination 141(3), 223-236.

Uchymiak, M., Bartman, A. R., Daltrophe, N., Weissman, M., Gilron, J., Christofides, P. D., Kaiser, W. J., Cohen, Y., 2009. Brackish water reverse osmosis (BWRO) operation in feed flow reversal mode using an ex situ scale observation detector (EXSOD), Journal of Membrane Science 341(1–2), 60-66.

Uchymiak, M., Rahardianto, A., Lyster, E., Glater, J., Cohen, Y., 2007. A novel RO ex situ scale observation detector (EXSOD) for mineral scale characterization and early detection, Journal of Membrane Science 291(1–2), 86-95.

Valladares Linares R., Fortunato, L., Farhat, N. M., Bucs, S. S., Staal, M., Fridjonsson, E. O., Johns, M. L., Vrouwenvelder, J. S., Leiknes, T., 2016. Mini-review: novel non-destructive in situ biofilm characterization techniques in membrane systems, Desalination and Water Treatment 3994(June), 1-8.

Vilker, V. L., Colton, C. K., Smith, K. A., 1981. Concentration polarization in protein ultrafiltration. Part I: An optical shadowgraph technique for measuring concenration profiles near a solution-membrane interface, AIChE Journal 27(4), 632-636.

Voutchkov, N., Semiat, R., 2008. Seawater Desalination, 47-86.

Vrouwenvelder, J. S., Hinrichs, C., Van der Meer,W.G.J., Van Loosdrecht,M.C.M., Kruithof, J. C., 2009a. Pressure drop increase by biofilm accumulation in spiral wound RO and NF membrane systems: role of substrate concentration, flow velocity, substrate load and flow direction, Biofouling 25(6), 543-555.

Vrouwenvelder, J. S., Buiter, J., Riviere, M., van der Meer, W.,G.J., van Loosdrecht, M.,C.M., Kruithof, J. C., 2010a. Impact of flow regime on pressure drop increase and

biomass accumulation and morphology in membrane systems, Water research 44(3), 689-702.

Vrouwenvelder, J. S., Graf von der Schulenburg, D. A., Kruithof, J. C., Johns, M. L., van Loosdrecht, M. C. M., 2009b. Biofouling of spiral-wound nanofiltration and reverse osmosis membranes: A feed spacer problem, Water research 43(3), 583-594.

Vrouwenvelder, J. S., Hinrichs, C., Sun, A. R., Royer, F., van Paassen, J. A. M., Bakker, S. M., van der Meer, W. G. J., Kruithof, J. C., van Loosdrecht, M. C. M., 2008. Monitoring and control of biofouling in nanofiltration and reverse osmosis membranes, Water Science and Technology: Water Supply 8(4), 449-458.

Vrouwenvelder, J. S., Kruithof, J. C., Van Loosdrecht, M.,C.M., 2010b. Integrated approach for biofouling control, Water Science and Technology 62(11), 2477-2490.

Vrouwenvelder, J. S., van Loosdrecht, M.,C.M., Kruithof, J. C., 2011. Early warning of biofouling in spiral wound nanofiltration and reverse osmosis membranes, Desalination 265(1-3), 206-212.

Vrouwenvelder, J. S., van Paassen, J.,A.M., Wessels, L. P., van Dam, A. F., Bakker, S. M., 2006. The Membrane Fouling Simulator: A practical tool for fouling prediction and control, Journal of Membrane Science 281(1-2), 316-324.

Vrouwenvelder, J. S., van Paassen, J. A. M., Kruithof, J. C., van Loosdrecht, M. C. M., 2009c. Sensitive pressure drop measurements of individual lead membrane elements for accurate early biofouling detection, Journal of Membrane Science 338(1–2), 92-99.

Yu, J., Baek, Y., Yoon, H., Yoon, J., 2013. New disinfectant to control biofouling of polyamide reverse osmosis membrane, Journal of Membrane Science 427, 30-36.

Zhang, W., Ethier, C. R., 2001. Direct pressure measurements in a hyaluronan ultrafiltration concentration polarization layer, Colloids and Surfaces A: Physicochemical and Engineering Aspects 180(1–2), 63-73.

Zinn, M. S., Kirkegaard, R. D., Palmer Jr., R. J., White, D. C., 1999. Laminar flow chamber for continuous monitoring of biofilm formation and succession, Methods in enzymology 310, 224-232.

# Appendices

**Appendix A: List of antiscalants products from chemical supplier.**

**Appendix B: List of biocides products from chemical supplier.**

**Appendix C: List of cleaning chemicals products form chemical supplier.**

## Appendix A: List of antiscalants products

Table A-1: Avista company antiscalants

| Company | Product name | Calcium Carbonate | Calcium Sulfate | Calcium phosphate | Barium Sulfate | Strontium Sulfate | Calcium Fluoride | Silica | Iron/ Manganese | Appearance | pH | Specific gravity |
|---|---|---|---|---|---|---|---|---|---|---|---|---|
| | | **($CaCO_3$)** | **($CaSO_4$)** | **($Ca_3(PO_4)_2$)** | **($BaSO_4$)** | **($SrSO_4$)** | **($CaF_2$)** | **($SiO_2$)** | | | | |
| Avista | Vitec 1000 (Non-phosphorus Containing) | X | X | - | X | X | X | - | - | Clear liquid | (10% solution) : 3.0 - 5.0 | (@ 20°C): 1.15 - 1.25 |
| | Vitec 2000 | X | X | - | X | X | X | X | - | Amber to light yellow | 4.5-5.5 | (@20°C): 1.1-1.2 |
| | Vitec 3000 (Wide Spectrum Inhibitor) | X | X | - | X | X | X | X | - | Clear, amber liquid | 10.7-11.8 | (@25°C): 1.2-1.3 |
| | Vitec 4000 | X | X | - | X | X | X | X | - | Clear, amber liquid | 4.5-6.5 | (@25°C): 1.1-1.2 |
| | Vitec 5000 (Municipal or Potable Drinking Water) | X | X | - | X | X | X | X | - | Light amber liquid | 2.0-3.0 | (@ 20°C): 1.12-1.22 |
| | Vitec 5100 (Wide Spectrum Inhibitor) | X | X | - | X | X | X | X | - | Clear, amber liquid | (2% solution) 5.0-6.5 | (@25°C): 1.05 - 1.15 |
| | Vitec 7000 (Coagulant Polymer Compatible) | X | X | - | X | X | X | X | - | Clear, amber liquid | 5.0-7.0 | (@ 20°C): 1.15-1.25 |
| | Vitec 8200 Green (Free of phosphate and phosphonate) | X | X | - | X | X | X | X | - | Colorless to light amber liquid | 10.5-11.5 | (@ 20°C): 1.15-1.20 |

| | | | | | |
|---|---|---|---|---|---|
| X | Effective | - | Not effective | NA | No available information |

Table A-2: Genesys International company antiscalants

| Company | Product -me | Calcium Carbonate **($CaCO_3$)** | Calcium Sulfate **($CaSO_4$)** | Calcium phosphate **($Ca_3(PO_4)_2$)** | Barium Sulfate **($BaSO_4$)** | Strontium Sulfate **($SrSO_4$)** | Calcium Fluoride **($CaF_2$)** | Silica **($SiO_2$)** | Iron/ Manganese | Appearance | pH | Specific gravity |
|---|---|---|---|---|---|---|---|---|---|---|---|---|
| Genesys International | Genesys LF | X | X | X | X | X | - | X | X | straw coloured liquid | 9.8 - 10.2 | 1.34 - 1.37 |
| | Genesys LS | X | X | X | X | X | - | X | X | pale coloured liquid | 9.7 – 10.3 | 1.08 – 1.11 |
| | Genesys SW | X | X | X | - | - | - | - | - | pale yellow liquid | 8.3 – 8.7 | 1.15 – 1.17 |
| | Genesys CAS | X | X | - | X | X | - | X | X | pale clear liquid | 8.3 – 8.7 | 1.31 – 1.33 |
| | Genesys MG | X | X | X | X | X | - | X | X | amber liquid | 8.0 – 8.5 | 1.24 – 1.26 |
| | Genesys LF | X | X | X | X | X | - | X | X | straw coloured liquid | 9.8 - 10.2 | 1.34 - 1.37 |
| | Genesys SI | X | X | X | X | X | - | X | X | pale amber liquid | 9.8 – 10.2 | 1.13 – 1.17 |
| | Genesys PHO | X | X | X | X | X | - | X | - | pale clear liquid | 6.0 – 6.4 | 1.14 – 1.16 |
| | Genesys RC (Magnesium hydroxide) | X | X | X | X | X | - | - | X | pale liquid | 10.7 – 11.3 | 1.08 – 1.12 |
| | Genesys WB | X | X | X | X | X | - | - | X | colourless liquid | 6.0 - 6.5 | 1.09 - 1.13 |
| | Genesys MP | X | X | X | X | X | - | X | X | straw coloured liquid | 9.8 - 10.2 | 1.28 - 1.30 |

| | | | | | |
|---|---|---|---|---|---|
| X | Effective | - | Not effective | NA | No available information |

Table A-3: American Water Chemicals (AWC) company antiscalants

| Company | Product name | Calcium Carbonate **($CaCO_3$)** | Calcium Sulfate **($CaSO_4$)** | Calcium phosphate **($Ca_3(PO_4)_2$)** | Barium Sulfate **($BaSO_4$)** | Strontium Sulfate **($SrSO_4$)** | Calcium Fluoride **($CaF_2$)** | Silica **($SiO_2$)** | Iron/ Manganese | Appearance | pH | Specific gravity |
|---|---|---|---|---|---|---|---|---|---|---|---|---|
| American Water Chemicals (AWC) | AWC A-102 ULTRA | X | X | X | X | X | X | X | - | Clear colorless to yellow liquid | 3 – 4 | 1.10 ± 0.05 |
| | AWC A-101 | - | X | - | X | X | - | - | - | Clear colorless to light yellow liquid | 4 – 6 | 1.20 ± 0.05 |
| | AWC A-102 C8X | X | X | X | X | X | X | X | - | Clear colorless to light yellow liquid | < 2.0 | 1.40 ± 0.1 |
| | AWC A-102 PLUS | X | X | X | X | X | X | - | - | Clear colorless to light yellow liquid | 3 – 4 | 1.10 ± 0.05 |
| | AWC A-103 | X | X | X | X | X | X | - | - | Clear colorless to yellow liquid | 2 – 3 | 1.21 ± 0.05 |
| | AWC A-104 | X | X | - | X | X | - | - | - | Clear colorless to yellow liquid | 3 – 5 | 1.10 ± 0.05 |
| | AWC A-105 | X | X | X | - | X | X | - | X | Clear colorless to yellow liquid | 1 – 2 | 1.12 ± 0.05 |
| | AWC A-108 | X | X | X | X | X | - | X | - | Clear colorless to yellow liquid | < 2.0 | 1.30 ± 0.05 |
| | AWC A-108Fe (fully biodegradable) | X | X | X | X | X | - | X | X | Pale yellow liquid | < 2.0 | 1.35 ± 0.1 |
| | AWC A-109 | X | X | - | X | X | - | - | X | Clear light yellow to amber liquid | 2.0 ± 0.05 | 1.25 ± 0.05 |
| | AWC A-110 | X | X | X | X | X | X | X | X | Clear colorless to light yellow liquid | < 2 | 1.25 ± 0.05 |
| | AWC A-111 PLUS | X | X | - | X | X | - | X | - | Clear colorless to light yellow liquid | 3.0 – 5.0 | 1.02 ± 0.05 |
| | Ultratek 11X | X | X | - | X | X | - | X | - | Clear colorless to light yellow liquid | 3.0 – 5.0 | 1.20 ± 0.05 |

| X | Effective | - | Not effective | NA | No available information |
|---|---|---|---|---|---|

Table A-4: Accepta, Italmatch, and BWA companies' antiscalants

| Company | Product name | Calcium Carbonate **($CaCO_3$)** | Calcium Sulfate **($CaSO_4$)** | Calcium phosphate **($Ca_3(PO_4)_2$)** | Barium Sulfate **($BaSO_4$)** | Strontium Sulfate **($SrSO_4$)** | Calcium Fluoride **($CaF_2$)** | Silica **($SiO_2$)** | Iron/ Manganese | Appearance | pH | Specific gravity |
|---|---|---|---|---|---|---|---|---|---|---|---|---|
| Accepta | Accepta 2651 | X | X | X | - | - | X | - | X | Clear, pale yellow | 10.5 @25 ºC | 1.35 @20 C |
| | Accepta 2091 | X | X | X | - | - | - | X | - | Amber | 9.2 - 10.2 | 1.22 (15.6 °C) |
| DEQUEST® Italmatch chemicals | SPE 0001 | X | - | - | - | - | X | - | - | NA | NA | NA |
| | SPE 0106 | X | X | - | - | - | X | - | - | NA | NA | NA |
| | SPE 0107 | X | - | - | - | - | X | - | X | NA | NA | NA |
| | SPE 0108 | - | - | X | X | X | - | X | X | NA | NA | NA |
| | SPE 0109 | - | - | X | X | X | - | X | X | NA | NA | NA |
| | SPE 0109 POT | - | - | X | X | X | - | X | X | NA | NA | NA |
| | SPE 0111 | X | - | - | - | - | X | - | - | NA | NA | NA |
| | SPE 0112 | X | - | - | - | - | X | - | - | NA | NA | NA |
| | SPE 0125 | X | - | - | - | - | X | - | - | NA | NA | NA |
| BWA, water Additives | Flocon® 135 | Scale inhibitor for units operating at high recovery | | | | | | | | Pale yellow liquid | 3.5 to 4.5 | (@ 20°C): 1.13 to 1.18 |
| | Flocon® 190 | Non polymeric inorganic scale inhibitor | | | | | | | | Colourless to pale yellow liquid | > 10 | (@ 20°C): 1.22 to 1.32 |
| | Flocon® 260 | Scale inhibitor, antifoulant for unit operating at high recovery | | | | | | | | Pale yellow liquid | < 2 | (@ 20°C): 1.14 to 1.165 |
| | Flocon® Plus N | Inorganic scale inhibitor for salt water reverse osmosis (SWRO) | | | | | | | | Clear amber liquid | 8.0 to 8.5 | (@ 20°C): 1.10 to 1.15 |

| | | | | | |
|---|---|---|---|---|---|
| X | Effective | - | Not effective | NA | No available information |

Table A-5: Kemira company antiscalants

| Company | Product name | Calcium Carbonate | Calcium Sulfate | Calcium phosphate | Barium Sulfate | Strontium Sulfate | Calcium Fluoride | Silica | Iron/ |
|---|---|---|---|---|---|---|---|---|---|
| | | **($CaCO_3$)** | **($CaSO_4$)** | **($Ca_3(PO_4)_2$)** | **($BaSO_4$)** | **($SrSO_4$)** | **($CaF_2$)** | **($SiO_2$)** | Manganese |
| Kemira | KemGuard 5800 | - | X | - | X | X | NA | - | X |
| | KemGuard 5804 E | X | X | - | X | X | NA | - | - |
| | KemGuard 5811 | X | X | - | X | X | NA | - | - |
| | KemGuard 5835 | X | X | - | X | X | NA | - | - |
| | KemGuard 5840 | - | - | X | - | - | NA | X | X |
| | KemGuard 5876 | X | X | - | X | X | NA | - | X |
| | KemGuard 5853 | - | X | - | X | X | NA | - | X |
| | KemGuard 5892 (Biodegredable) | X | X | - | X | X | NA | - | - |
| | KemGuard PA-100 | X | X | - | - | - | NA | - | - |
| | KemGuard PA-105 | - | X | - | - | - | NA | - | - |
| | KemGuard PB 10211 | X | X | - | X | X | NA | - | - |
| | KemGuard PB 20412 | X | X | X | - | - | NA | X | X |

| X | Effective | - | Not effective | NA | No available information |
|---|---|---|---|---|---|

## Appendix B: List of biocides products

| Company | Product name | Contaminant | | | Method of use | | | Appearance | pH | Specific gravity |
|---|---|---|---|---|---|---|---|---|---|---|
| | | Bacteria | Fungi | Algae | Clean-in-place (CIP) | Continuous Dosing | Shock Treatment | | | |
| Avista | RoCide DB5 | X | X | X | X | | X | Clear yellow liquid | 1.5-5.0 | (@20°C): 1.1-1.2 |
| | RoCide DB20 | X | X | X | X | | X | Clear, light yellow to amber liquid | 2.0-5.0 | ($H_20$ = 1): 1.2-1.3 |
| | RoCide IS2 | X | X | X | | X | | Clear, pale green liquid | 1.5-5.0 | (@25°C): 1.0-1.1 |
| | | | | | | | | | | |
| BWA, water Additives | Flocon® B38, Biocide for biofilm growth | X | X | X | | | | Colorless to amber liquid | - | (@25°C): 1.04 to 1.08 |
| | | | | | | | | | | |
| GE Power, Water & Process Technologies | BioMate* Biocides for Membrane Systems | | | | | | | | | |
| | | | | | | | | | | |
| Genesys International | Genesol 30 | | | | | | | pale amber liquid | 1.5 – 5.0 | 1.20 - 1.30 |
| | Genesol 32 | | | | | | | colourless/yellow liquid | 3.0 – 5.0 | 1.04 - 1.09 |
| | Genefloc ABF | | | | | | | colourless liquid | 4.0 – 5.0 | 1.00 – 1.10 |
| | | | | | | | | | | |
| American Water Chemicals (AWC) | AWC C-226 | | | | | | | White to tan powder | 11 – 12 | |
| | AWC C-227 | | | | | | | White to tan powder | 11 – 12 | |
| | AWC C-230 | | | | | | | Clear colorless liquid | 11 – 12 | 1.04 ± 0.05 |

## Appendix C: List of cleaning chemicals products

| Company | Product name | Appearance | pH | Specific gravity |
|---|---|---|---|---|
| Avista | AvistaClean L011 | Colorless to pale yellow liquid | (2% solution): 10.5-11.8 | (@25°C): 1.05-1.15 |
| | AvistaClean P312 | White powder | (2% solution): 11.9-12.4 | |
| | AvistaClean P611 Green | White powder | (2% solution): 10.8-11.3 | |
| | RoClean L211 | Clear, colorless to amber liquid | (2% solution): 10.5-11.5 | (@25°C): 1.05-1.20 |
| | RoClean L212 Green | Clear, colorless to amber liquid | (2% solution): 11.7-12.7 | (@25°C): 1.1-1.2 |
| | RoClean L403 | Clear, colorless to amber liquid | (2% solution): 2.5-3.5 | (@25°C): 1.3-1.4 |
| | RoClean L404 Green | Pale yellow liquid | (2% solution): 3.5-4.5 | (@25°C): 1.15-1.25 |
| | RoClean L607 | Clear, amber liquid | (2% solution): 7.0-8.0 | (@25°C): 1.1 ± 0.05 |
| | RoClean L811 | Clear, to amber liquid | (2% solution): 10.0-11.5 | (@25°C): 1.2-1.3 |
| | RoClean P112 | White powder | (1% solution): 12.0-12.9 | |
| | RoClean P303 | White powder | (2% solution): 2.4-3.8 | |
| | RoClean P703 | White powder | (2% solution): 2.5-3.5 | |
| | RoClean P911 | White powder | (4.5% solution): 11.5-12.8 | |
| Genesys International | Genesol 34 | colourless to pale liquid | 11.0 - 11.5 | 1.33 - 1.35 |
| | Genesol 36 | pale yellow liquid | 7.0 - 9.0 | 1.01 - 1.05 |
| | Genesol 37 | pale liquid | <1 | 1.30 - 1.34 |
| | Genesol 38 | colourless liquid | 3.5 – 4.0 | 1.17 - 1.20 |
| | Genesol 40 | pale liquid | > 13.0 | 1.12 - 1.24 |
| | Genesol 50 | pale yellow liquid | 13 | 1.29 - 1.31 |
| | Genesol 61 | pale liquid | 7.0 – 7.8 | 1.09 – 1.12 |
| | Genesol 701 | white powder | (1% solution): 2.5 | 1.04 g/cm2 |
| | Genesol 703 | white powder | 11.5 -12.5 | 1.3 - 1.4 g/cm2 |
| | Genesol 704 | white powder | (1% solution): 12 | 1.3 - 1.4 g/cm2 |

| | | | | |
|---|---|---|---|---|
| American Water Chemicals (AWC) | AWC C-205 | White crystalline powder | <2 | |
| | AWC C-209 | White crystalline powder | 2 – 3 | |
| | AWC C-225 | White to tan powder | 4 – 5 | |
| | AWC C-234 | Clear colorless to light yellow liquid | < 2 | 1.15 ± 0.05 |
| | AWC C-235 | Clear, colorless to light yellow liquid | 2 – 3 | 1.15 ± 0.05 |
| | AWC C-236 | Clear yellow to amber liquid | >12 | 1.30 ± 0.10 |
| | AWC C-237 | Clear colorless to light yellow liquid | >12 | 1.1 ± 0.10 |
| | AWC C-238 | Clear Yellow to yellow liquid | 7.0 – 9.0 | 1.05 ± 0.05 |
| | AWC C-239 | Clear Yellow to Amber Liquid | 9.0 – 10.0 | 1.35 ± 0.05 |
| Accepta | Accepta 2069 | Colourless liquid | 14 | 1.12 |
| | Accepta 2066 | Light yellow liquid | 12.0-13.0 | 1.3 |